AD-784 332

NUMERICAL SOLUTION OF THE NAVIER-STOKES EQUATIONS FOR ROCKET PLUMES AT 120 KM ALTITUDE

L. C. Himmell, et al

Applied Theory, Incorporated

Prepared for:

Office of Naval Research
Advanced Research Projects Agency

July 1974

ATR-74-33-1

NUMERICAL SOLUTION OF THE NAVIER-STOKES EQUATIONS
FOR ROCKET PLUMES AT 120 KM ALTITUDE
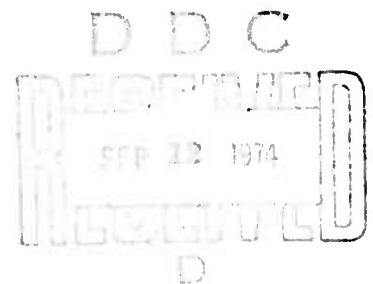
by

L. C. Himmell
J. G. Trulio

The views and conclusions contained in this document
are those of the authors and should not be interpreted
as necessarily representing the official policies,
either expressed or implied, of the Advanced Research
Projects Agency or the U.S. Government.

1 (a)

79

ABSTRACT

Results are presented of a first-principle calculation
of steady flow to a distance of 300 ft aft of an Atlas booster
emitting exhaust gases. Agreement between the air shock
locus reported here, and the locus predicted by the simpler
model of Boynton, improves with distance from the vehicle.
Boynton's air-plume shock radius is smaller than ours by
factors of 2.2, 1.8 and 1.5, at distances of 100, 200, and
300 ft, respectively, aft of the vehicle. For the jet shock,
the corresponding ratios at the same three downstream loca-
tions are 1.5, 1.1 and 1.0, respectively. No evidence of
Helmholtz instability was found in our calculated flow-field.

ACKNOWLEDGMENT

TABLE OF CONTENTS

REPORT DOCUMENTATION PAGE		READ INSTRUCTIONS BEFORE COMPLETING FORM
1. REPORT NUMBER	2. GOVT ACCESSION NO.	3. RECIPIENT'S CATALOG NUMBER AD-784 332
4. TITLE *(and Subtitle)* NUMERICAL SOLUTION OF THE NAVIER-STOKES EQUATIONS FOR ROCKET PLUMES AT 120 KM ALTITUDE		5. TYPE OF REPORT & PERIOD COVERED Final Technical Report
		6. PERFORMING ORG. REPORT NUMBER ATR-74-33-1
7. AUTHOR(s) L. C. Himmell J. G. Trulio		8. CONTRACT OR GRANT NUMBER(s) ARPA Order No. 1801 for Contract N00014-71-C-0331
9. PERFORMING ORGANIZATION NAME AND ADDRESS Applied Theory, Inc. 1010 Westwood Boulevard Los Angeles, California 90024		10. PROGRAM ELEMENT, PROJECT, TASK AREA & WORK UNIT NUMBERS
11. CONTROLLING OFFICE NAME AND ADDRESS Advanced Research Projects Agency 1400 Wilson Boulevard Arlington, Virginia 22209		12. REPORT DATE July 1974
		13. NUMBER OF PAGES 79
14. MONITORING AGENCY NAME & ADDRESS(If different from Controlling Office) Office of Naval Research 800 Quincy Street Arlington, Virginia 22217		15. SECURITY CLASS. (of this report) Unclassified
		15a. DECLASSIFICATION DOWNGRADING SCHEDULE

16. DISTRIBUTION STATEMENT *(of this Report)*

17. DISTRIBUTION STATEMENT *(of the abstract entered in Block 20, If different from Report)*

18. SUPPLEMENTARY NOTES

19. KEY WORDS *(Continue on reverse side if necessary and identify by block number)*

Rocket Plumes
Navier-Stokes Equations
Hypersonic Flow

20. ABSTRACT *(Continue on reverse side if necessary and identify by block number)*

Results are presented of a first-principle calculation of steady flow to a distance of 300 ft aft of an Atlas booster emitting exhaust gases. Agreement between the air shock locus reported here, and the locus predicted by the simpler model of Boynton, improves with distance from the vehicle. Boynton's air-plume shock radius is smaller than ours by factors of 2.2, 1.8 and 1.5, at distances of 100, 200, and 300 ft, respectively, aft of the vehicle. For the jet shock, the corresponding ratios at the same three downstream locations are 1.5, 1.1 and 1.0, respectively. No evidence of Helmholtz instability was found in our calculated flow-field.

SECTION 1

INTRODUCTION AND SUMMARY

1.1 Background

In this paper we describe the continuation of a calculation from first principles of the interaction of a hypersonic airstream with the exhaust plume of a typical launch vehicle during ascent. Since there were large differences between the results of the previous calculation for the near-field of the vehicle[1] relative to results based on simpler plume interaction models (in particular, the model of Boynton[2]), it became important to determine whether similar discrepancies would be found farther downstream. The properties of the flow-field were therefore computed from the previous downstream boundary location of 71 ft, to a cross-flow plane about 300 ft aft of the vehicle. It also proved necessary to extend the field of calculation in the radial direction, even within 71 ft of the vehicle.

To recapitulate, the procedure for computing fluid-mechanical fields in the present program is one of numerical integration of the full time-dependent Navier-Stokes equations using the AFTON 2A computer code.[3,4] In the case at hand, a hypersonic airstream interacts with an ATLAS launch vehicle that emits rocket exhaust. The flow, which is assumed to be steady, proceeds under the following conditions:

U_∞	=	10150 fps	freestream flow speed
M_∞	=	8.054	freestream Mach number
Re_∞/ft	=	1.17	freestream Reynolds number per foot

1

$$\lambda_\infty \quad = \quad 10.26 \text{ ft} \qquad \text{freestream mean free path}$$

$$\dot{\omega} \quad = \quad 285 \text{ lb/sec} \qquad \text{plume weight flow}$$

$$T_v \quad = \quad 82,600 \text{ lbs} \qquad \text{vacuum thrust}$$

$$R \quad = \quad 1.895 \text{ ft} \qquad \text{Atlas rocket nozzle radius}$$

The rocket exhaust gases have the following properties:

$$M* \quad = \quad 3.86 \qquad \text{Mach number}$$

$$T* \quad = \quad 2118^\circ \text{ R} \qquad \text{Temperature}$$

$$P* \quad = \quad .158 \text{ atmospheres} \qquad \text{Pressure}$$

Both the air and rocket exhaust are defined as polytropic gases with a heat capacity ratio equal to 1.4 and a molecular weight of 28, and having a viscosity propertional to the local temperature raised to the power .70.

With respect to the field generated earlier by ATI,[1] a question remained as to whether steady-state conditions had been attained over the whole region of calculation. That question is addressed below by comparing the earlier field with the field reported here. The results of the present calculation are also compared herein with those predicted by the plume model of Boynton.

1.2   Summary of Results

A velocity vector plot of the entire steady-state flow field is presented in Figure 1. The field was generated in piecewise fashion (Sections 2 and 3), and the finite difference meshes used on individual portions of the overall computational domain did not always fit smoothly together. Thus, an abrupt change in mesh-point distribution is evident in
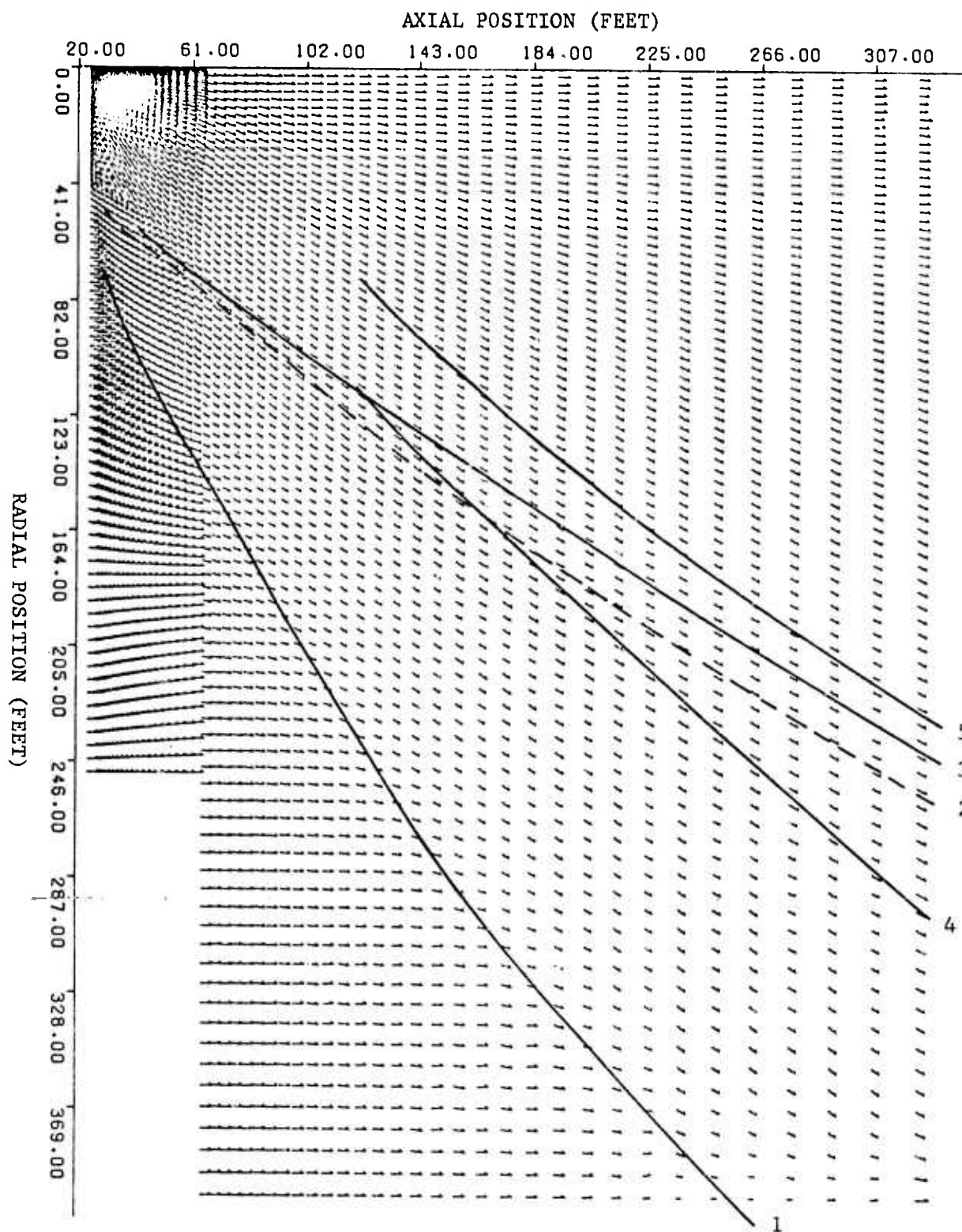
Figure 1.   Steady-State Velocity Field Aft of an Atlas Booster During Ascent. Each arrow gives the direction of flow at the mesh point from which it emanates, and flow speeds are proportional to the lengths of the arrows. The field, which is shown between planes 3.58 ft and 302.01 ft behind the body was computed with the AFTON 2A code. The air shock, dividing streamline and jet shock are denoted by Curves 1, 2 and 3, respectively, while Curves 4 and 5 represent, respectively, the air and jet shocks of Boynton.[8] The field was determined by calculation on six separate portions of the overall region shown. (Problem 590.1; Altitude 394 kft; U_∞ = 10150 fps; M_∞ = 8.054; Re_∞ = 1.17/ft)

3

Figure 1 on a line 44.36 ft aft of the vehicle; in fact even the radius of the region of calculation changes substantially 44.36 ft behind the exhaust nozzle. However, care was taken to insure that the field itself varied smoothly with position throughout the calculational domain.

The AFTON 2A air shock, dividing streamline and jet shock, as well as the air and jet shocks of Boynton,[5] are shown in Figure 1. Evidently the final AFTON 2A air-shock leaves the nozzle with a different slope — steeper by more than a factor of 3 — than that found by Boynton. However, the ratio of the radii of the two air-shocks continually decreases with distance aft of the nozzle, attaining a value of about 1.5 at the furthest downstream position calculated with the AFTON code (~300 ft). Boynton's results extend 2 kilometers downstream, and the consequent uncertainty in the position of his shock locus on a 300-ft scale is therefore substantial (~15 ft). Similar uncertainty attends the location of Boynton's jet-shock locus, whose radius 300 ft aft of the nozzle is about 233 ft. The corresponding final radius found with the AFTON 2A code is 241 ft, while the slope of the AFTON jet-shock locus at the nozzle is about 1.5 times that of Boynton's curve. No dividing streamline locus appeared in the final account of Boynton's results received at ATI.

In the AFTON 2A field, gases exiting from the exhaust nozzle turn through a much larger angle than is predicted by Boynton's model. Thus, a relatively large volume of air is intercepted by the AFTON 2A air-plume shock, and that air is relatively strongly heated. Downstream, the region of expanding shocked air is therefore relatively thick. Also the

4

hotter shocked air in the AFTON 2A field delivers heat to the exhaust gases by conduction more rapidly than in Boynton's field, which leads to a radial expansion of the exhaust gases near the dividing streamline. More important, however, is the result that the difference between the AFTON 2A and Boynton fields decreases with increasing downstream distance. Indeed, the two jet-shocks are already coincident, for all practical purposes, 200 ft aft of the nozzle.

Once again we find that an assumption basic to plume models (including the Boynton model), namely that streamlines and isotherms coincide, is not verified by the final AFTON 2A field. However, departures from that rule are large only in the region of the air shock, and even those differences decrease considerably with downstream distance.

The present AFTON 2A flow field was developed over a much longer period of problem time than the earlier field, to insure the attainment of steady conditions. The region of calculation common to both fields extended from 3.58 ft to 71 ft aft of the nozzle. On that region, it can be seen by comparing Figures 1 and 2 that the air-plume shock loci found in the two AFTON calculations generally differ by less than 10% in radius. However, the present dividing streamline and jet-shock loci are smaller in radius than the earlier AFTON loci (by factors of about 0.7 and 0.6, 60 ft aft of the nozzle), indicating that the earlier field was not steady over the domain in question. Little of the former difference now remains between the AFTON jet-shock position, and that of Boynton.

AXIAL POSITION (FEET)
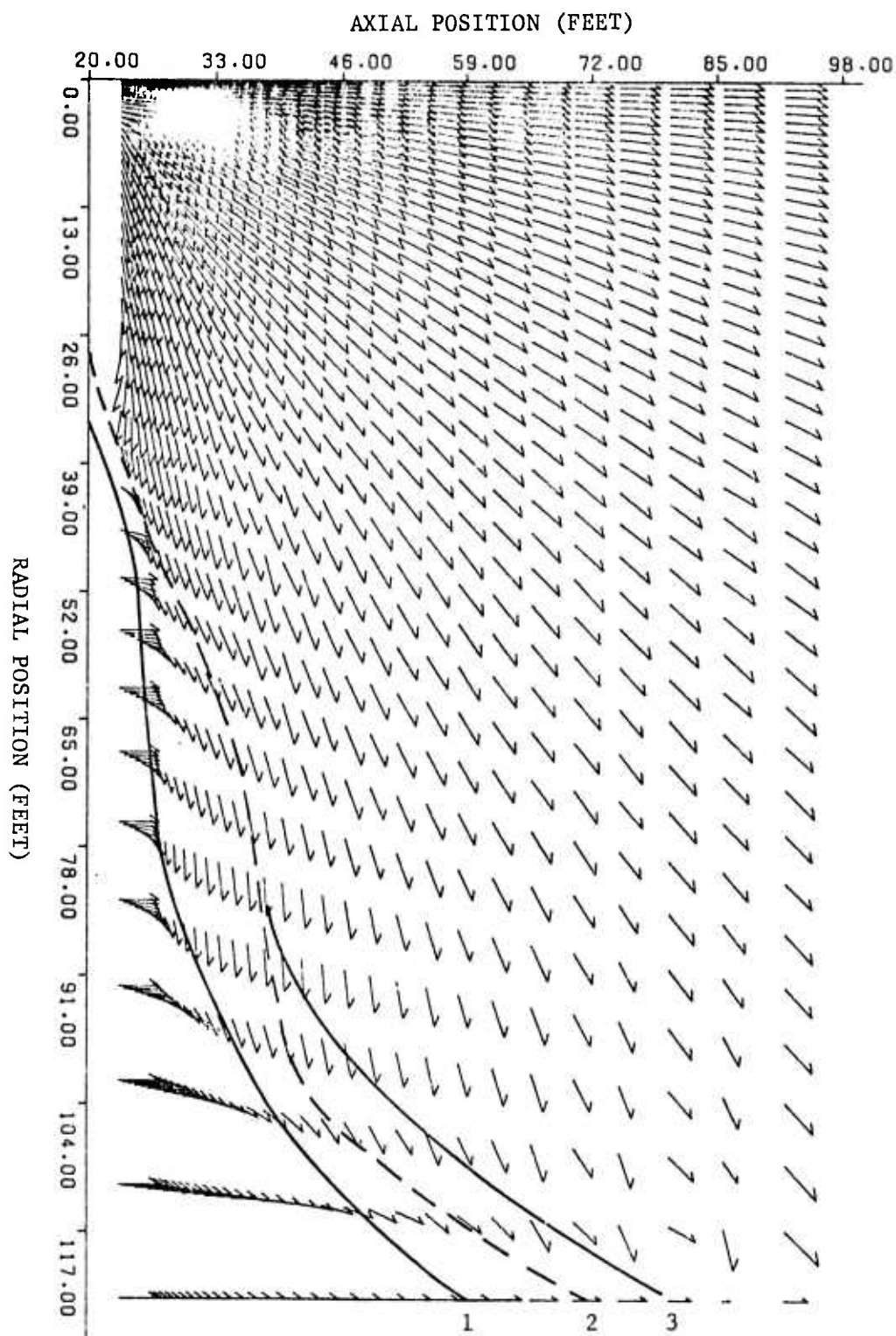
Figure 2. Velocity Field Aft of an Atlas Booster During Ascent, as
Calculated with the AFTON 2A Code Prior to the Work Reported
Here.[1] The field is shown between planes 2.53 ft and 71.28 ft
behind the body. The air shock, dividing streamline and jet
shock are denoted by Curves 1, 2 and 3, respectively. The
points at the tails of the vector-arrows comprise Mesh 1.
(Problem 590.1; Altitude 394 kft; $U_\infty = 10150$ fps; $M_\infty = 8.054$;
$Re_\infty = 1.17/ft$)

6

SECTION 2

MAIN FEATURES OF THE CALCULATION

To proceed efficiently with the calculation, despite
uncertainty as to the air shock locus, and despite an
upper limit to the number of streamline-like lines permitted
by the AFTON 2A code, advantage was taken of the hypersonic
character of the flow. Thus, when it was found that the
field obtained in the previous calculation[1] was not steady
in its outer radial regions, a line in the steady inner
region was employed as an inner radial boundary for further
calculation. The new region of computation covered the same
streamwise interval as before, but extended to a larger
radius. The Mach number was large enough over the region
of calculation to insure that changes in flow-field proper-
ties due to displacement of the outer boundary, would not
disturb the field within the inner boundary. On that same
principle, the field to a downstream distance of 300 ft
behind the vehicle, and roughly bounded by the air shock,
was computed in sections. Specifically, for a given axial
interval, motion was computed over a series of radial inter-
vals whose inner boundaries, in turn, lay in regions on
which the calculated flow field had become steady; the pro-
cedure was then repeated for an adjacent axial interval
further downstream. The number of radial intervals asso-
ciated with each axial interval was dictated by both the
radius of the air shock and the need to maintain mesh-point
densities that would lead to consistent accuracy of integra-
tion throughout the region of calculation. Details follow.

7

2.1   Continuation of the Previous Calculation

It was planned that the field calculated to a distance of 71 ft behind the booster before the present effort began would be used to provide boundary conditions at about 45 ft for the calculation of flow further downstream. It was therefore important that the field to 71 ft be steady, within numerical error. For that reason, the numerical field provided by previous work was used without any change as an initial field for a preliminary test calculation (Stage 1 of the overall calculation). Boundary conditions, mesh-point locations, etc., were not modified in any way; the earlier calculation was simply continued for an additional 12.96 units of characteristic time, where a unit of characteristic time is defined as the time taken by a free-stream particle to travel a distance equal to one exit-nozzle radius (1.895 ft). Careful examination of the resulting distribution of velocity, specific internal energy, pressure, etc., showed that the original field of flow was indeed steady near the symmetry axis. However, as can be seen in Figure 3, the air shock moved outward in the region of the lateral boundary during Stage 1. In fact, the radial boundary itself was evidently interfering with the growth of the plume. It was therefore clear that the previous mesh would have to be extended greatly in the radial direction, and the flow field developed on the enlarged radial domain, before calculating motion further downstream. The finite difference mesh defined for that purpose will now be described.

AXIAL POSITION (FEET)

23.00   35.50   48.00   60.50   73.00   85.50   98.00

RADIAL POSITION (FEET)

0.00
12.50
25.00
37.50
50.00
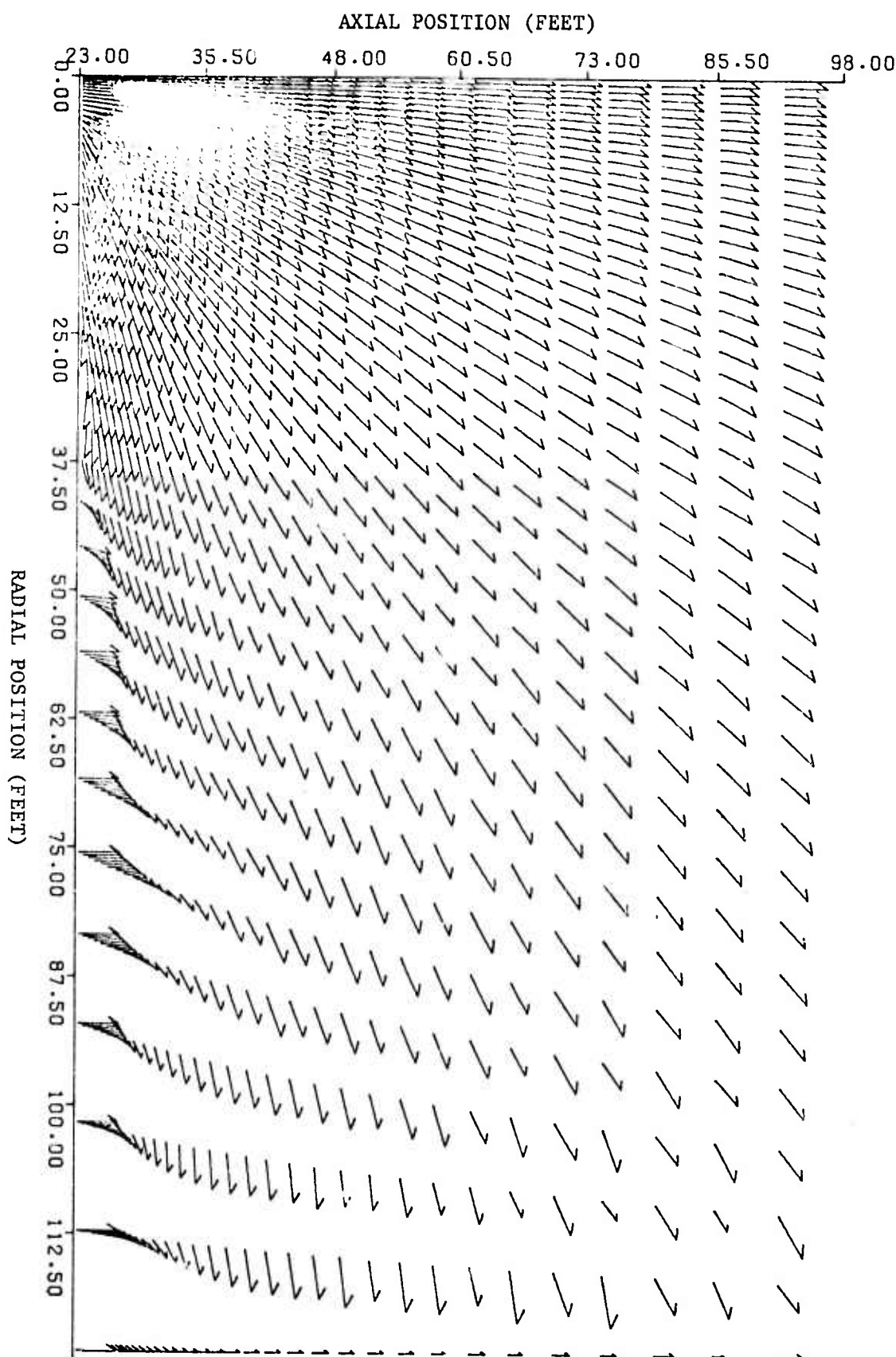62.50
75.00
87.50
100.00
112.50

Figure 3. Velocity Field Aft of an Atlas Booster During Ascent. Evolution of the flow field has been computed with the AFTON 2A code for 12.96 units of characteristic time, starting from the field of Figure 2. Again Mesh 1 was used. (Problem 590.1; Altitude 394 kft; $U_\infty = 10150$ fps; $M_\infty = 8.054$; $Re_\infty = 1.17/\text{ft}$)

9

2.2   The Mesh, Boundary Conditions and Initial Conditions for Stage 2 of the Calculation

The finite difference mesh used in previous work[1] and in Stage 1 of the present effort, will be referred to hereafter as Mesh 1. Mesh 1 was traced in the flow-plane by 45 streamline-like lines and 31 potential-like lines. The mesh covered a rectangular region of the flow-plane that ran from the symmetry axis to a radius of about 120 feet, and extended axially to about 69 ft from an upstream boundary located 2.53 ft aft of the exit nozzle.

A new Mesh (Mesh 2) was constructed to cover a region with a radial boundary at 180 ft, but with axial boundaries coincident with the first interior K-lines of Mesh 1. However, due to limited high-speed computer memory, it was not possible to form Mesh 2 simply by adding more streamline-like lines to Mesh 1. Moreover, such a procedure would have been wasteful in that (a) it was not necessary to perform further calculations for the region near the axis, where the flow already seemed steady, and (b) the timestep for stable calculation was limited for the entire mesh by the near-axis region, since the density of mesh-points was greatest near the exhaust nozzle. Thus, in forming Mesh 2, zones were removed from Mesh 1 near the axis of symmetry, and were added above the lateral boundary of Mesh 1. Furthermore, since the region near the lateral boundary of Mesh 1, and beyond, was of primary interest, the radial distribution of mesh points was altered relative to Mesh 1. The new mesh — Mesh 2 — is exhibited in Figure 4.

Mesh 2 contains 55 streamline-like lines (J-lines) and 29 potential-like lines (K-lines). As usual the J-lines and K-lines were labeled with positive integral indices. In both Mesh 1 and Mesh 2, the first J-line — the line
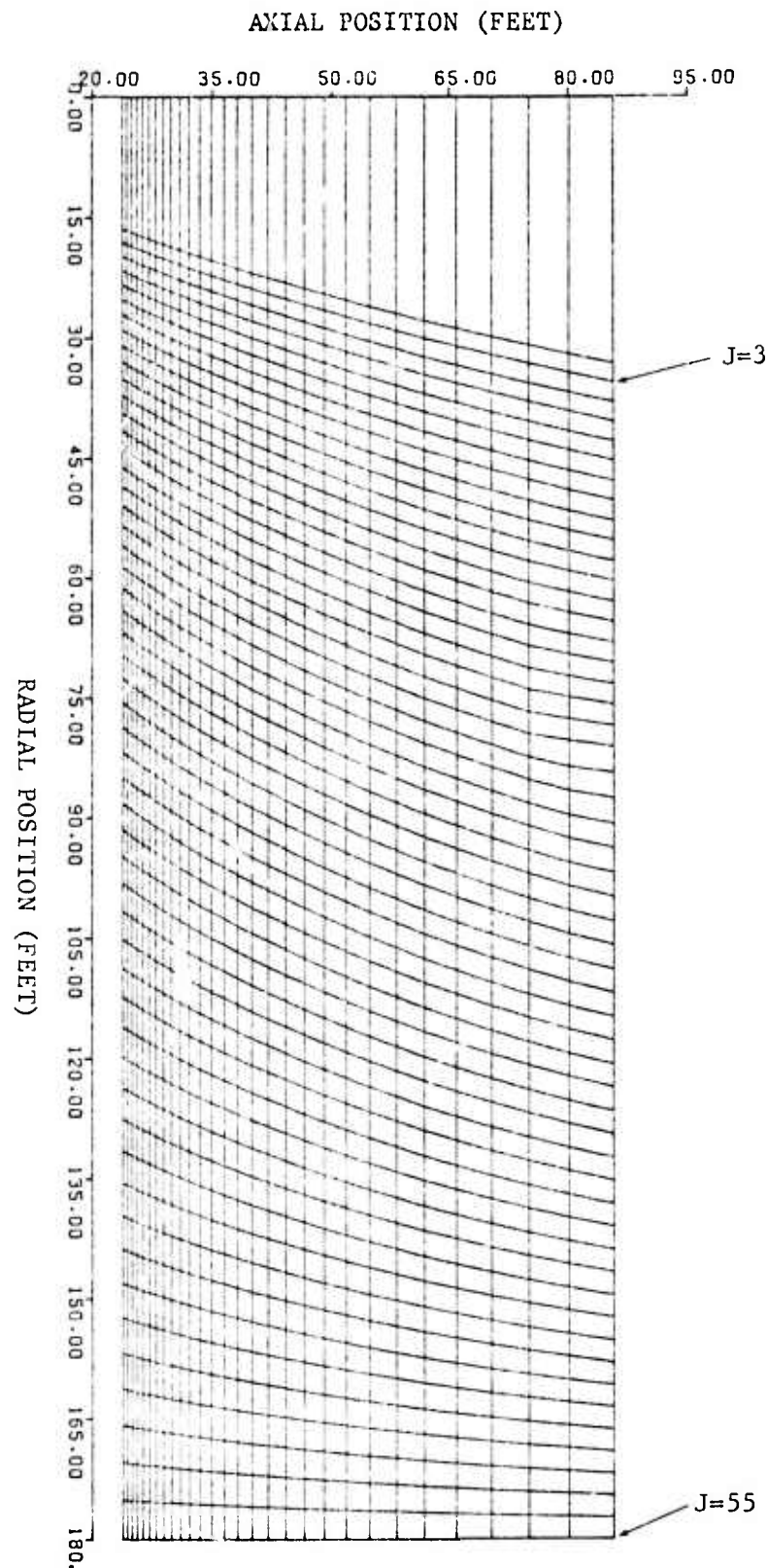
10

AXIAL POSITION (FEET)

Figure 4. Plot of Mesh 2, Which Was Used to Compute Steady Flow on a Portion of the Field Behind an Atlas Booster During Ascent. The region on which the field was determined with Mesh 2 is bounded by the lines labeled J=3 and J=55 and extends from 3.03 ft to 64.89 ft behind the exhaust nozzle. The mesh is composed of 55x29 points.

11

labeled J=1 — was coincident with the symmetry axis. Also
the J-lines were ordered so that at any given axial position,
lines of increasing J-index lay at increasing distances from
the symmetry axis. However, the 25th J-line of Mesh 1 (J=25),
whose radius increased smoothly from 16.45 ft at its upstream
end to 33.15 ft at its downstream end, was chosen as the sec-
ond J-line (J=2) of Mesh 2. For J > 2, positions were assigned
to the J-lines of Mesh 2 in such a way that their increasing
distances of separation formed a geometric progression. The
lines J=2 and J=3 were the most closely-spaced J-lines of
Mesh 2, and those two lines were separated by almost the
same distance at each axial location as the lines J=25 and
J=26 of Mesh 1. The positions of the K-lines were the same
in both meshes. The flow found previously with Mesh 1 was
assumed to be steady out to the line J=3 of Mesh 2 — an assump-
tion that was verified even beyond that line.

Out to the lateral (radial) boundary of Mesh 1, thermo-
dynamic variables such as specific internal energy and density,
as well as values of the velocity, were found for Mesh 2 by
interpolation. In particular, values of thermodynamic vari-
ables, which are cell-centered, were determined at any given
point of Mesh 1 by taking a mass-weighted-average of the
values of each variable over the cells sharing the given
point as a common vertex. Having determined values of thermo-
dynamic quantities at the vertices of the cells of Mesh 1,
values were determined at the points of Mesh 2, by taking
advantage of the fact that the same K-lines were used in the
two meshes. Thus a quantity at any given point of Mesh 2 was
found from its values at the points of Mesh 1 by linear
interpolation with respect to radial position along a K-line.
Within each cell of Mesh 2, a value was then computed for each

thermodynamic variable as a density-weighted average, using the densities and specific internal energies just found for the cell's vertices. Since values for velocity were known at the start at points of Mesh 1, it was only necessary to determine their values at points of Mesh 2 by linearly interpolating with respect to radial position along a K-line. At the conclusion of the process just described, initial conditions were available for calculation with Mesh 2.

The properties found along the lines J=2 and J=3 by interpolation in the field that resulted from Stage 1, were maintained thereafter as boundary values. In that way, motion at smaller radii was precluded in Stage 2 from having any effect on the field outside the line J=3. Along the lateral boundary of the system (i.e., at a radius of 180 ft), the usual conditions of frictionless axially-directed flow were imposed. Also, on both the upstream and downstream boundaries, the boundary conditions of Stage 1 were again utilized; as in many previous applications of the AFTON codes, flow through the downstream boundary was dictated by equations based on the method of characteristics for uniaxial flow.[6] In fact, only the treatment of flow in the vicinity of the inner radial boundary of the region of calculation represents an extension of previous numerical technique.

Stage 2 of the calculation was carried out using Mesh 2, subject to the initial and boundary conditions just discussed.

2.3   Results Obtained with Mesh 2; Definition of
        Meshes 3 and 4

A vector plot of the initial velocity field on Mesh 2 is presented in Figure 5. Figure 6 contains a corresponding
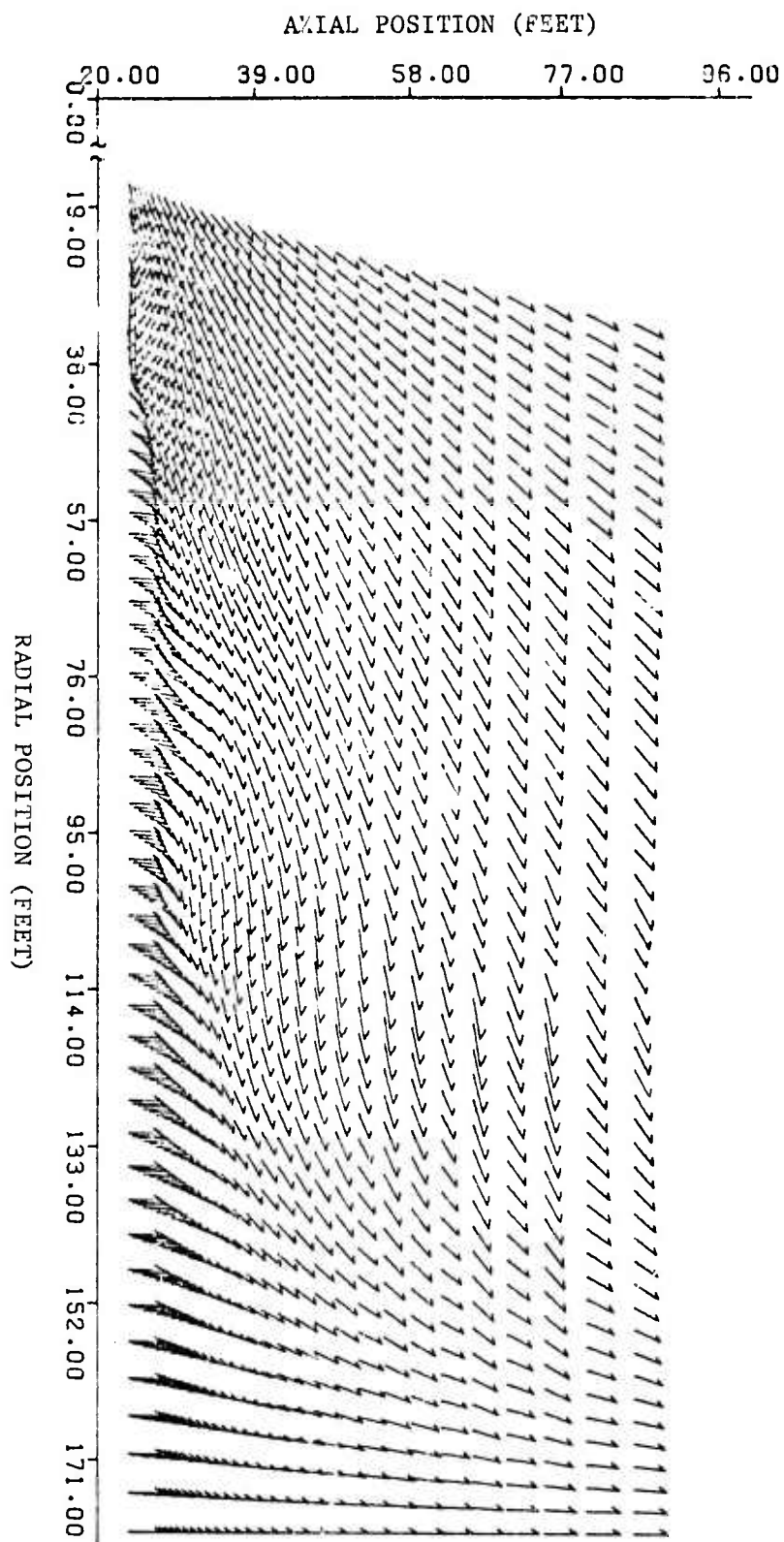
Figure 5. Initial Velocity Field for the Calculation of Flow on Mesh 2.
The region shown lies between between planes 3.03 ft and 64.89 ft
behind an Atlas booster during ascent. (Problem 590.1; Altitude
394 kft; $U_\infty = 10150$ fps; $M_\infty = 8.054$; $Re_\infty = 1.17/ft$)
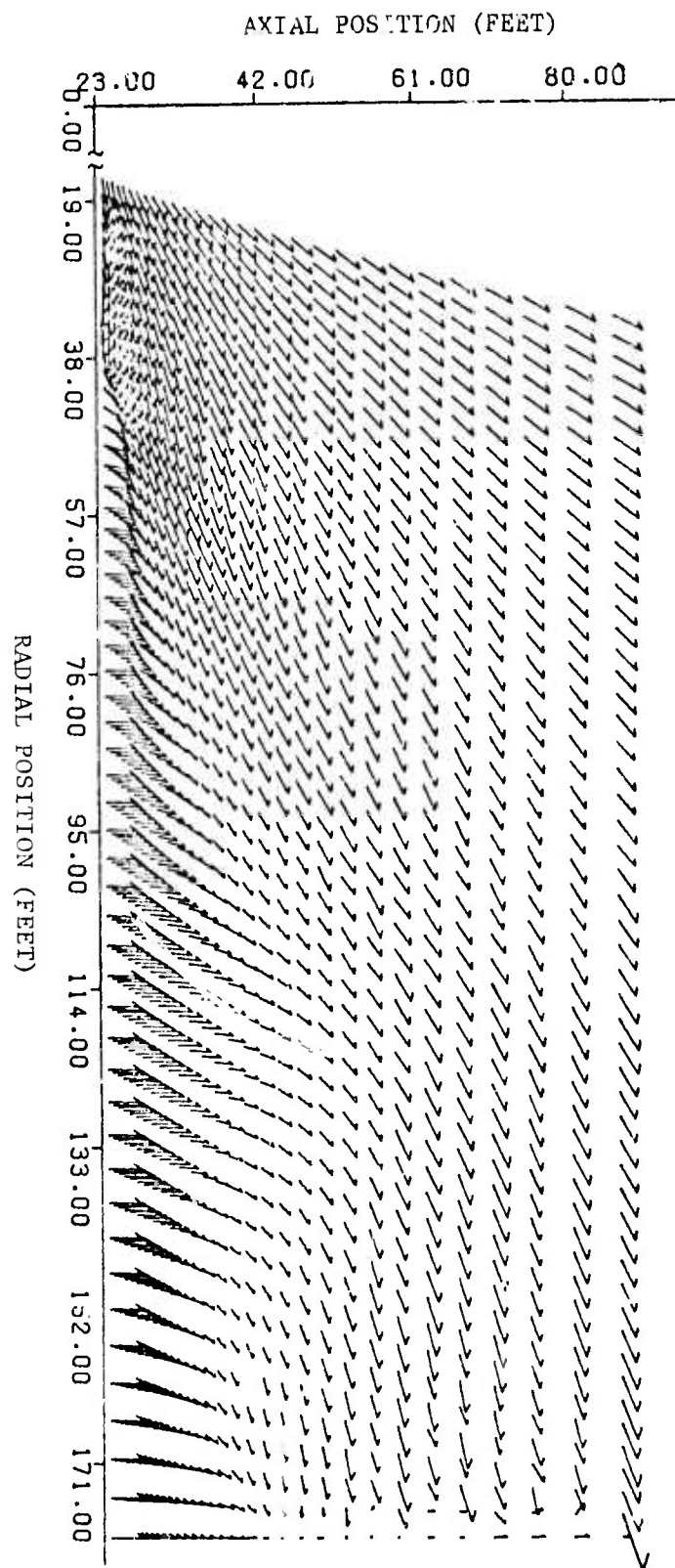
Figure 6. Velocity Field Behind an Atlas Booster During Ascent. Evolution of the flow field has been computed for 33.2 units of characteristic time on Mesh 2. The field, which is shown between planes 3.03 ft and 64.89 ft aft of the body, was computed with the AFTON 2A code. (Problem 590.1; Altitude 394 kft; $U_\infty =$ 10150 fps; $M_\infty = 8.054$; $Re_\infty = 1.17/ft$)

15

plot of the velocity field after having advanced the numerical solution in Stage 2 by 33.2 units of characteristic time.

Figure 6 attests to the need to move the lateral boundary of the region of calculation outward from its radial position of 180 feet in Mesh 2, in order to permit unimpeded development of the plume. However, since the Boynton model predicts an air-shock locus that is amply contained within Mesh 2, a further attempt was made to develop the steady field without enlarging the region of calculation. Specifically, we decided to find out whether a field similar to Boynton's would emerge if the calculation were run far enough to achieve steady conditions at the lateral boundary of Mesh 2. Since the time required to reach such a state was not known at the outset, the K-lines of Mesh 2 were moved so that their smallest distance of separation would increase by a factor of 2.5 relative to Mesh 2, with a corresponding increase in timestep. In the resulting mesh (Mesh 3), the distances of separation of consecutive K-lines (which increased in the downstream direction) formed a geometric progression characterized by the factor 1.053. The axial interval of 61.9 ft covered by Mesh 2 was reduced by 6.2 ft in Mesh 3, mostly at the downstream edge; also, Mesh 3 contained 24 K-lines rather than 29.

Initial conditions for calculation with Mesh 3 were obtained from the field generated on Mesh 2, using the interpolation procedure described above for Mesh 2 (Section 2.2). Also, the conditions imposed along the boundaries of Mesh 2 were retained for Mesh 3.

Evolution of the flow field was computed for 12.85 characteristic units of time using Mesh 3. During that period

16

the timestep was controlled by cells near the line J=2, and was larger by a factor of 3.3 than the timestep during calculation with Mesh 2. Near the lateral boundary, changes in the flow field became progressively more pronounced during the period in question. We therefore decided that the desired field could only be found if the radius of the region of calculation were increased, and another mesh (Mesh 4) was created for that purpose.

In Mesh 4, the outer radial boundary was displaced outward relative to Mesh 3, to a radius of 260 ft. The inner radial boundary was also moved outward when it was found from velocity vector plots that the field computed with Mesh 3 appeared to be steady within the line J=28; the radius of the line J=28 was 76.1 ft at its upstream end and 101.5 ft downstream. The line J=1 again coincided with the centerline of the system. The lines J=2 through J=29 of Mesh 4 were identical to the lines J=28 through J=55 of Mesh 3; beyond J=29, the J-lines of Mesh 4 were almost equally spaced out to the lateral boundary of the region of calculation (J=55, a line parallel to the symmetry axis at a distance of 260 ft).

The K-line distribution in Mesh 4 was identical to that of Mesh 3. Thus, in both the J- and K-directions, the cells of Mesh 4 were larger than those of Mesh 2, and the sound-speed-controlled timestep for stable computation with Mesh 4 was therefore relatively large. The timestep also rose relative to that employed with Mesh 3 because the region of highest mesh-point-density was located in Mesh 3 near the symmetry axis and upstream boundary, and was excluded from Mesh 4. In fact, on resuming the calculation of air-plume interaction

17

with Mesh 4, it was found that the timestep had increased by factors of 5.7 and 1.7, respectively, relative to the time-steps employed during numerical integration with Meshes 2 and 3.

2.4   Calculation with Mesh 4

Up to and including the line J=19 of Mesh 4, the field obtained from calculation with Mesh 3 defined initial conditions for Mesh 4. Above the line J=19, initial conditions were determined for Mesh 4 by linear interpolation between J=19 and the lateral boundary, where the flow variables were assumed to take on their free-stream values. Further, when calculation was resumed with Mesh 4, the boundary conditions employed on Mesh 3 were again utilized. The problem was run for 224.1 units of characteristic time. Observations of successive velocity vector plots up to that time, and of the change with time of flow variables at specific field-points, indicated that the computed field of flow had then become steady; conditions under which flows are considered "steady" are described in Sections 2.6 and 3.2.

Figure 7 presents a plot of the velocity vector field found by calculating the flow on Mesh 4 for 224.1 units of characteristic time. The solid curve of Figure 7, which defines the air shock, evidences a dimple at a radius of about 120 feet. A similar dimple had appeared at a radius of about 60 ft in the field generated prior to those reported here.[1] There seems to be no physical reason for the presence of such dimples in the steady field; it is true that a "no-slip" boundary condition was not employed on the surface of
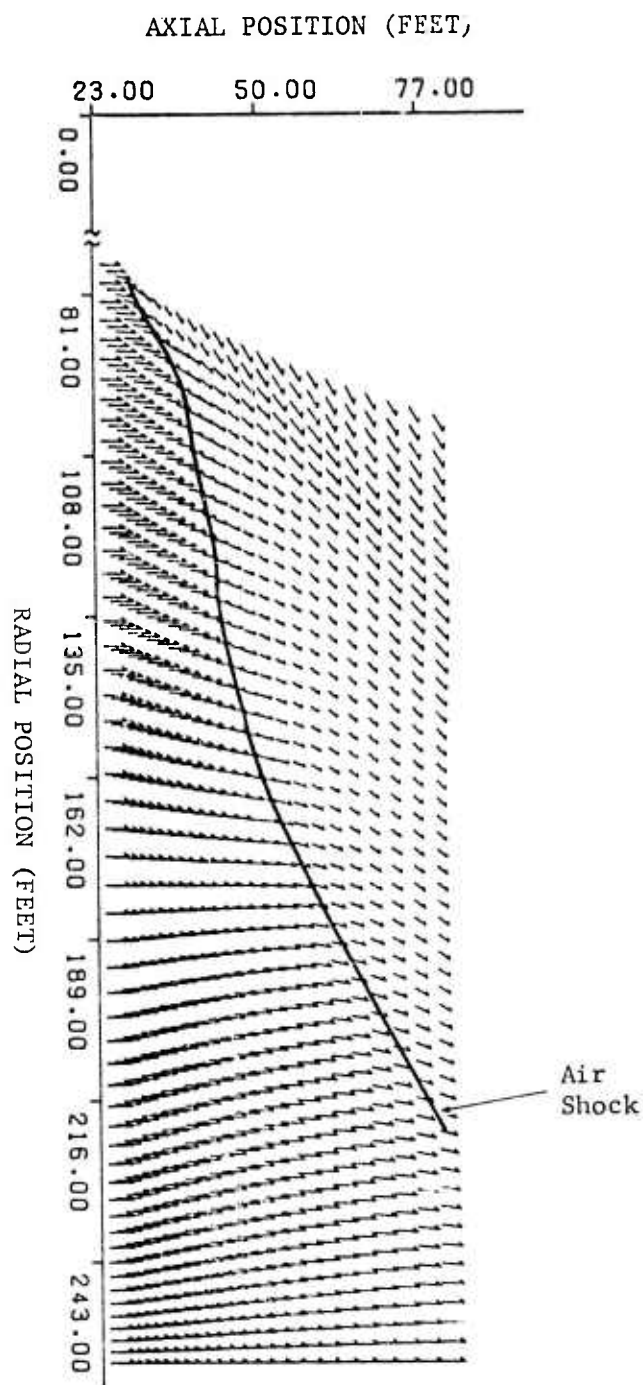
18

Figure 7. Velocity Field Aft of an Atlas Booster During Ascent.
Evolution of the flow has been computed for 224.1 units of
characteristic time using Mesh 4. The mesh consists of the
points at the tails of the vector-arrows shown. The field,
which is shown between planes 3.58 ft and 59.27 ft behind
the body, was computed with the AFTON 2A code. The solid
curve denotes the air shock. (Problem 590.1; Altitude 394 kft;
$U_\infty = 10150$ fps; $M_\infty = 8.054$; $Re_\infty = 1.17/ft.$)

the rocket in the original calculation, but the effects
produced thereby should have been confined to distances of
the order of a few boundary layers from the body. Since
the dimple in the air shock of Mesh 4 was intuitively diffi-
cult to accept, we were led to question the steadiness of
the field obtained with previous meshes — particularly Mesh 3.
The grounds on which that field had been judged steady on
Mesh 3 were not as firm as in the case of Mesh 4. In fact,
applying all the criteria of Sections 2.6 and 3.2, we con-
cluded that (a) steady conditions had not been obtained
with Mesh 2 to as large a radius as had been thought, and
that (b) a dimple had appeared in the air shock found with
Mesh 4 because boundary conditions imposed in that mesh
along the line J=2 were not representative of a truly steady
field. Accordingly, further calculations were made of the
field from 3.58 to 59.3 ft aft of the nozzle, as will now
be described.

2.5   Resolution of the "Dimple": Meshes 5 and 6

The possibility that the conditions imposed along the
lines J=2 and J=3 of Mesh 4 were not those of steady flow,
was investigated by means of further flow-field calculation
with Mesh 5.

Mesh 5 covered the total region occupied by both
Meshes 3 and 4. Between J-lines whose upstream radii lay
between about 16 ft and 76 ft (i.e., on Mesh 3 and below
Mesh 4), Mesh 5 was made identical to Mesh 3. At greater
radii, and up to 175 ft, Mesh 5 was identical to Mesh 4. A
final J-line was placed at 260 ft (as in Mesh 4), making

20

55 J-lines in all. On the portion of Mesh 5 identical to
Mesh 3, the final flow-field of Mesh 3 became the initial
field for Mesh 5. Elsewhere on Mesh 5, the initial field
was identical to the final field of Mesh 4, which had reached
a later stage of evolution toward a steady state than had the
field obtained with Mesh 3. Along the lines J=2 and J=3, and
along J=53 and J=54, the initial conditions of flow were main-
tained as boundary conditions; calculation with Mesh 5 was
thereby restricted to the radial interval from about 16 ft
to 175 ft. Relative to Meshes 3 and 4, there was no change
in Mesh 5 in either the position or conditions of flow asso-
ciated with the upstream and downstream boundaries. A vector
plot of the initial velocity field on Mesh 5 is presented in
Figure 8.

The field of flow was calculated using Mesh 5 for
197.3 units of characteristic time, during which period the
motion became steady below a radial height of about 70 ft.
Another mesh — Mesh 6 — was then constructed to cover the
region between the line J=17 of Mesh 5, and a lateral bound-
ary located at a radius of 250 ft. Initial conditions for
Mesh 6 were obtained from the results of the calculation
with Mesh 5 out to a radius of 175 ft, and at greater radii
from the field calculated earlier using Mesh 4. Boundary
conditions were imposed in the same manner as on the previous
meshes.

The initial velocity field for Mesh 6 is depicted in
Figure 9. After advancing the field in time for 279 charac-
teristic time-units, a study of successive velocity-vector
plots, and of the change with time of thermodynamic variables
at many field points, indicated that the computed field was

21

AXIAL POSITION (FEET)

23.00   50.00   77.00

RADIAL POSITION (FEET)

0.00
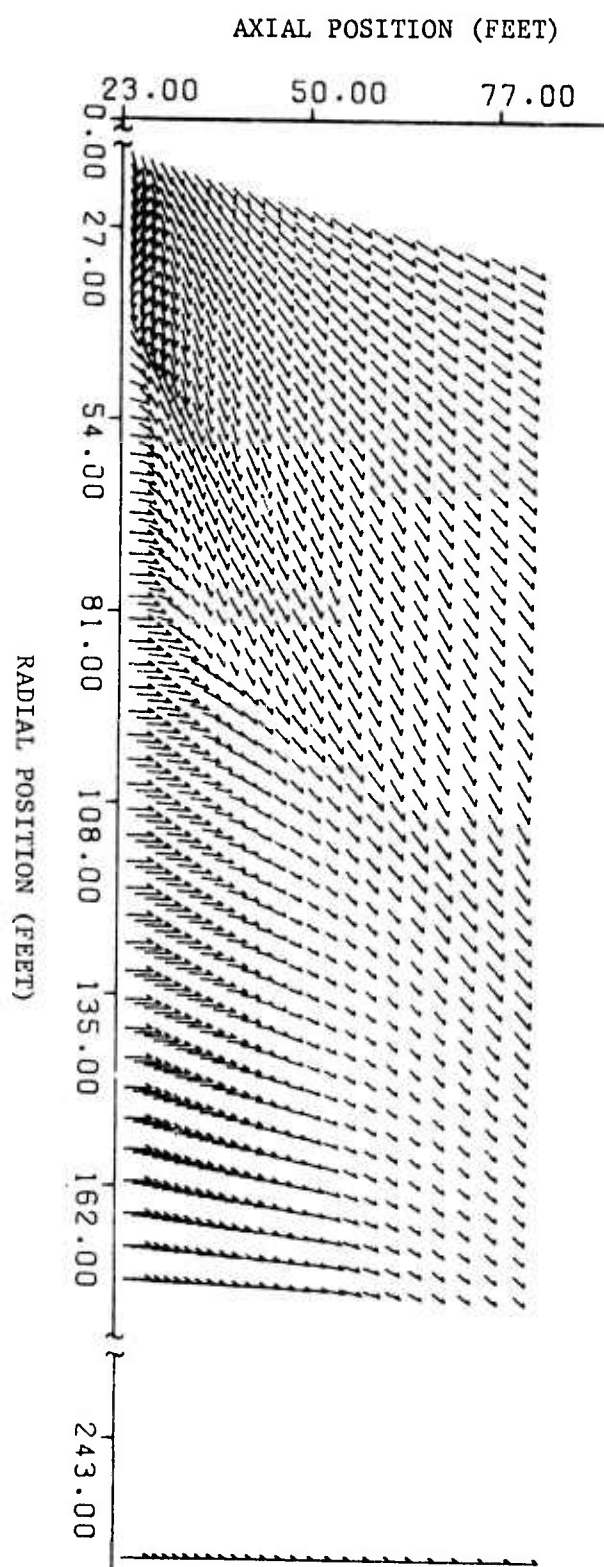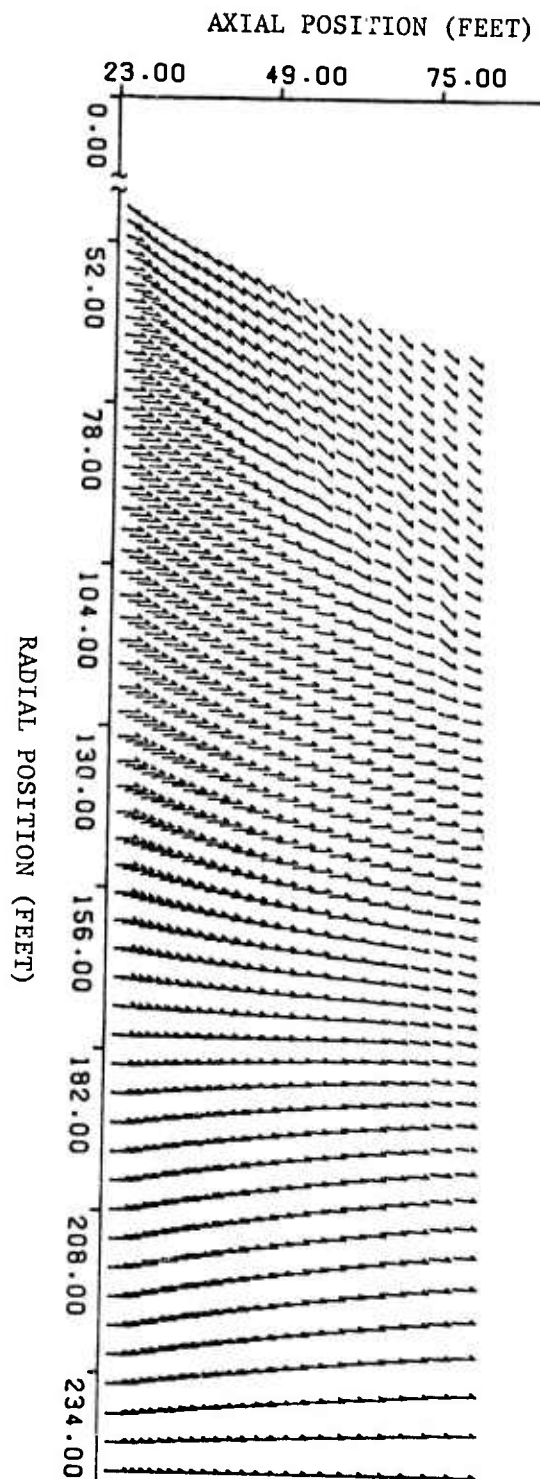27.00
54.00
81.00
108.00
135.00
162.00

243.00

Figure 8. Initial Velocity Field for the Calculation of Flow Using Mesh 5. The mesh consists of the points at the tails of the vector-arrows shown. The region covered by the mesh lies between planes 3.58 ft and 59.27 ft behind an Atlas Booster during ascent. (Problem 590.1; Altitude 394 kft; $U_\infty = 10150$ fps; $M_\infty = 8.054$; $Re_\infty = 1.17/ft.$)

AXIAL POSITION (FEET)

23.00   49.00   75.00

RADIAL POSITION (FEET)

0.00
52.00
78.00
104.00
130.00
156.00
182.00
208.00
234.00

Figure 9.   Initial Velocity Field for the Calculation of Flow Using Mesh 6.
            The mesh consists of the points at the tails of the vector-
            arrows shown.   The region covered by the mesh lies between planes
            3.58 ft and 59.27 ft behind an Atlas Booster during ascent.
            (Problem 590.1; Altitude 394 kft; $U_\infty = 10150$ fps; $M_\infty = 8.054$;
            $Re_\infty = 1.17$/ft.)

23

steady enough (Section 2.6) to make calculation feasible further downstream. The final flow-field obtained with Mesh 6 is shown in Figure 10 along with the dividing streamline and the air- and jet-shocks. No trace remains of the earlier air-shock dimple.

2.6 The Computed Field to a Distance of About 60 ft Behind the Vehicle; Steadiness of the Flow

As computation went forward for each particular mesh, successive velocity-vector plots were carefully examined to determine the extent to which steady flow conditions had been attained. For the same purpose, plots were made of specific internal energy, density and the two components of velocity, as functions of time, at a variety of points within Meshes 1, 4, 5 and 6. With regard to final flow-field properties calculated to a distance of about 60 ft aft of the vehicle (the "near-field"), the various indices of steady flow will now be reviewed.

A velocity-vector plot for the entire near-field is presented in Figure 11. The figure was obtained by piecing together those portions of the flow-fields computed with Meshes 1, 5 and 6 that were deemed steady; the portions in question cover three radial intervals defined by the sequence of radii 0, 16.66, 46.59 and 250.0 ft. In the region near the upstream boundary it can be seen that plume gas, which is axially directed as it leaves the exhaust nozzle, acquires a considerable radial component. The collision of plume-gas with the airstream then abruptly turns the gas downstream toward the symmetry axis — in some regions by as much as 45°.
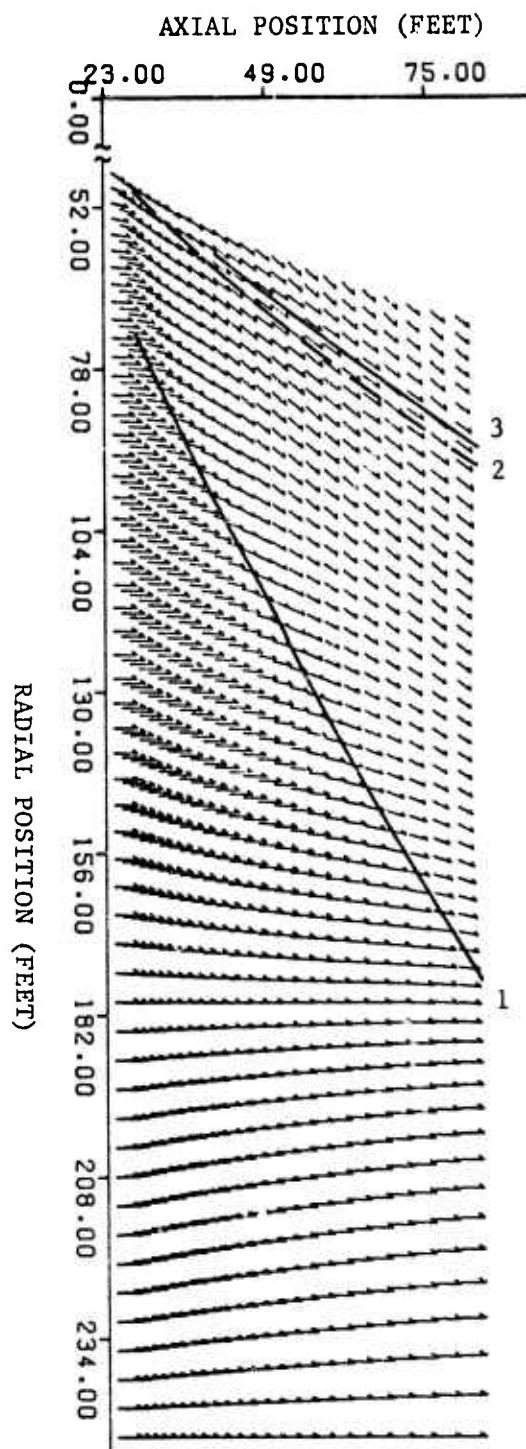
24

Figure 10. Velocity Field Aft of an Atlas Booster During Ascent. Evolution of the flow has been computed for 279 units of characteristic time starting from field of Figure 9. Mesh 6 was used for the calculation. The field, which is shown between planes 3.58 ft and 59.27 ft behind the body, was computed with the AFTON 2A code. The air shock, dividing streamline and jet shock are denoted by Curves 1, 2 and 3, respectively. (Problem 590.1; Altitude 394 kft; $U_\infty = 10150$ fps; $M_\infty = 8.054$; $Re_\infty = 1.17/ft.$)

25

AXIAL POSITION (FEET)
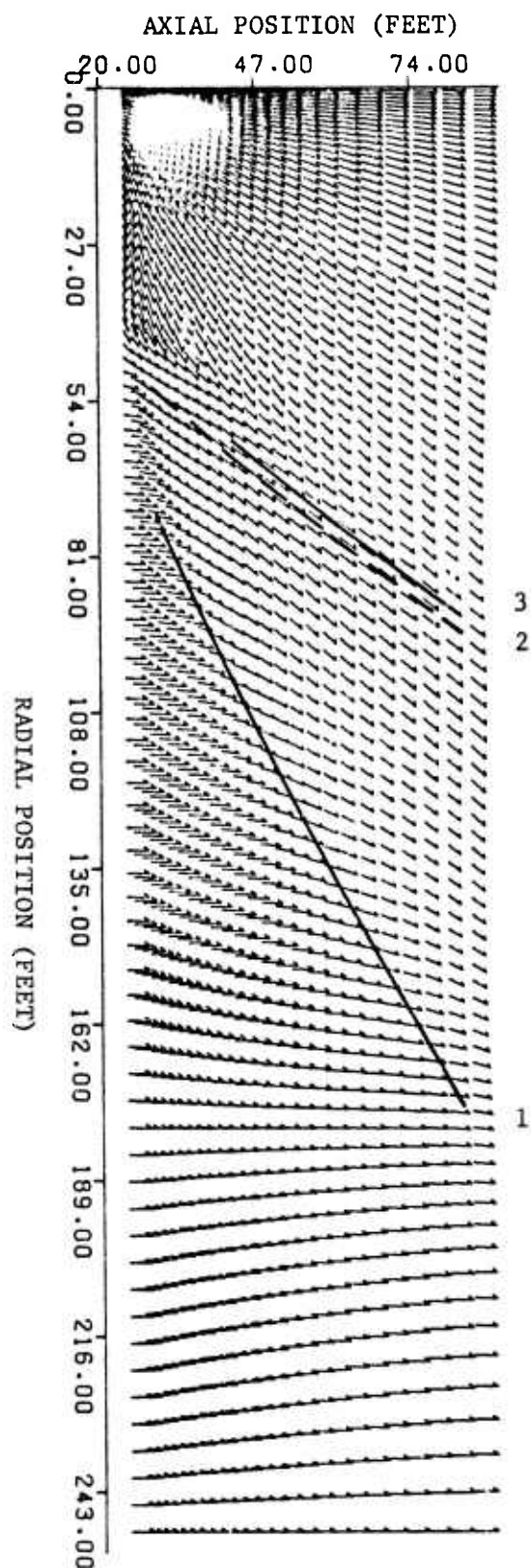
Figure 11. Steady-State Velocity Field Aft of an Atlas Booster During Ascent. The field, which is shown between planes 3.58 ft and 59.27 ft behind the body, was computed with the AFTON 2A code. The air shock, dividing streamline and jet shock are denoted by Curves 1, 2 and 3, respectively. The field was determined by calculation on portions of Meshes 1, 5 and 6. (Problem 590.1; Altitude 394 kft; $U_\infty = 10150$ fps; $M_\infty = 8.054$; $Re_\infty = 1.17/\text{ft.}$)

26

Curves 1, 2 and 3 of Figure 11 label the air shock, the dividing streamline and the jet shock, respectively. Corresponding curves, reported earlier,[1] are reproduced in Figure 2. It is evident on comparing Figures 11 and 2 that the shocks found in the final field are free of earlier wiggles, and also that as one progresses downstream the dividing streamline and jet-shock have moved considerably closer to the centerline. However, no substantial change has occurred in the position of the air shock. It is worth noting that the two shock loci were defined with the aid of an artificial viscosity function proportional to the square of the divergence of the local velocity, although no artificial viscosity entered the calculation of fluid motion. Specifically, points of the air- and jet-shock loci were identified as relative maxima of the artificial viscosity along individual streamlines.

The variation with time of velocity, specific internal energy and density at two axial stations is presented in Figures 12 through 19. At the first axial position, located 22.3 ft behind the exhaust nozzle, the evolution of field variables is shown for radii of 29.0, 40.0, 64.6, 78.5, 93.4, 102.8, 115.6, 139.4, 164.7 and 192.0 ft (Figures 12, 13, 14 and 15). Figures 16 through 19 refer, respectively, to radii of 37.3, 50.0, 76.0, 90.2, 105.1, 120.1, 135.1, 150.0, 165.0 and 180.0 ft at an axial position 51.45 ft aft of the nozzle.

Only the components of fluid velocity show significant changes with time in Figures 12 through 19, and then only in shock regions — at radii of 20 and 40 ft at the first axial station, and 37, 50 and 90 ft at the second
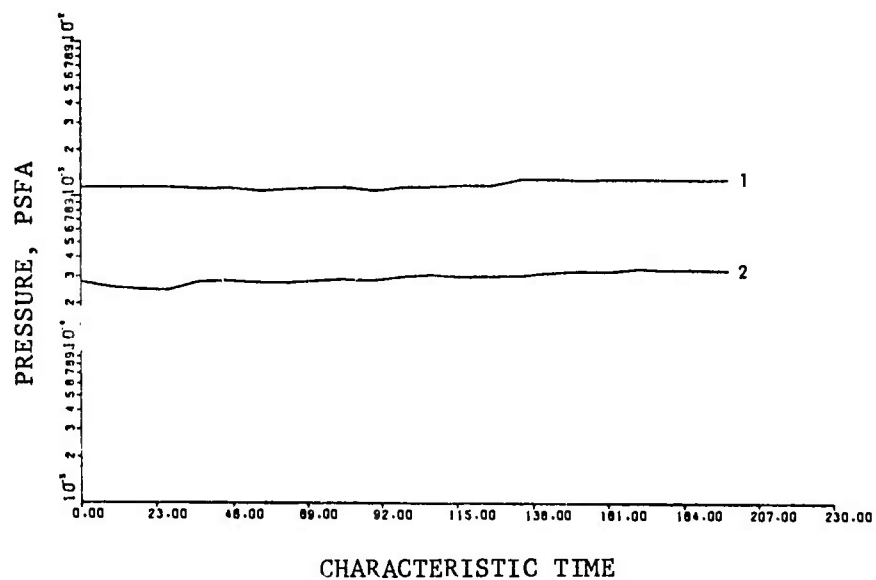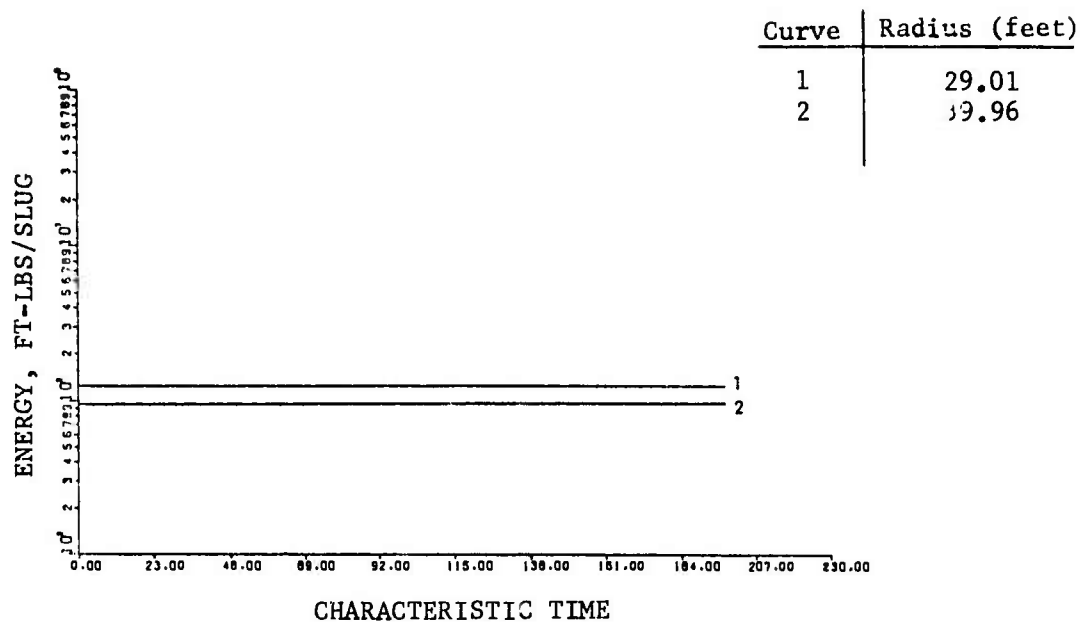
27

Figure 12. Specific Internal Energy and Pressure, vs. Time, at Various Points Along a Line Normal to the Centerline of an Atlas Booster During Ascent, and 22.31 ft Behind the Exit Nozzle. Data for the curves shown were generated by the AFTON 2A code using Mesh 5. (Problem 590.1; Altitude 394 kft; $E_\infty = .2836 \times 10^7$ ft-lbs/slug; $P_\infty = .5671 \times 10^{-4}$ psfa; $M_\infty = 8.054$; $Re_\infty = 1.17/ft$.)

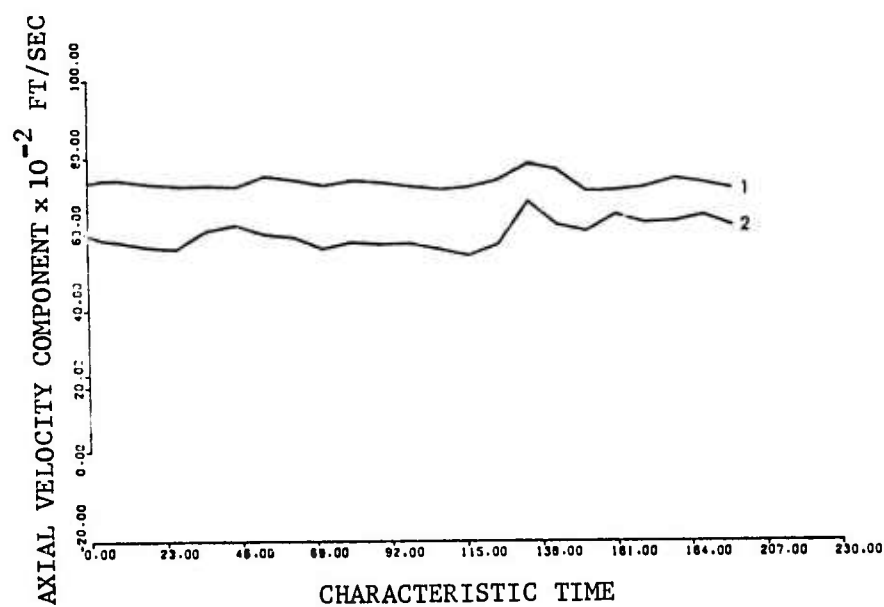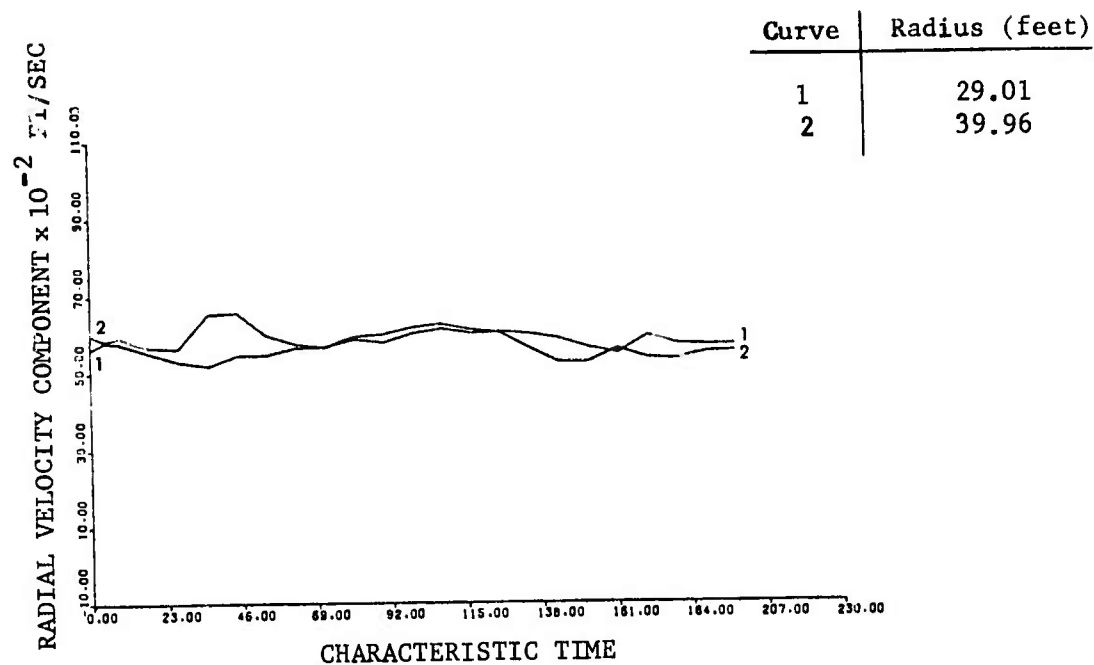| Curve	Radius (feet)
1	29.01
2	39.96

Figure 13. Radial and Axial Components of Velocity, vs. Time, at Various Points Along a Line Normal to the Centerline of an Atlas Booster During Ascent, and 22.31 ft Behind the Exit Nozzle. Data for the curves shown were generated by the AFTON 2A code using Mesh 5. (Problem 590.1; Altitude 394 kft; $U_\infty = 10150$ fps; $M_\infty = 8.054$; $Re_\infty = 1.17$/ft.)

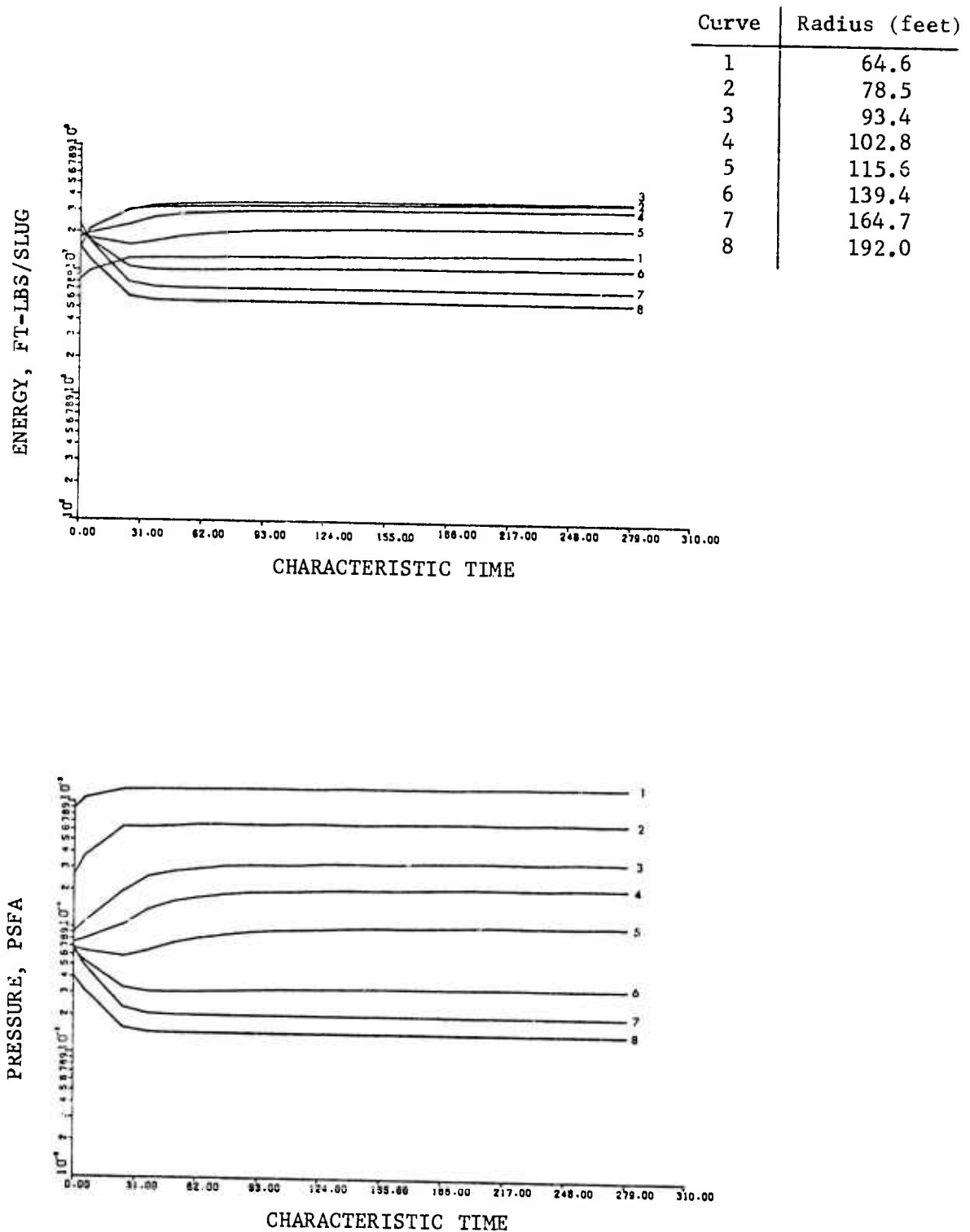| Curve	Radius (feet)
1	64.6
2	78.5
3	93.4
4	102.8
5	115.6
6	139.4
7	164.7
8	192.0

Figure 14. Specific Internal Energy and Pressure, vs. Time, at Various Points Along a Line Normal to the Centerline of an Atlas Booster During Ascent, and 22.31 ft Behind the Exit Nozzle. Data for the curves shown were generated by the AFTON 2A code using Mesh 6. (Problem 590.1; Altitude 394 kft; $E_\infty = .2836 \times 10^7$ ft-lbs/slug; $P_\infty = .5671 \times 10^{-4}$ psfa; $M_\infty = 8.054$; $Re_\infty = 1.17/\text{ft.}$)

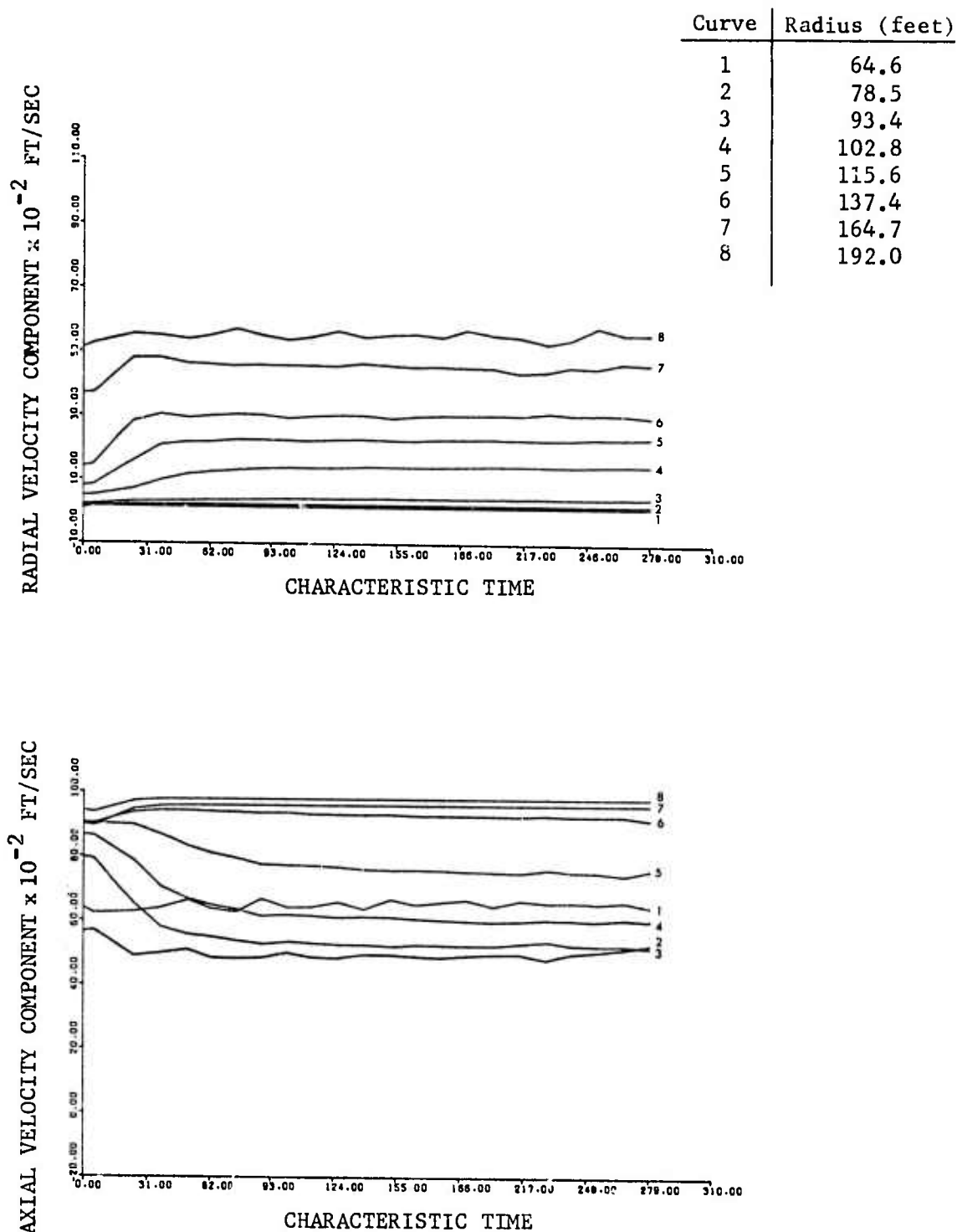| Curve	Radius (feet)
1	64.6
2	78.5
3	93.4
4	102.8
5	115.6
6	137.4
7	164.7
8	192.0

Figure 15. Radial and Axial Components of Velocity, vs. Time, at Various Points Along a Line Normal to the Centerline of an Atlas Booster During Ascent, and 22.31 ft Behind the Exit Nozzle. Data for the curves shown were generated by the AFTON 2A code using Mesh 6. (Problem 590.1; Altitude 394 kft; U_∞ = 10150 fps; M_∞ = 8.054; Re_∞ = 1.17/ft.)

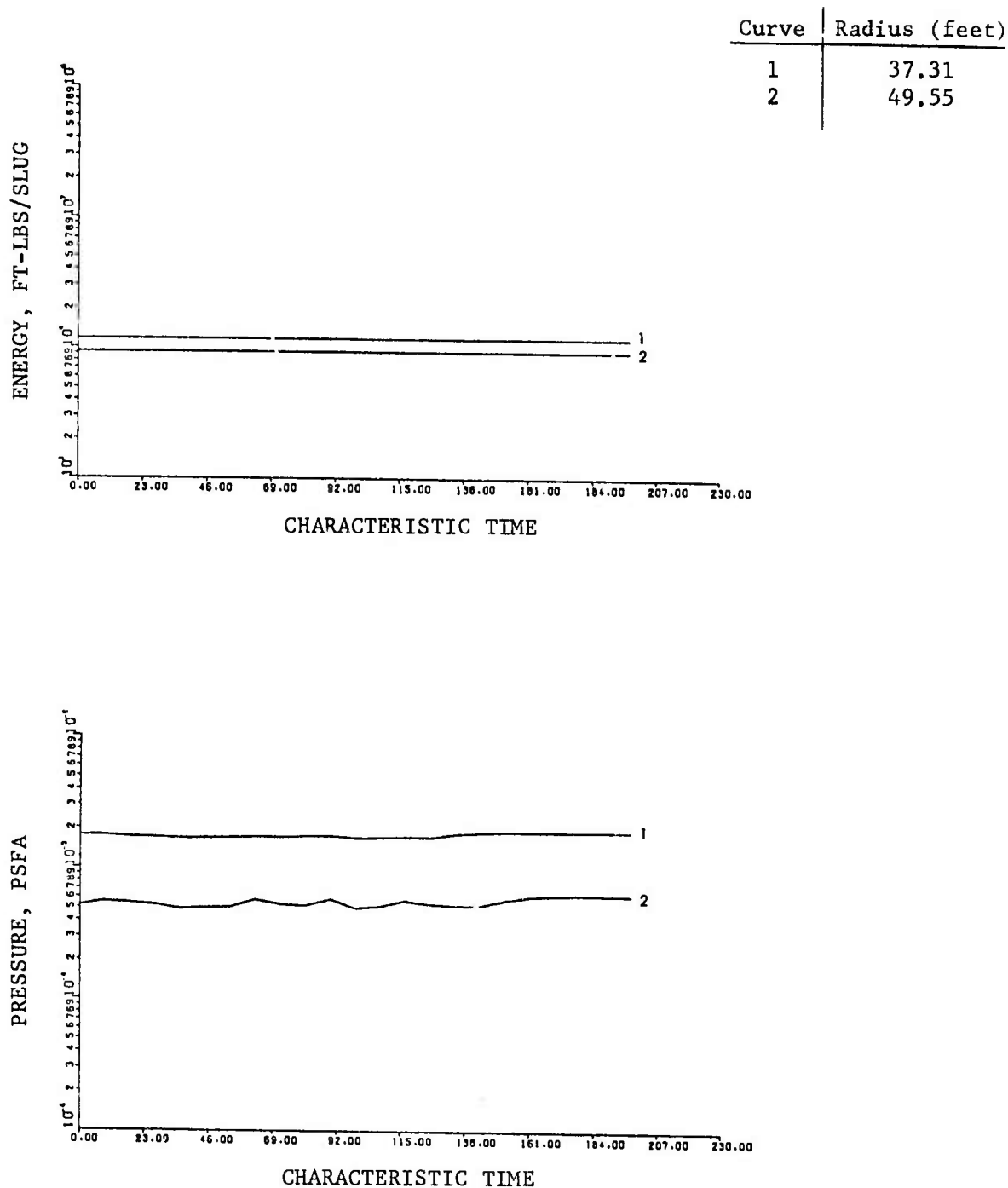| Curve	Radius (feet)
1	37.31
2	49.55

Figure 16. Specific Internal Energy and Pressure, vs. Time, at Various Points Along a Line Normal to the Centerline of an Atlas Booster During Ascent, and 51.45 ft Behind the Exit Nozzle. Data for the curves shown were generated by the AFTON 2A code using Mesh 5. (Problem 590.1; Altitude 394 kft; $E_\infty = .2836 \times 10^7$ ft-lbs/slug; $P_\infty = .5671 \times 10^{-4}$ psfa; $M_\infty = 8.054$; $Re_\infty = 1.17/ft$.)

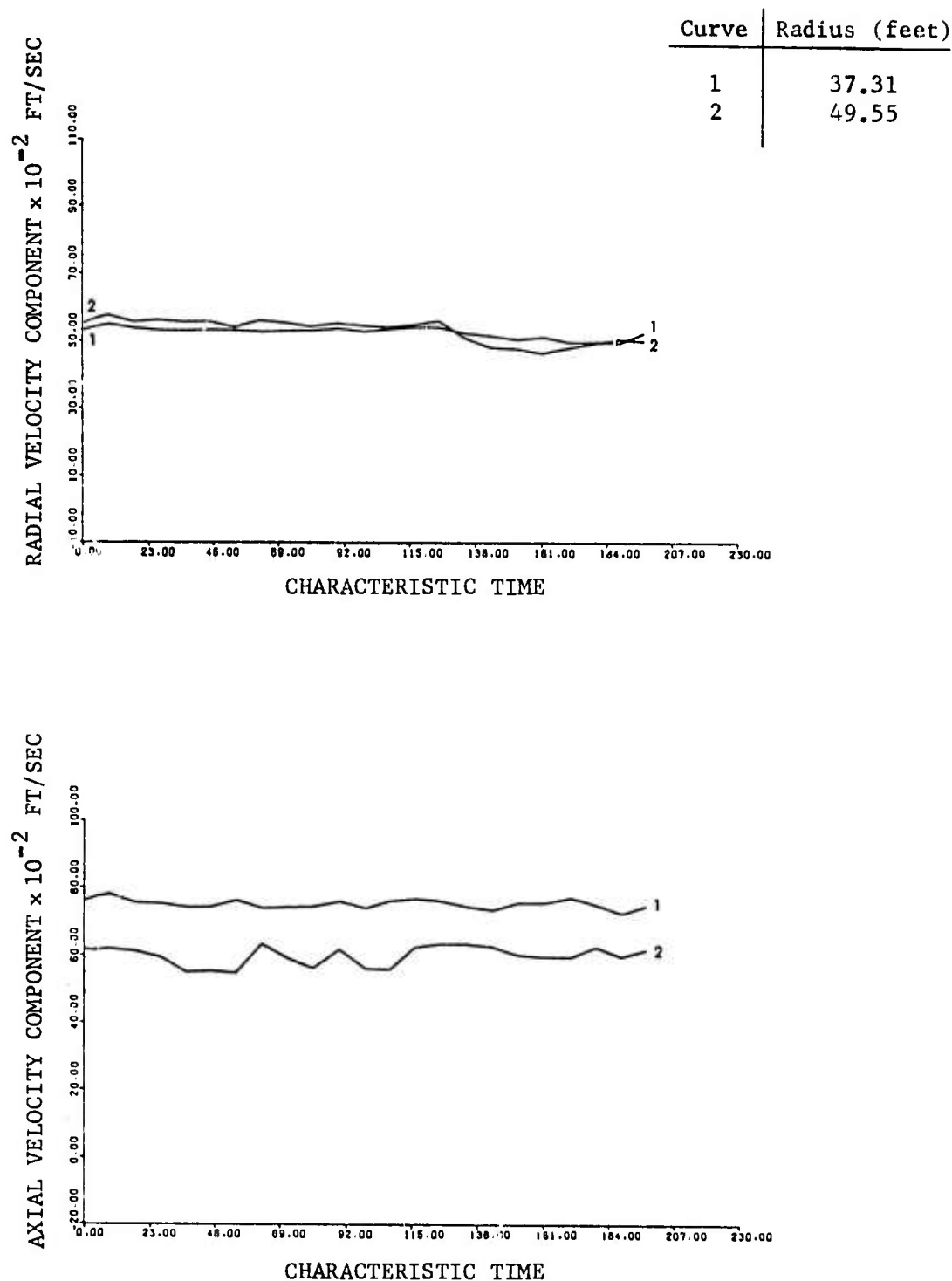| Curve	Radius (feet)
1	37.31
2	49.55

Figure 17. Radial and Axial Components of Velocity, vs. Time, at Various Points Along a Line Normal to the Centerline of an Atlas Booster During Ascent, and 51.45 ft Behind the Exit Nozzle. Data for the curves shown were generated by the AFTON 2A code using Mesh 5. (Problem 590.1; Altitude 394 kft; $U_\infty = 10150$ fps; $M_\infty = 8.054$; $Re_\infty = 1.17/ft.$)

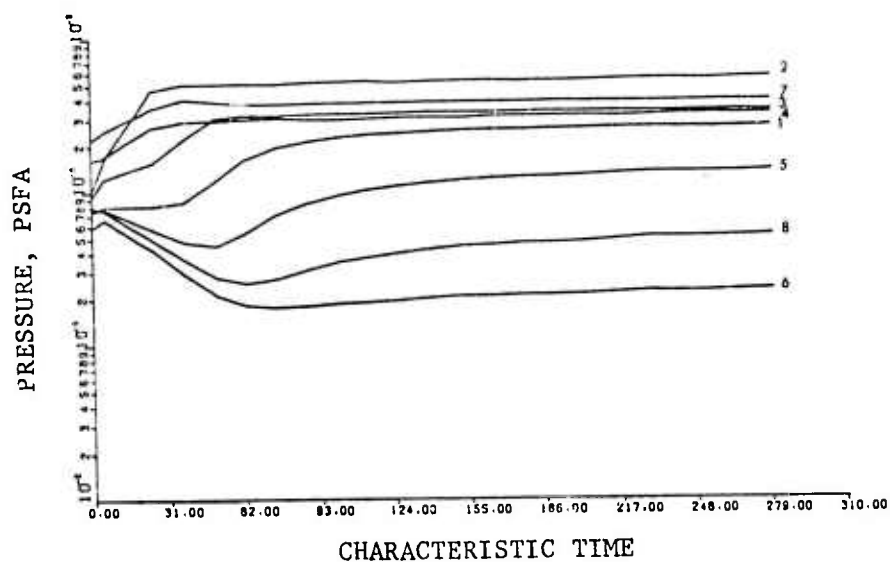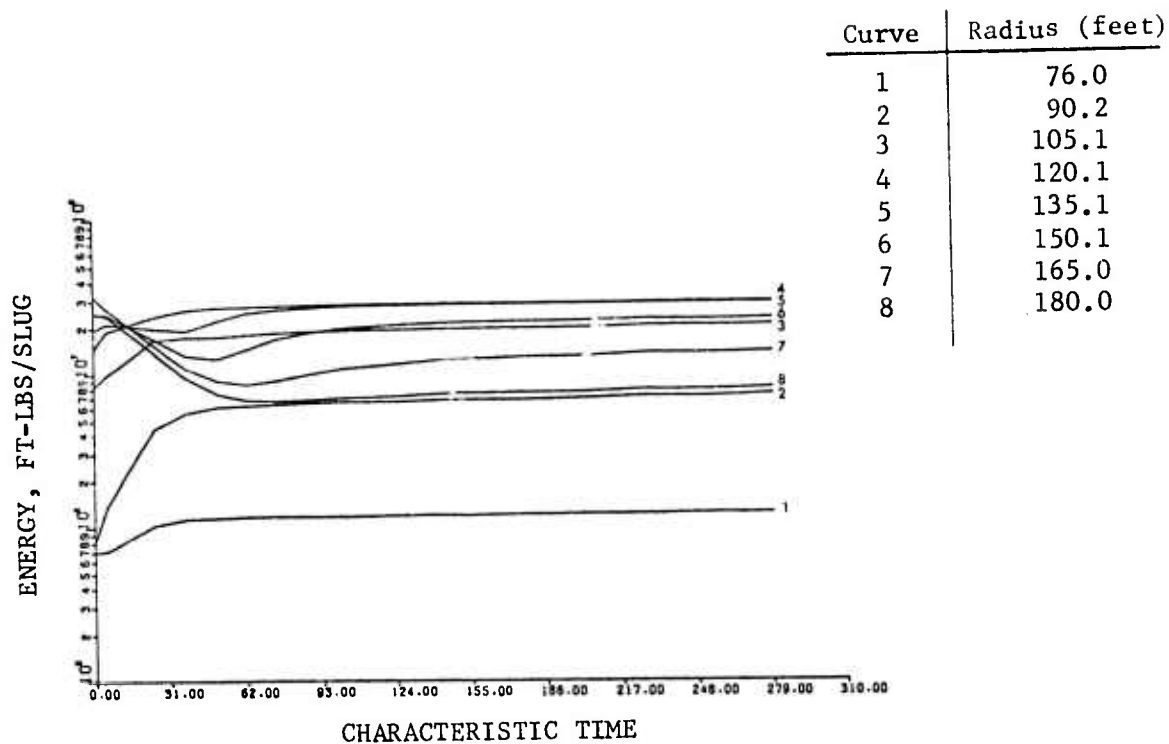| Curve	Radius (feet)
1	76.0
2	90.2
3	105.1
4	120.1
5	135.1
6	150.1
7	165.0
8	180.0

Figure 18. Specific Internal Energy and Pressure, vs. Time, at Various Points Along a Line Normal to the Centerline of an Atlas Booster During Ascent, and 51.45 ft Behind the Exit Nozzle. Data for the curves shown were generated by the AFTON 2A code using Mesh 6. (Problem 590.1; Altitude 394 kft; $E_\infty = .2836 \times 10^7$ ft-lbs/slug; $P_\infty = .567 \times 10^{-4}$ psfa; $M_\infty = 8.054$; $Re_\infty = 1.17/ft.$)

34

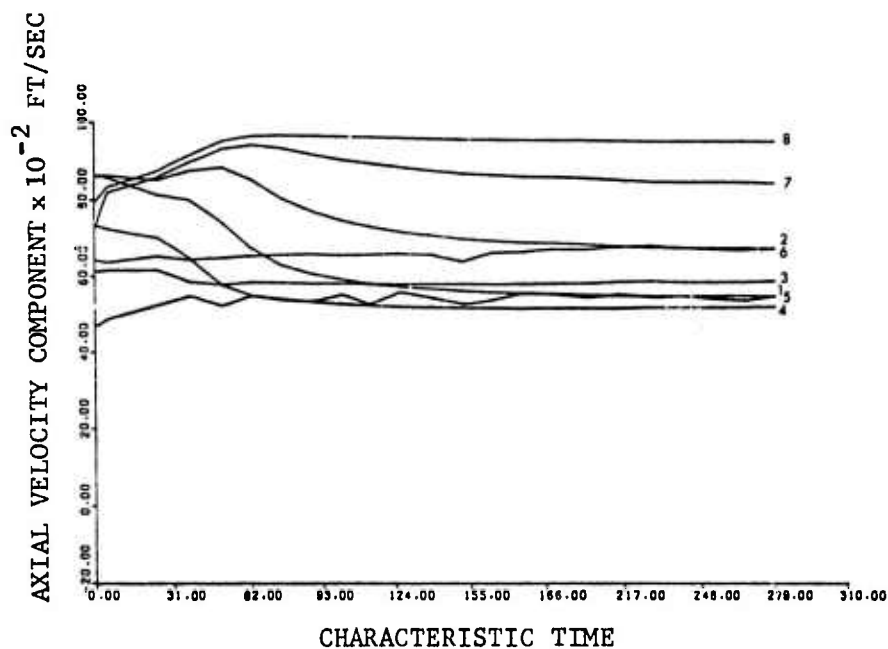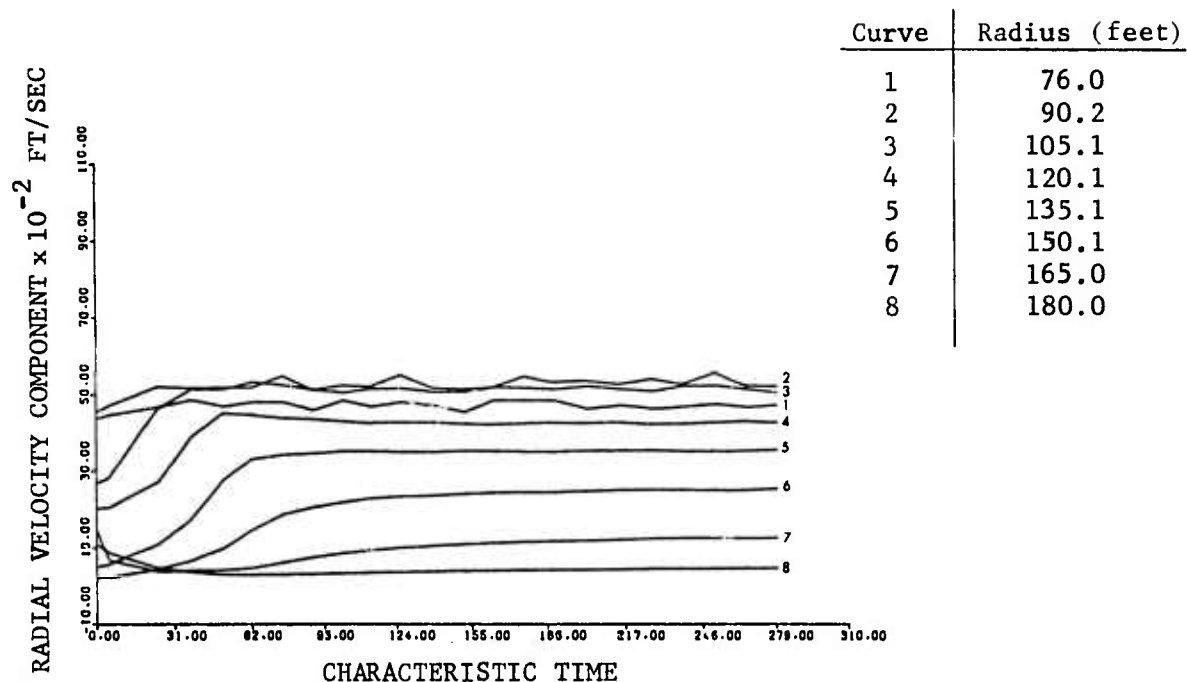| Curve	Radius (feet)
1	76.0
2	90.2
3	105.1
4	120.1
5	135.1
6	150.1
7	165.0
8	180.0

Figure 19. Radial and Axial Components of Velocity, vs. Time, at Various Points Along a Line Normal to the Centerline of an Atlas Booster During Ascent, and 51.45 ft Behind the Exit Nozzle. Data for the curves shown were generated by the AFTON 2A code using Mesh 6. (Problem 590.1; Altitude 394 kft; $U_\infty = 10150$ fps; $M_\infty = 8.054$; $Re_\infty = 1.17/ft$.)

35

station. The velocity variations noted are slow but not systematic, and previous experience suggests that they would not be eliminated by further calculation; part of the numerical error generated by time-marching discrete equations of motion lies in their lack of exactly-steady solutions, given exact boundary conditions. However, the other variables show no significant change with time toward the end of the calculation, on the scale of the figures. The fact that velocities can be noisy while other flow variables are not (which may seem strange), stems from a deep-rooted — but correctable — defect in time-marching methods as implemented to date: quadrilateral cells have one degree of freedom too many for the unique definition of strain and strain-rate, given the structure of the local field assumed (tacitly or otherwise) in the discrete equations of motion. As a result, some distortions of fluid elements meet with very little resistance, and velocity oscillations tend to persist. However, the other variables show no significant change with time toward the end of the calculation, on the scale of the figures.

SECTION 3

CALCULATION OF THE FIELD TO A DISTANCE OF 300 FT
BEHIND THE VEHICLE

3.1   Meshes 7, 8 and 9

The calculations described in Section 2 defined the
field of steady flow to a distance of at least 50 ft down-
stream of the rocket nozzle. Accordingly, a new finite dif-
ference mesh (Mesh 7) was constructed with upstream and down-
stream boundaries located, respectively, about 45 ft and 300 ft
aft of the nozzle (Figure 20). The lateral boundary of Mesh 7
was fixed at 180 ft. The mesh contained 55 J-lines and 32
K-lines, which divided the flow-plane into rectangular cells.
The approximate dimensions of the smallest cell of Mesh 7
were 2.7 by 3.4 ft, while the corresponding dimensions of the
smallest cell of Mesh 5 were 1.3 by 1.7 ft. We therefore
expected that the timestep, which was sound-speed-controlled,
would increase by about a factor of two on passing from
Mesh 5 to Mesh 7; in fact, the timestep increased by a
factor of 2.4.

From 45 to 60 ft behind the nozzle, initial values of
flow-field variables for Mesh 7 were obtained by applying to
the final near-field (described in Section 2.6) the usual pro-
cedures for interpolation and for forming weighted averages
(Section 2.2). Further downstream, initial values were gen-
erated for Mesh 7 by extrapolating to free-stream conditions
on the downstream and lateral boundaries of that mesh (Sec-
tion 2.2). Initial values along the upstream boundary of
Mesh 7 were imposed thereafter as boundary conditions. A
vector plot of the initial velocity field on Mesh 7 is pre-
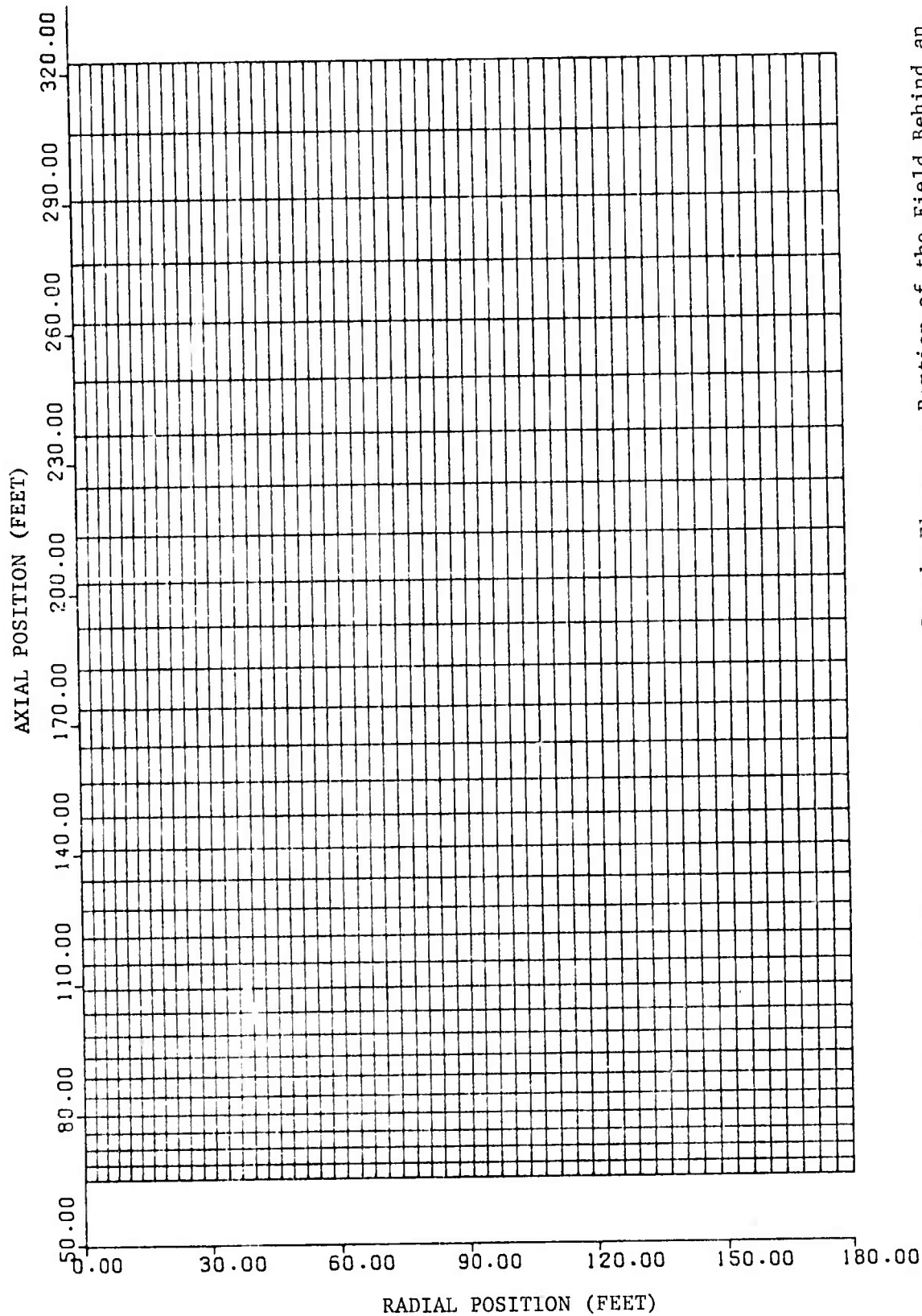sented in Figure 21.

37

Figure 20. Plot of Mesh 7, which was Used to Compute Steady Flow on a Portion of the Field Behind an Atlas Booster During Ascent. The region on which the field was determined with Mesh 7 extends from 44.32 ft to 302.01 ft behind the body. The mesh is composed of 55x32 points.

38

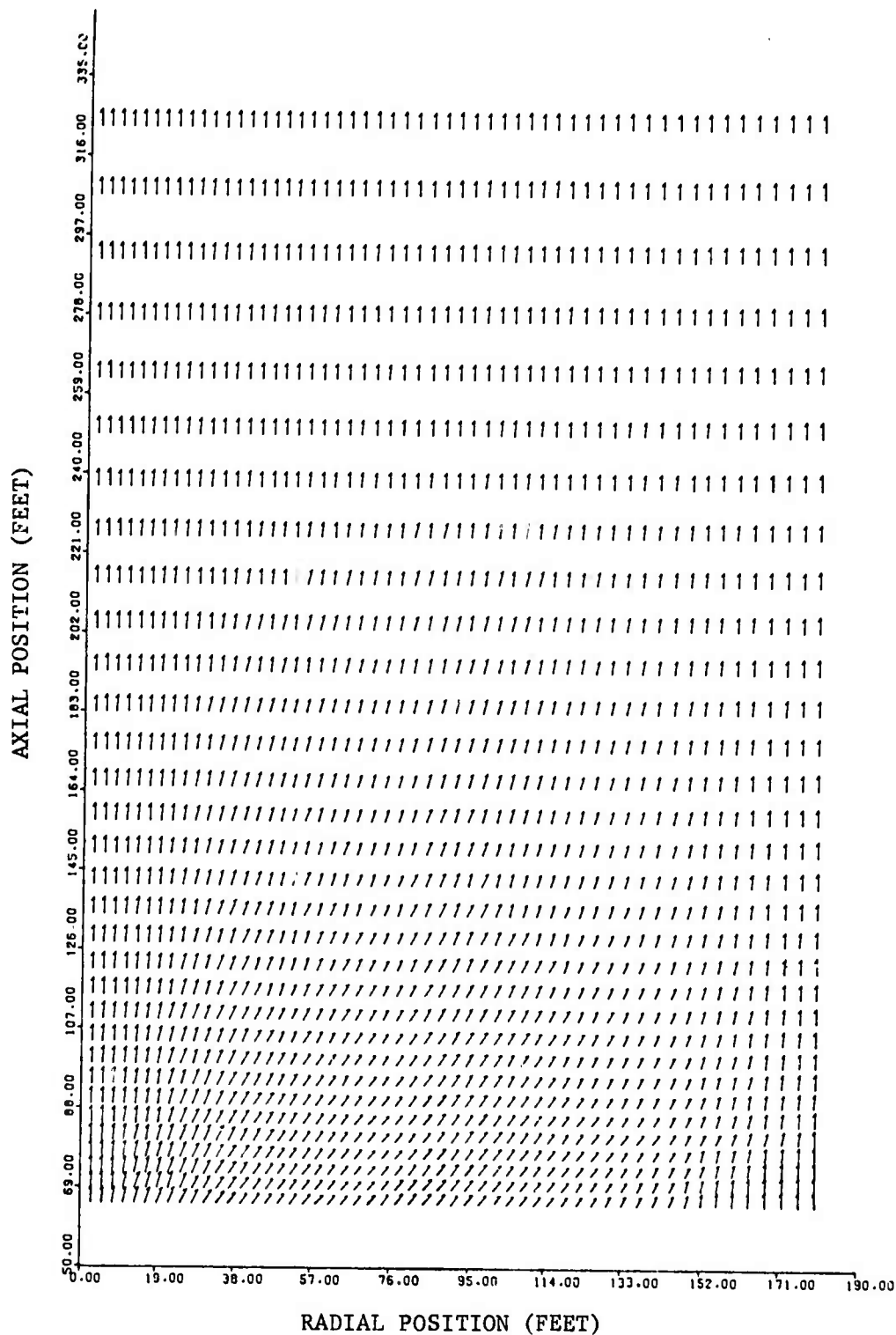AXIAL POSITION (FEET)

RADIAL POSITION (FEET)

Figure 21. Initial Velocity Field for the Calculation of Flow Using Mesh 7. The region shown lies between planes 44.36 ft and 302.01 ft behind an Atlas Booster during ascent. (Problem 590.1; Altitude 394 kft; U_∞ = 10150 fps; M_∞ = 8.054; Re_∞ = 1.17/ft.)

39

With initial and boundary conditions established, the calculation was continued with Mesh 7 for 1011 units of characteristic time, when it was found that the flow-field had become steady near the symmetry axis (Figure 22). However, as had been noted in calculating motion further upstream, the lateral boundary again interfered with the development of the plume. To obviate that difficulty, a new mesh (Mesh 8) was constructed whose lateral boundary was located at a radius of 300 ft. The upstream and downstream boundaries of Mesh 7 were retained in Mesh 8, as was the line J=1. However, the line J=22 of Mesh 7 became the line J=2 of Mesh 8, and the final flow conditions found along the lines J=22 and J=23 of Mesh 7 were imposed for all time in Mesh 8 along the lines J=2 and J=3. Mesh 8 contained 55 J-lines and 32 K-lines, as in the case of Mesh 7.

In the region of Mesh 8 above 180 ft (the location of the lateral boundary of Mesh 7), values were generated for initial velocity, density, etc., using the same method of extrapolation to free-stream conditions on the new lateral boundary as had been used for Mesh 7. As before, initial conditions on the upstream boundary were used as boundary conditions. A plot of the initial velocity field on Mesh 8 is presented in Figure 23.

The smallest cell of Mesh 8 had the dimensions 3.46 ft by 3.45 ft, and the timestep was larger by a factor of 1.54 for Mesh 8 than it had been for Mesh 7. When the calculation had been run further with Mesh 8 for about 200 units of characteristic time, the field became steady below a radius of about 150 ft; a plot of the velocity field at that time
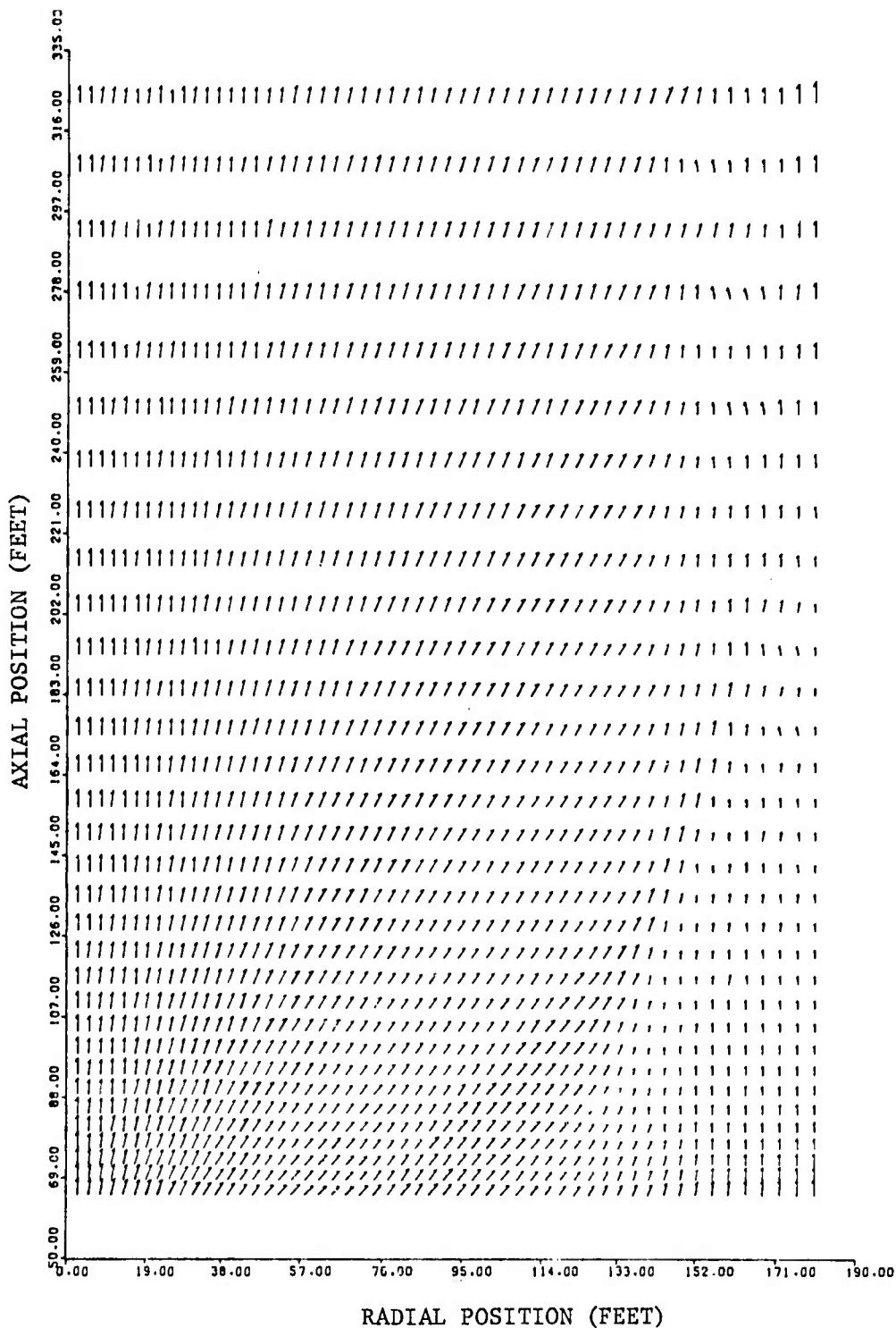
Figure 22. Velocity Field Aft of an Atlas Booster During Ascent. Evolution of the flow has been computed for 1011 units of characteristic time, starting from the field of Figure 21. Mesh 7 was used for the calculation. The field, which is shown between planes 44.36 ft and 302.01 ft behind the body, was computed with the AFTON 2A code. (Problem 590.1; Altitude 394 kft; $U_\infty = 10150$ fps; $M_\infty = 8.054$; $Re_\infty = 1.17/ft$.)

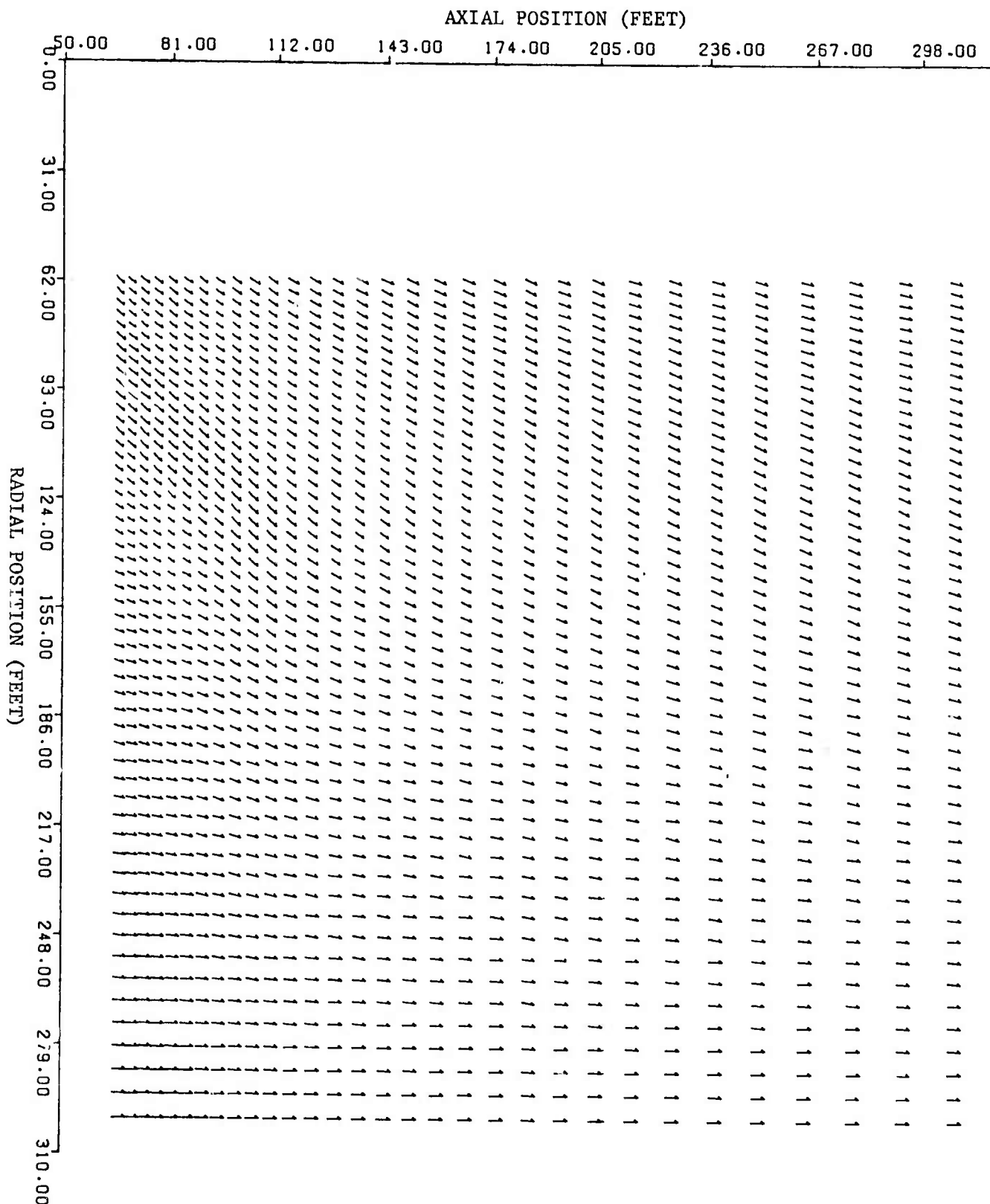AXIAL POSITION (FEET)

RADIAL POSITION (FEET)

41

Figure 23. Initial Velocity Field for the Calculation of Flow Using Mesh 8. The mesh consists of the points at the tails of the vector-arrows shown. The region covered by Mesh 8 lies between planes 44.36 ft and 302.01 ft behind an Atlas Booster during ascent. (Problem 590.1; Altitude 394 kft; U_∞ = 10150 fps; M_∞ = 8.054; Re_∞ = 1.17/ft.)

appears in Figure 24. As before (e.g., Mesh 2), the lateral boundary of the computational domain was not far enough from the axis to contain the plume, and another finite difference mesh (Mesh 9) was generated to complete the calculation. In Mesh 9, the line J=2 coincided with the line J=36 of Mesh 8, located at a radial position of about 108 ft. The lateral boundary of Mesh 9 was situated at a radius of 400 ft.

Initial and boundary conditions were obtained for Mesh 9 by the same procedures followed for Mesh 8, and the initial velocity field for Mesh 9 is shown in Figure 25. Calculation of the flow from that initial field ended when, after 512 units of characteristic time, the motion became steady (Figure 26).

3.2   The Field of Steady Flow to About 300 ft Behind the Exhaust Nozzle

Figure 27 shows a vector-plot of the entire steady velocity field from 45 to 300 ft aft of the nozzle. The air-shock, dividing streamline and jet-shock are the curves labeled 1, 2 and 3, respectively. In the region between the upstream and downstream boundaries, it can be seen that the plume radius increases by a factor of two (Figure 27). Stream-lines of the entire steady field, from 3.6 ft aft of the nozzle to 302 ft, are depicted in Figure 28, including the dividing streamline and the principal shocks. In the near-field portion of the figure, the location of the air-shock is roughly the same as that computed in the previous program.[1] However, in the final near-field region reported here, the dividing stream-line and jet shock have assumed positions substantially closer to the plume axis than in the earlier field.[1] It should be
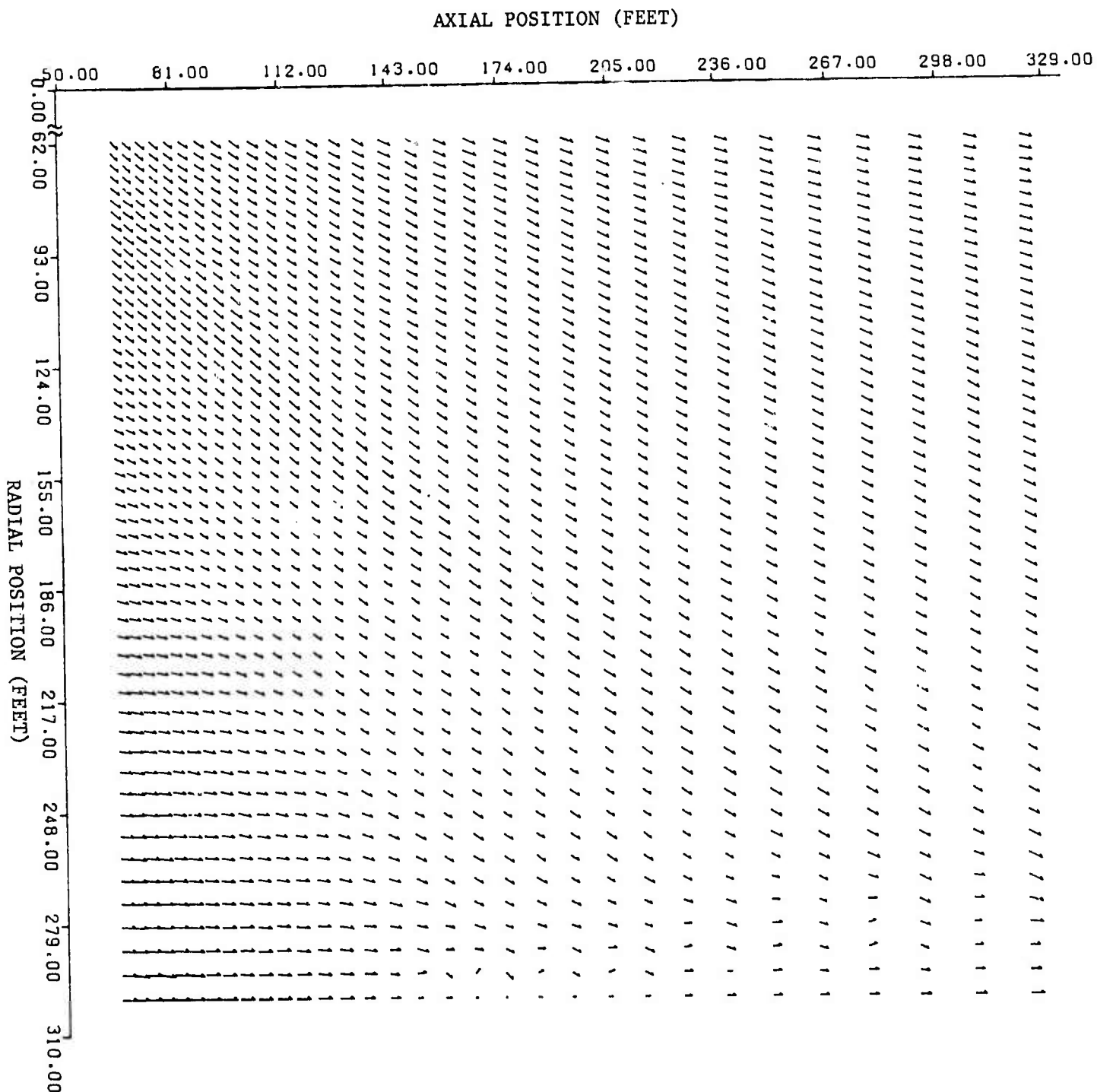
43

AXIAL POSITION (FEET)

Figure 24.   Velocity Field Aft of an Atlas Booster During Ascent. Evolution of
the flow has been computed for 200 units of characteristic time,
starting from the field of Figure 23. Mesh 8 was used for the
calculation. The field, which is shown between planes 44.36 ft and
302.01 ft behind the body, was computed with the AFTON 2A code.
(Problem 590.1; Altitude 394 kft; $U_\infty = 10150$ fps; $M_\infty = 8.054$;
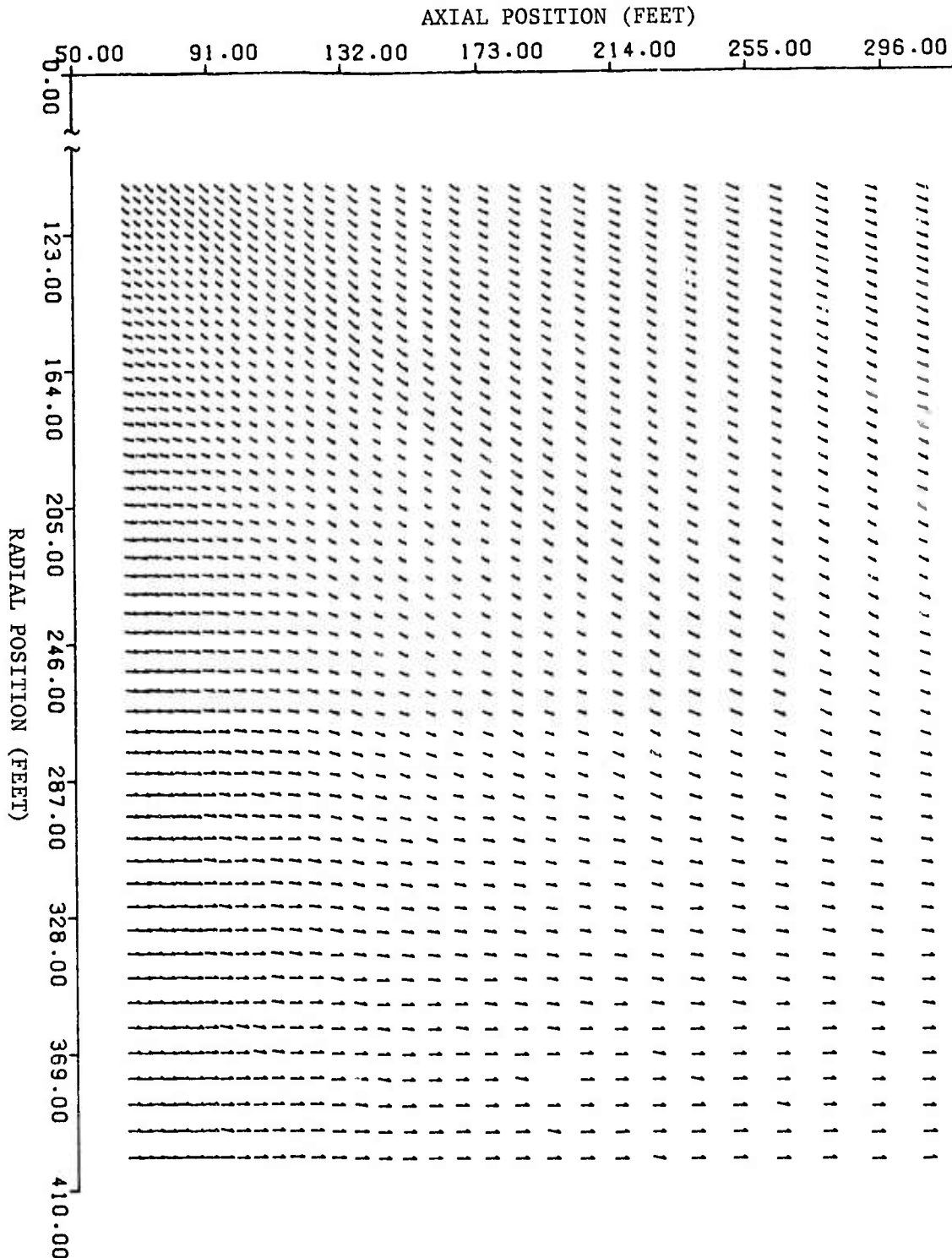$Re_\infty = 1.17/ft$.)

44

AXIAL POSITION (FEET)

Figure 25. Initial Velocity Field for the Calculation of Flow Using Mesh 9. The mesh consists of the points at the tails of the vector-arrows shown. The region covered by Mesh 9 lies between planes 44.36 ft and 302.01 ft behind an Atlas Booster during ascent. (Problem 590.1; Altitude 394 kft; U_∞ = 10150 fps; M_∞ = 8.054; Re_∞ = 1.17/ft.)

AXIAL POSITION (FEET)

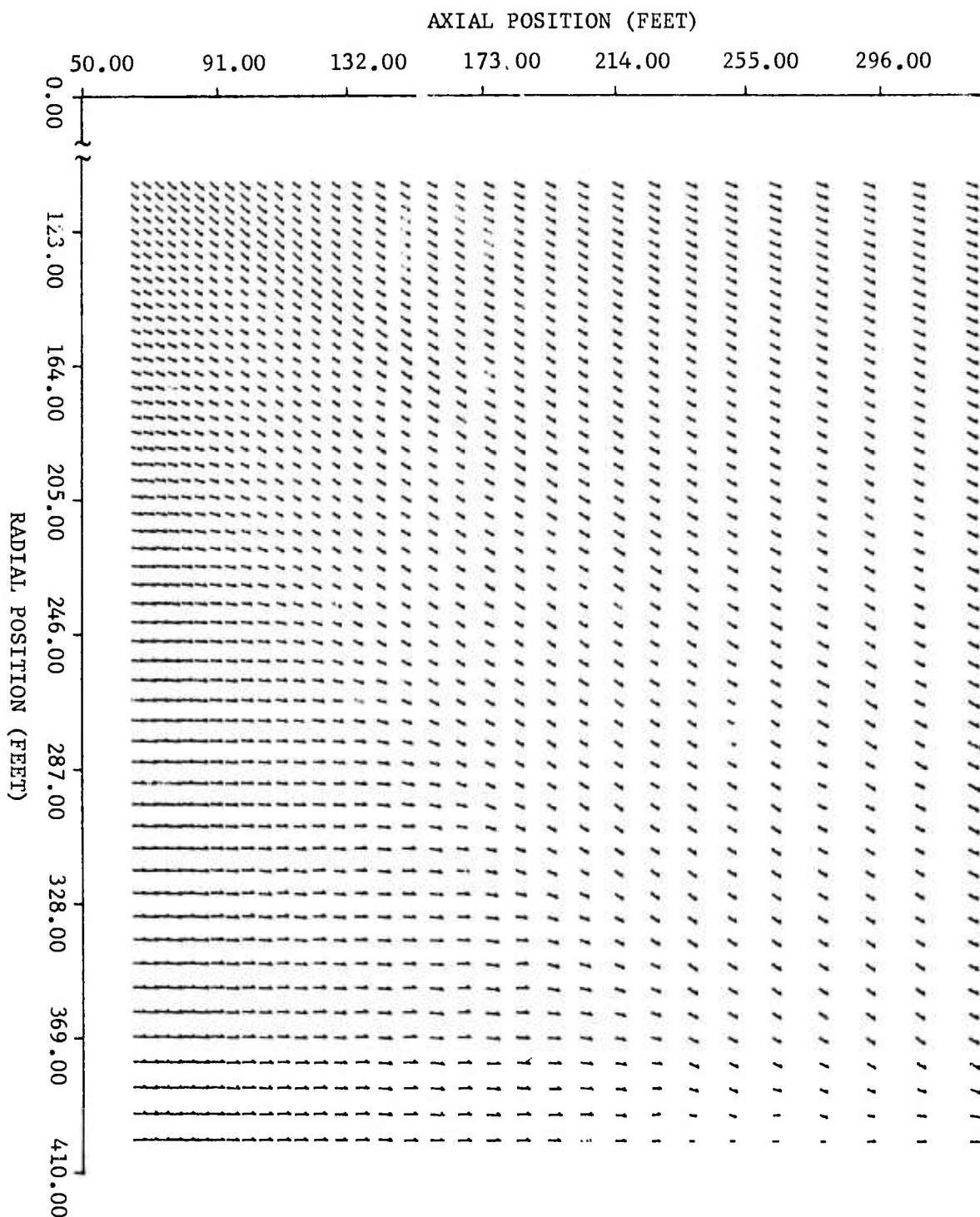50.00   91.00   132.00   173.00   214.00   255.00   296.00

Figure 26.   Velocity Field Aft of an Atlas Booster During Ascent.   Evolution of
the flow has been computed for 512 units of characteristic time,
starting from the field of Figure 25.   Mesh 9 was used for the
calculation.   The field, which is shown between planes 44.36 ft and
302.01 ft behind the body, was computed with the AFTON 2A code.
(Problem 590.1; Altitude 394 kft; $U_\infty = 10150$ fps; $M_\infty = 8.054$;
$Re_\infty = 1.17/ft.$)
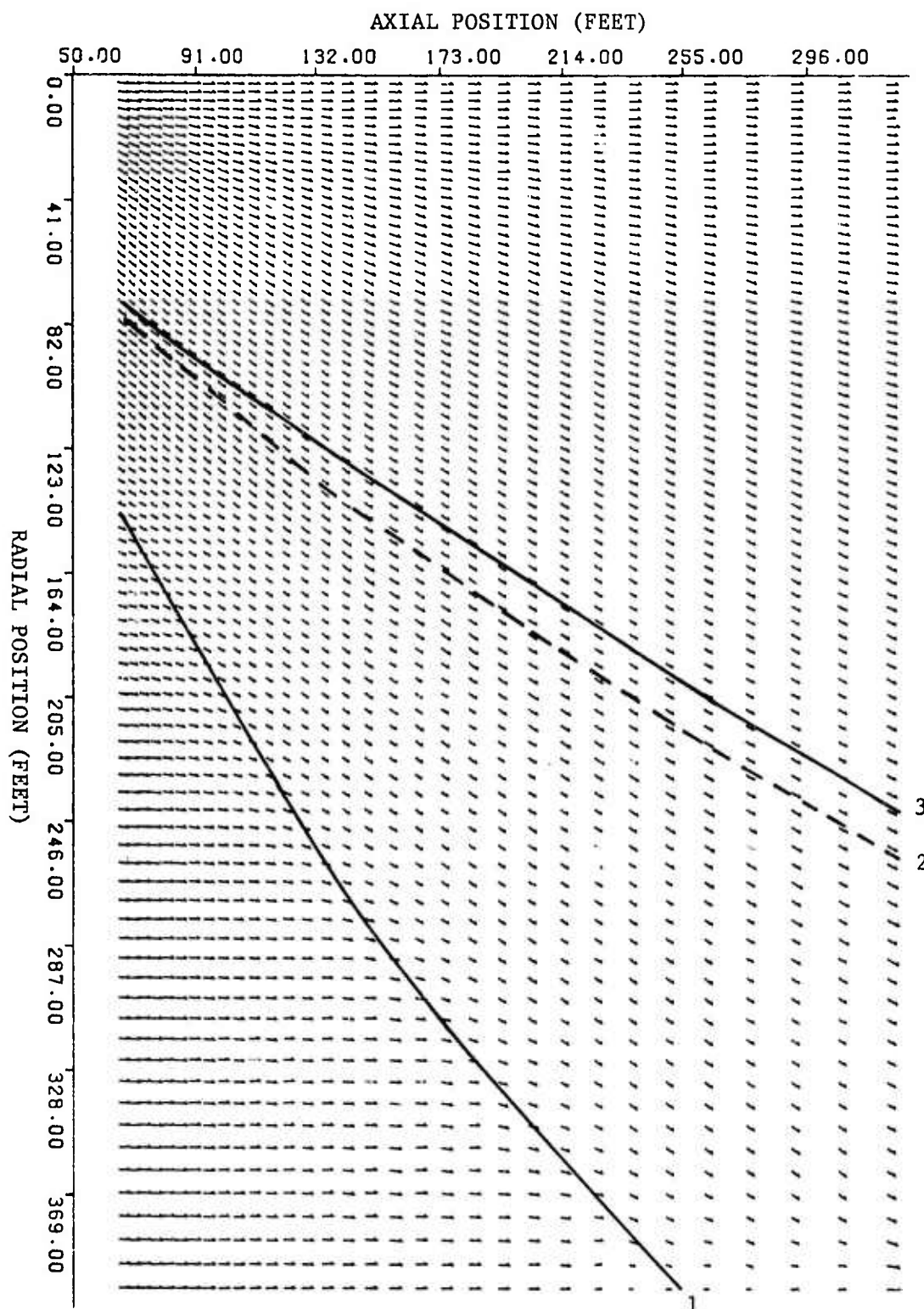
46

AXIAL POSITION (FEET)

Figure 27. Steady-State Velocity Field Aft of an Atlas Booster During Ascent.
The field, which is shown between planes 44.36 ft and 302.01 ft
behind the body, was computed with the AFTON 2A code. The air shock,
dividing streamline and jet shock are denoted by Curves 1, 2 and 3.
The field was determined by calculation on portions of Meshes 7, 8
and 9. (Problem 590.1; Altitude 394 kft; U_∞ = 10150 fps; M_∞ = 8.054;
Re_∞ = 1.17/ft.)

47

AXIAL POSITION (FEET)
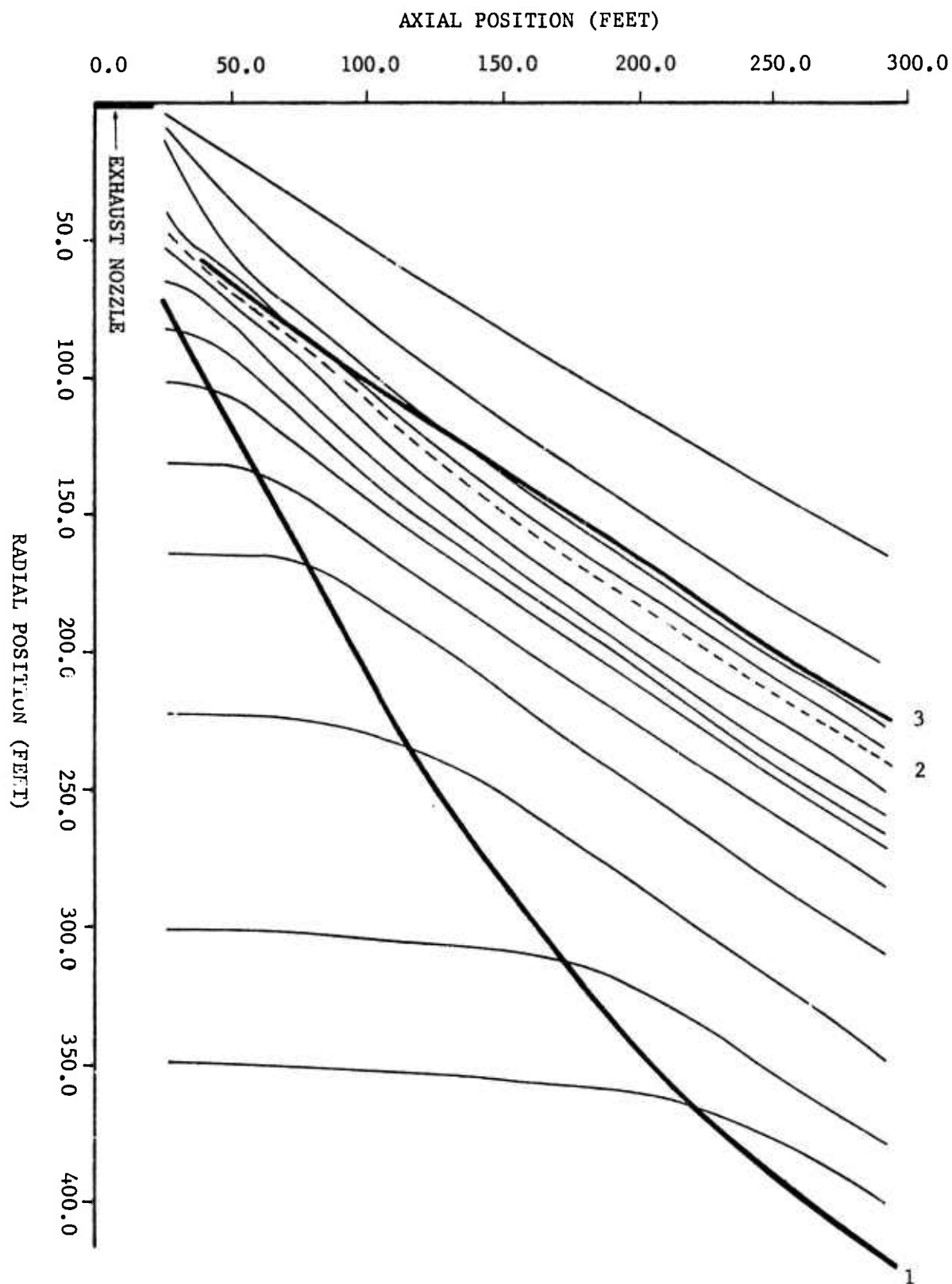
RADIAL POSITION (FEET)

EXHAUST NOZZLE

Figure 28. Streamlines of the Steady Field Behind an Atlas Booster During Ascent. The field, which is shown between planes 3.58 ft and 270 ft aft of the body, was computed using the AFTON 2A code. The air shock, dividing streamline and jet shock are denoted by Curves 1, 2 and 3, respectively. (Problem 590.1; Altitude 394 kft; $U_\infty = 10150$ fps; $M_\infty = 8.054$; $Re_\infty = 1.17/ft$.)

48

noted that in Figure 28, as in the earlier field, the calculated air shock is actually quite thick.

The variation of specific internal energy, pressure and velocity with time are shown in Figures 29-40, along radial lines about 94 ft and 172 ft aft of the exit nozzle. The figures cover the last stages of calculation with Meshes 7, 8 and 9. Only the components of fluid velocity show significant rates of change, as in the case of the near-field, but those changes again have the character of a slow random drift.

With respect to the approach of the field to a near-steady-state, such a state was expected to appear in a given mesh in about the time taken by a free-stream particle to move a small multiple of the distance L between the upstream and downstream boundaries. The results obtained with Mesh 7 show that the field did not become steady near the axis until a time of about 7.5 t_L, where t_L is the time taken by a free-stream particle to move through the distance L. The unexpectedly long period represented by 7.5 t_L reflects the fact that early in the calculation of flow with Mesh 7, oscillations were found in the field near the symmetry axis. Steady flow was established on a portion of Mesh 8 (as discussed above), and on Mesh 9, after the flow had been computed for times of 1.5 t_L and 3.8 t_L, respectively. Steady conditions were attained on those portions of Meshes 1, 5 and 6 that comprise the near-field region of Figure 28, in times of about .78 t_L, 3.7 t_L and 5.3 t_L.

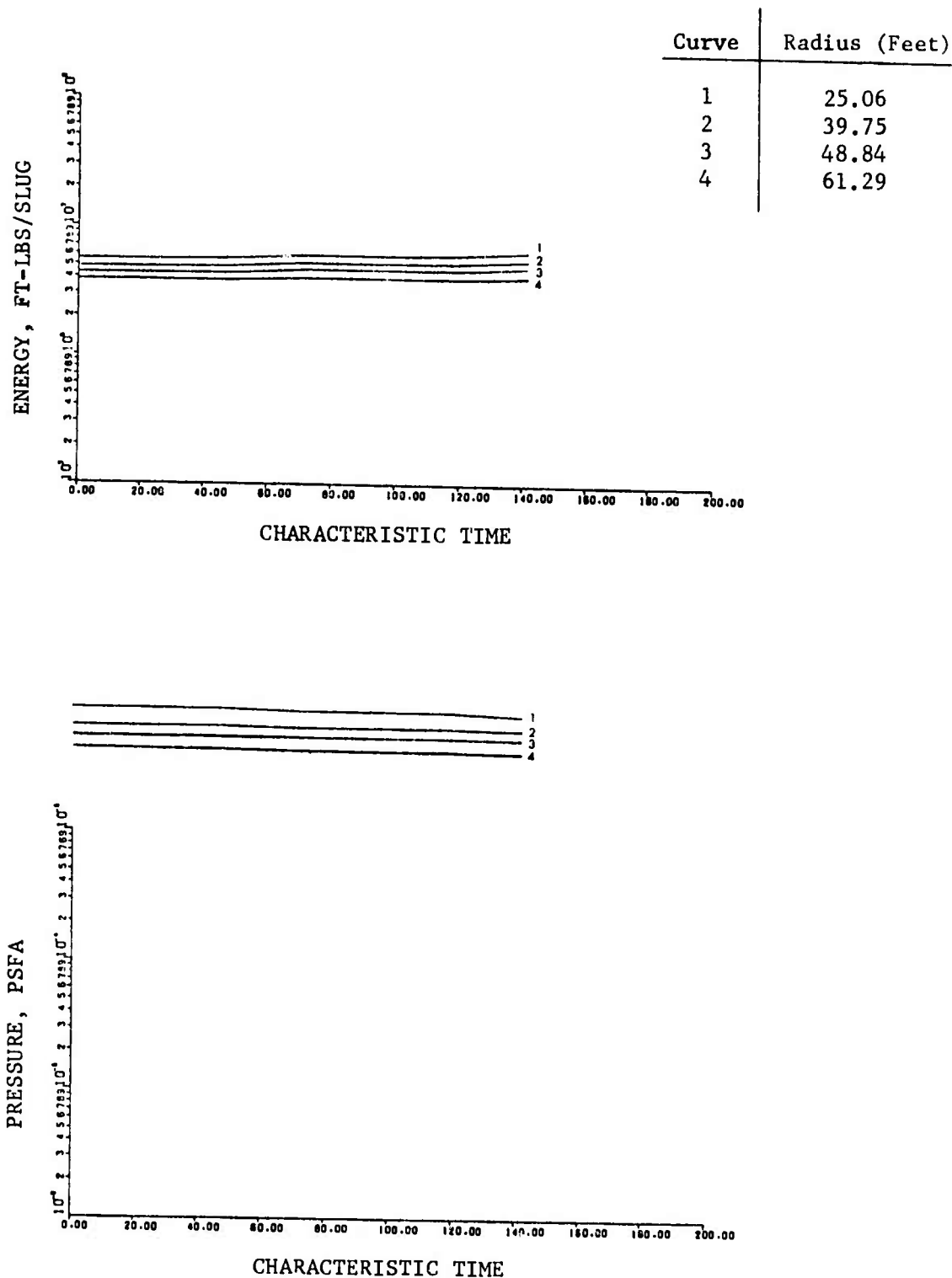| Curve	Radius (Feet)
1	25.06
2	39.75
3	48.84
4	61.29

Figure 29. Specific Internal Energy and Pressure, vs. Time, at Various Points Along a Line Normal to the Centerline of an Atlas Booster During Ascent, and 94.18 ft Behind the Exit Nozzle. Data for the curves shown were generated by the AFTON 2A code using Mesh 7. (Problem 590.1; Altitude 394 kft; $E_\infty = .2836 \times 10^7$ ft-lbs/slug; $P_\infty = .5671 \times 10^{-4}$ psfa; $M_\infty = 8.054$; $Re_\infty = 1.17/\text{ft.}$)

50

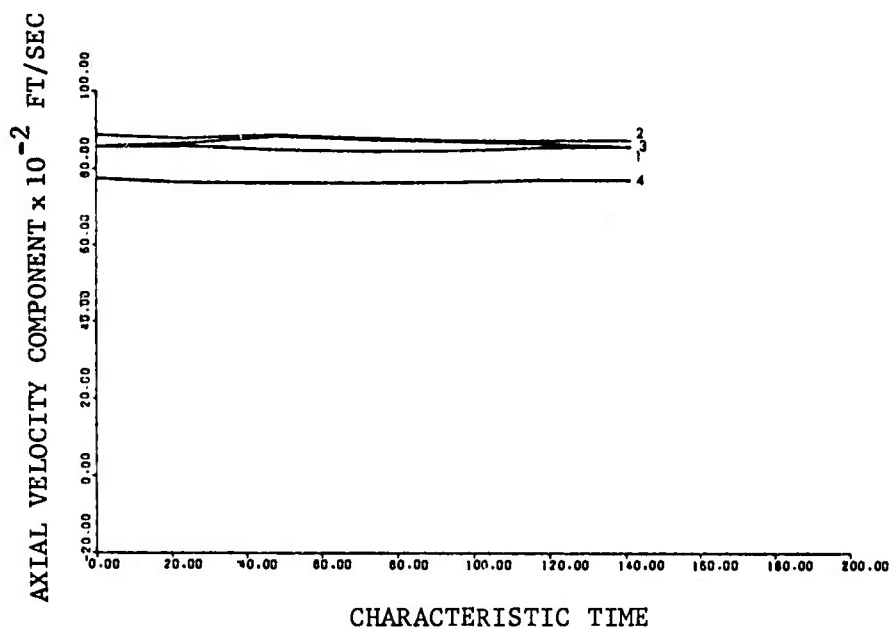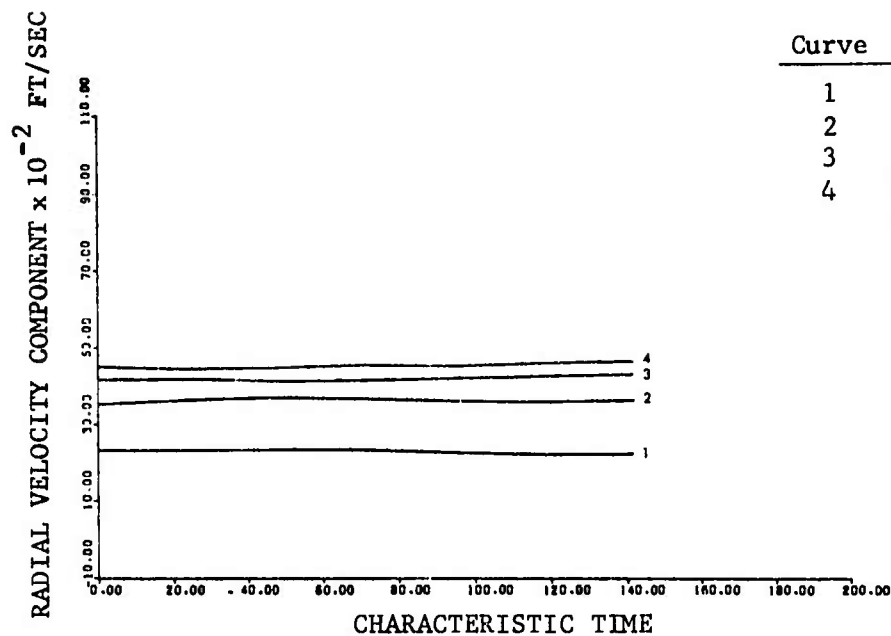| Curve	Radius (feet)
1	25.06
2	39.75
3	48.84
4	61.29

Figure 30. Radial and Axial Components of Velocity, vs. Time, at Various Points Along a Line Normal to the Centerline of an Atlas Booster During Ascent, and 94.18 ft Behind the Exit Nozzle. Data for the curves shown were generated by the AFTON 2A code using Mesh 7. (Problem 590.1; Altitude 394 kft; U_∞ = 10150 fps; M_∞ = 8.054; Re_∞ = 1.17/ft.)
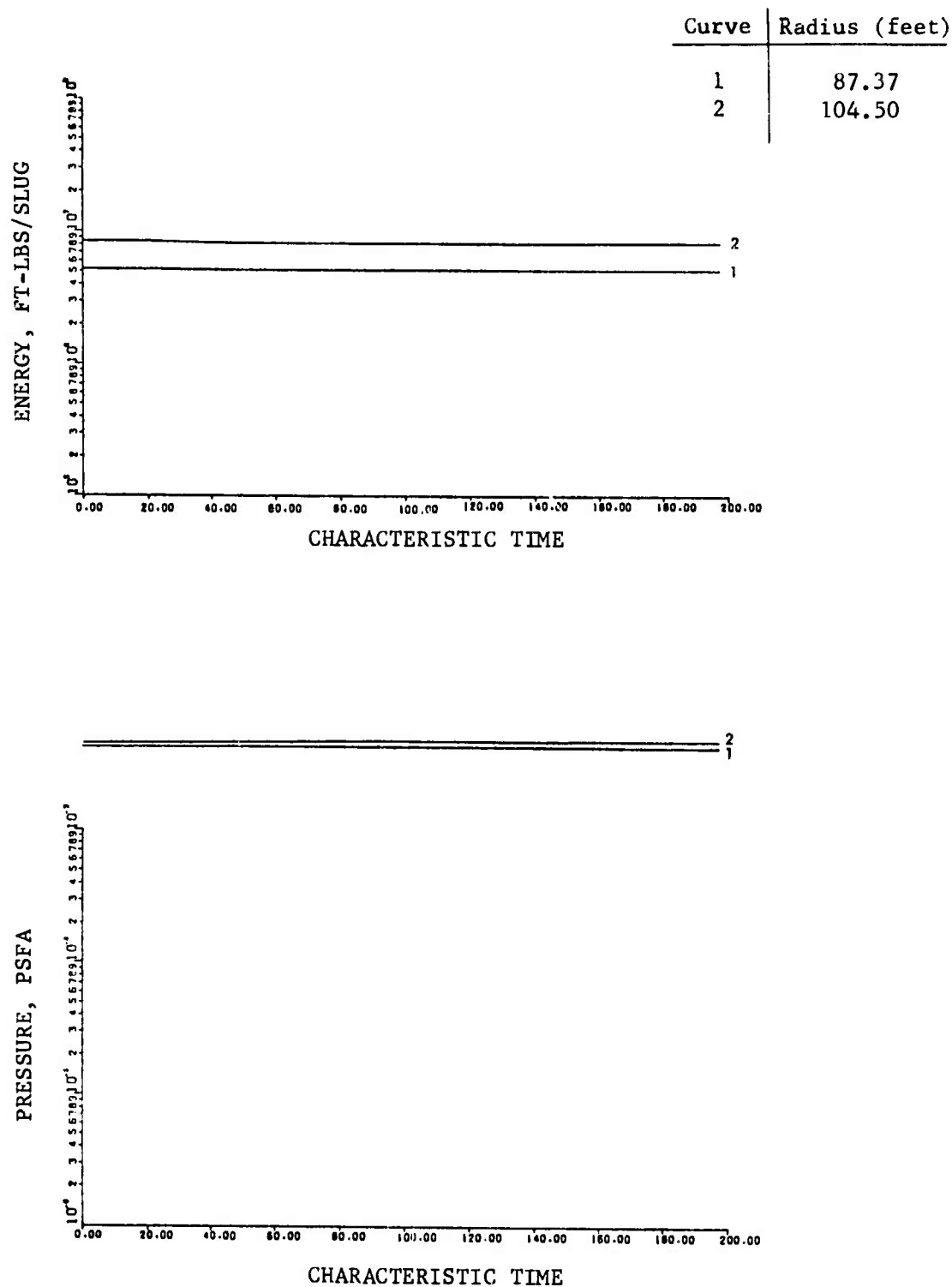
Figure 31. Specific Internal Energy and Pressure, vs. Time, at Various Points Along a Line Normal to the Centerline of an Atlas Booster During Ascent, and 94.18 ft Behind the Exit Nozzle. Data for the curves shown were generated by the AFTON 2A code using Mesh 8. (Problem 590.1; Altitude 394 kft; $E_\infty = .2836 \times 10^7$ ft-lbs/slug; $P_\infty = .5671 \times 10^{-4}$ psfa; $M_\infty = 8.054$; $Re_\infty = 1.17$/ft.)

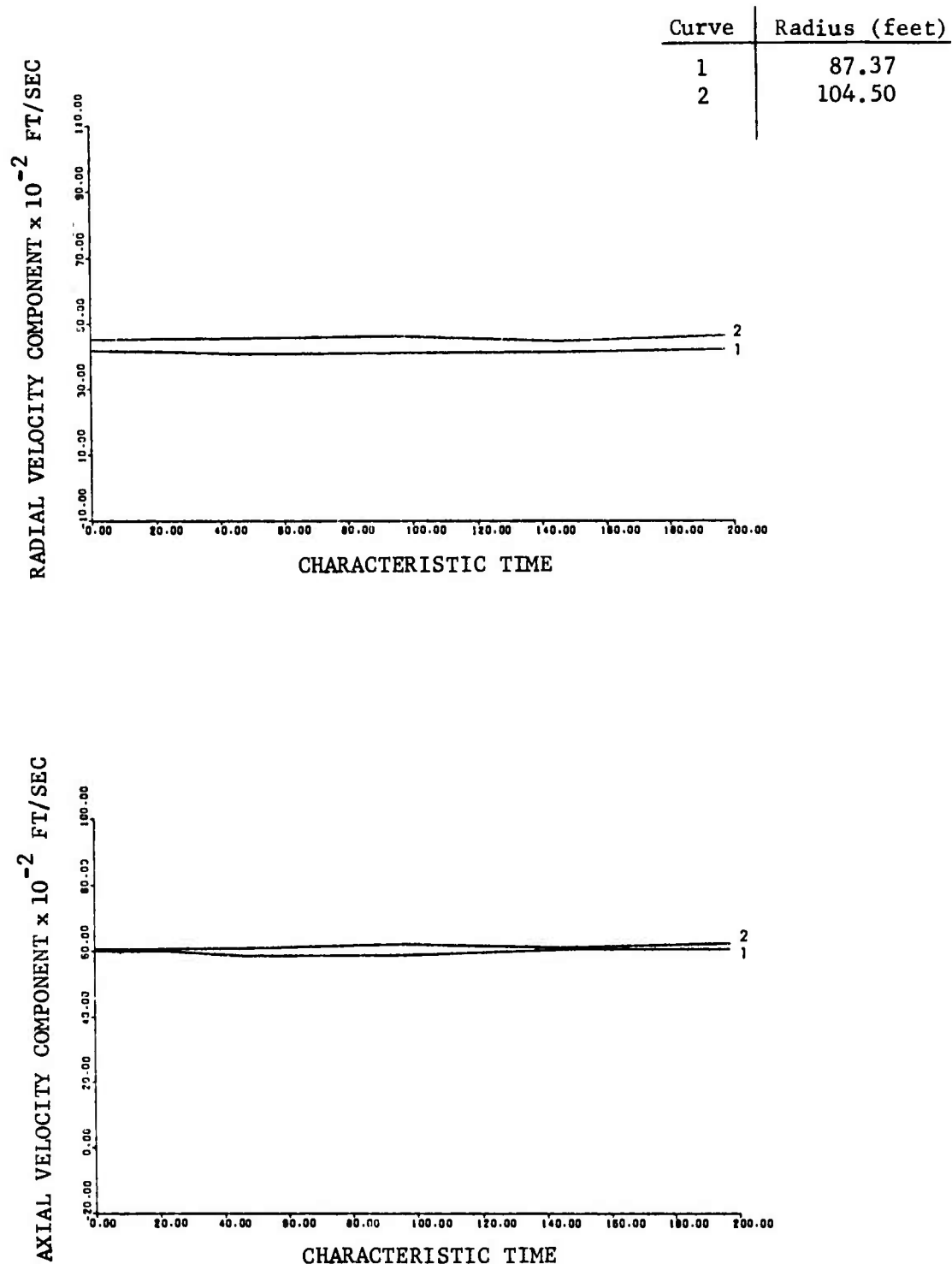| Curve	Radius (feet)
1	87.37
2	104.50

Figure 32. Radial and Axial Components of Velocity, vs. Time, at Various Points Along a Line Normal to the Centerline of an Atlas Booster During Ascent, and 94.18 ft Behind the Exit Nozzle. Data for the curves shown were generated by the AFTON 2A code using Mesh 8. (Problem 590.1; Altitude 394 kft; $U_\infty = 10150$ fps; $M_\infty = 8.054$; $Re_\infty = 1.17/\text{ft}$.)

53

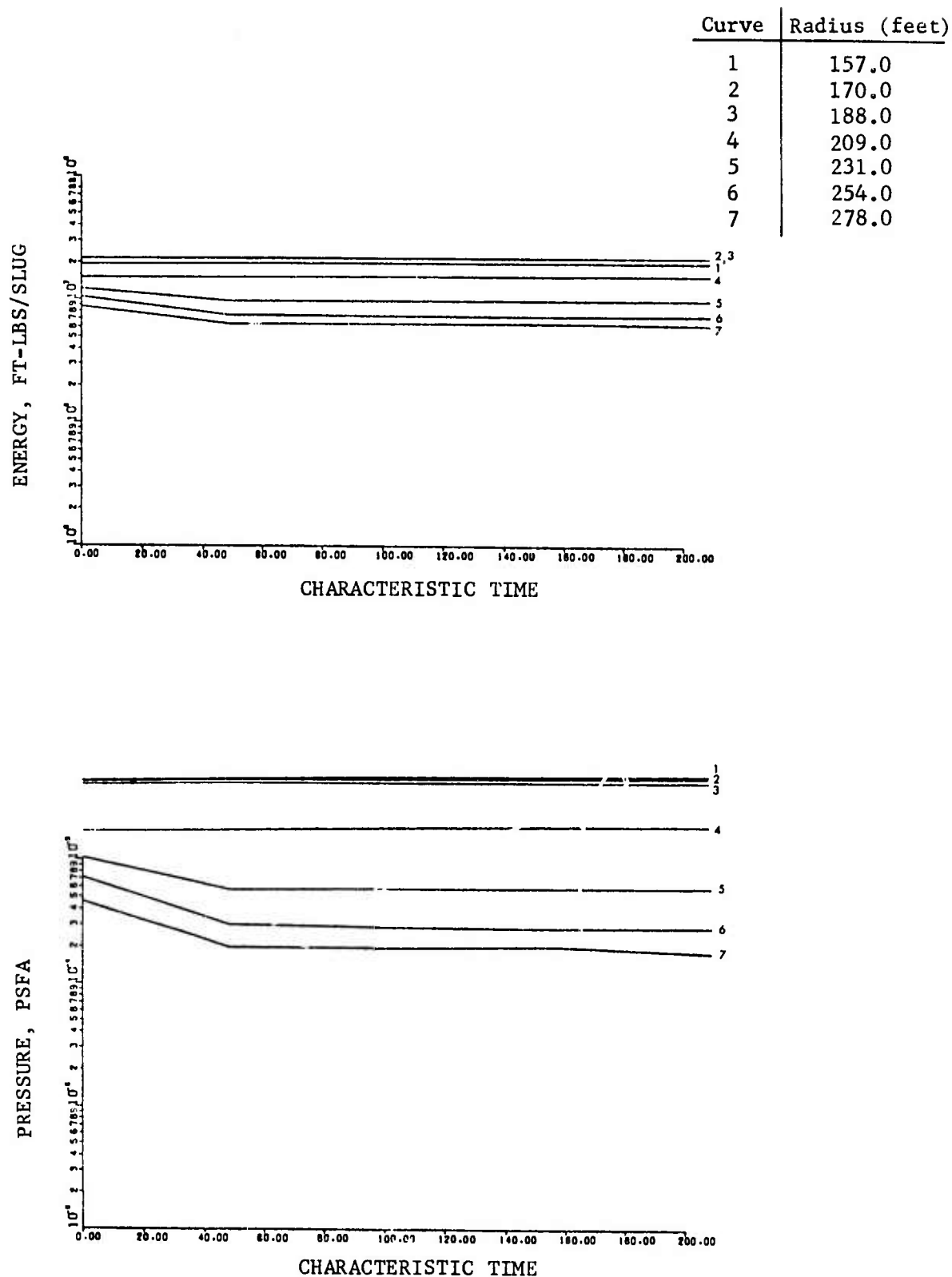| Curve	Radius (feet)
1	157.0
2	170.0
3	188.0
4	209.0
5	231.0
6	254.0
7	278.0

Figure 33. Specific Internal Energy and Pressure, vs. Time, at Various Points Along a Line Normal to the Centerline of an Atlas Booster During Ascent, and 94.18 ft Behind the Exit Nozzle. Data for the curves shown were generated by the AFTON 2A code using Mesh 9. (Problem 590.1; Altitude 394 kft; $E_\infty = .2836 \times 10^7$ ft-lbs/slug; $P_\infty = .5671 \times 10^{-4}$ psfa; $M_\infty = 8.054$; $Re_\infty = 1.17/\text{ft.}$)

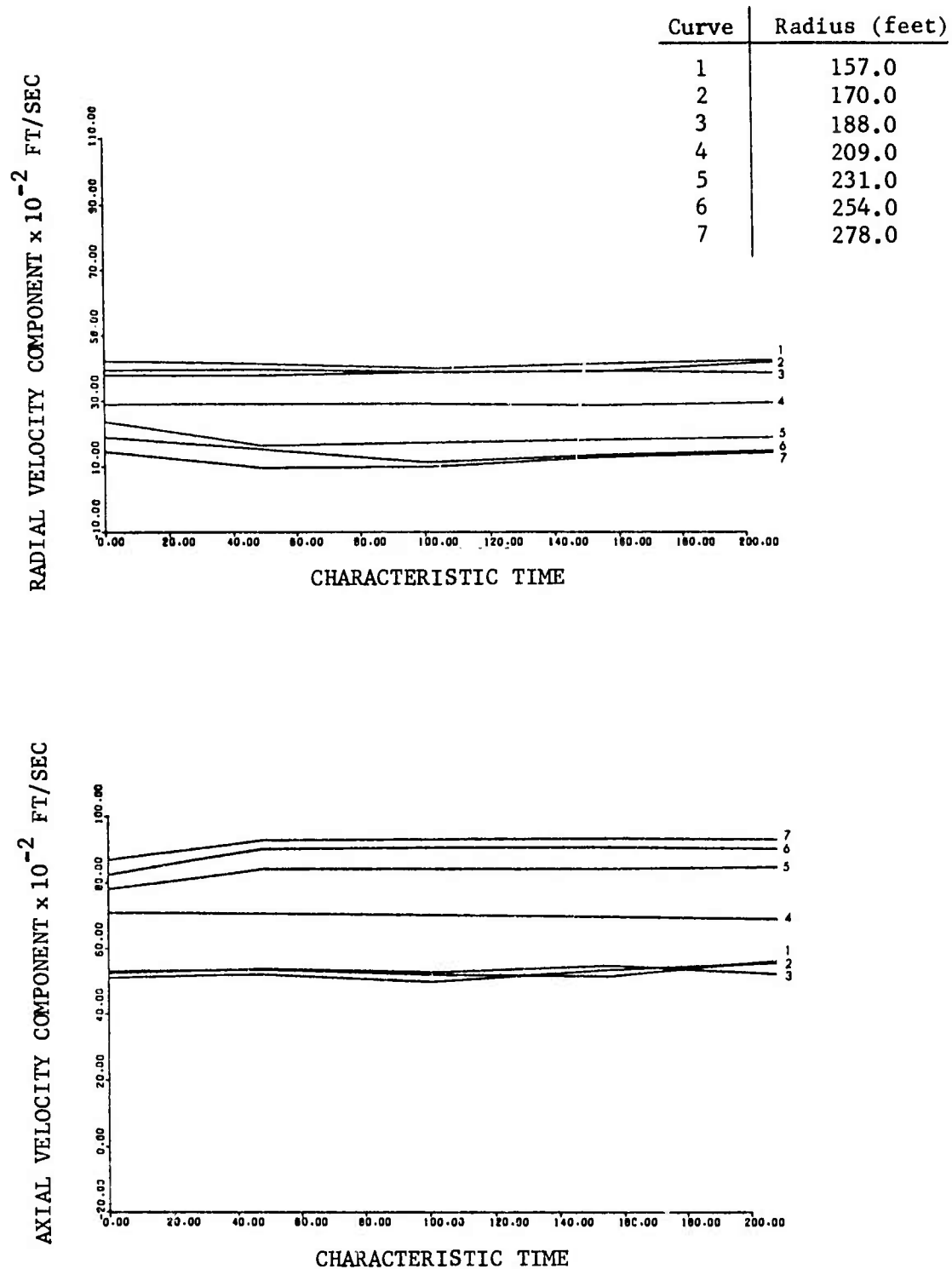| Curve	Radius (feet)
1	157.0
2	170.0
3	188.0
4	209.0
5	231.0
6	254.0
7	278.0

Figure 34. Radial and Axial Components of Velocity vs. Time, at Various
Points Along a Line Normal to the Centerline of an Atlas
Booster During Ascent, and 94.18 ft Behind the Exit Nozzle.
Data for the curves shown were generated by the AFTON 2A
code using Mesh 9. (Problem 590.1; Altitude 394 kft;
$U_\infty = 10150$ fps; $M_\infty = 8.054$; $Re_\infty = 1.17$/ft.)

55

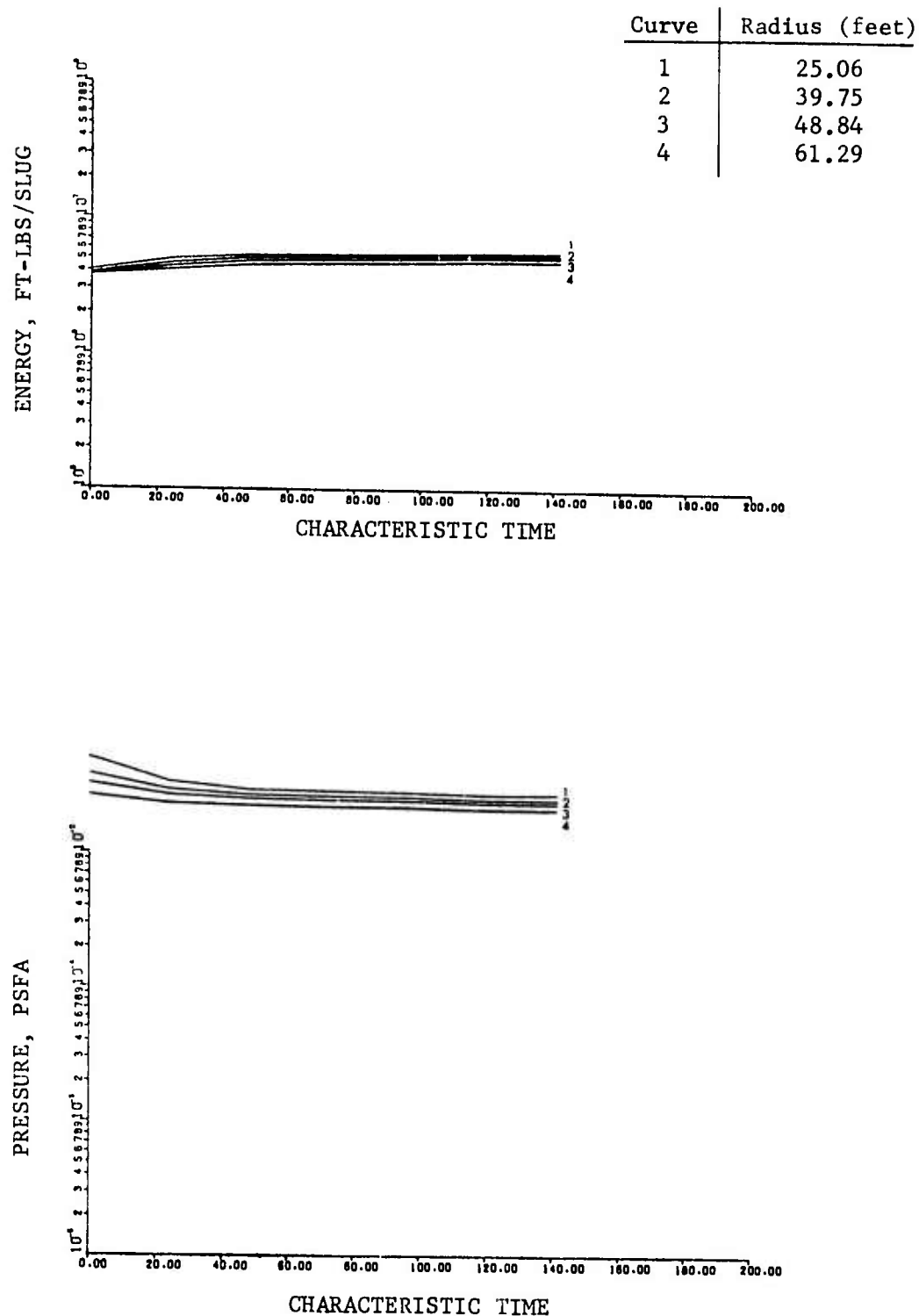| Curve	Radius (feet)
1	25.06
2	39.75
3	48.84
4	61.29

Figure 35. Specific Internal Energy and Pressure, vs. Time, at Various Points Along a Line Normal to the Centerline of an Atlas Booster During Ascent, and 171.86 ft Behind the Exit Nozzle. Data for the curves shown were generated by the AFTON 2A code using Mesh 7. (Problem 590.1; Altitude 394 kft; $E_\infty = .2836 \times 10^7$ ft-lbs/slug; $P_\infty = .5671 \times 10^{-4}$ psfa; $M_\infty = 8.054$; $Re_\infty = 1.17$/ft.)
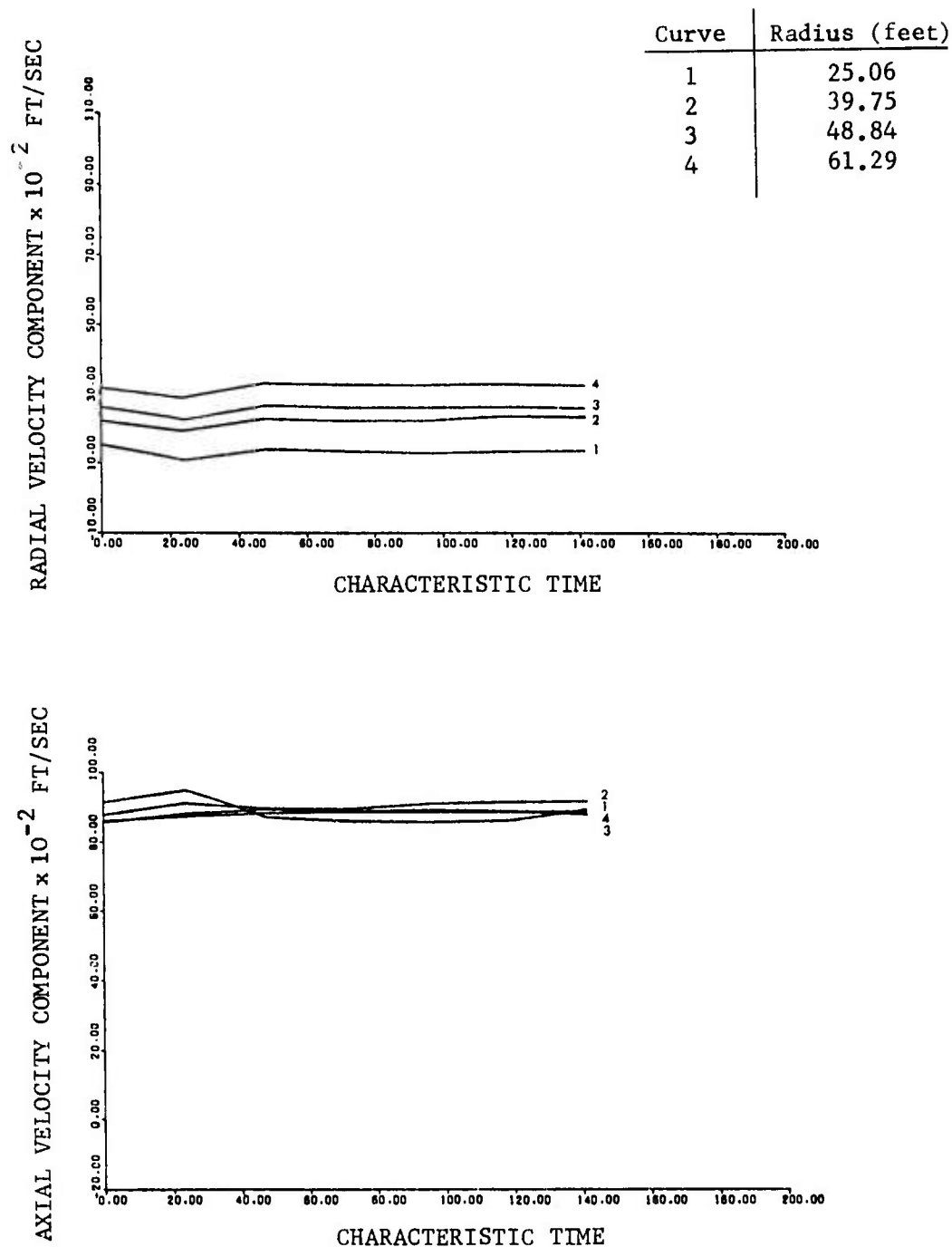
Figure 36. Radial and Axial Components of Velocity, vs. Time, at Various Points Along a Line Normal to the Centerline of an Atlas Booster During Ascent, and 171.86 ft Behind the Exit Nozzle. Data for the curves shown were generated by the AFTON 2A code using Mesh 7. (Problem 590.1; Altitude 394 kft; $U_\infty = 10150$ fps; $M_\infty = 8.054$; $Re_\infty - 1.17/ft$.)

57

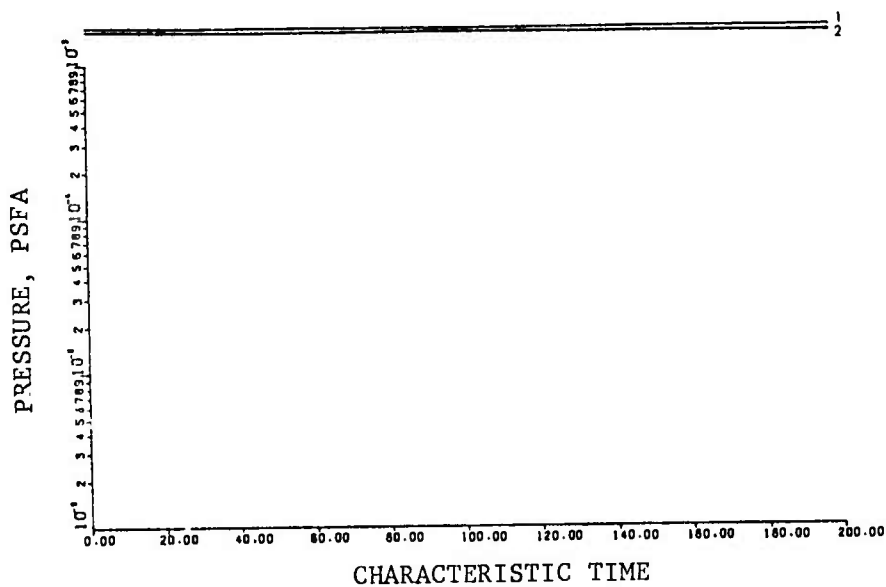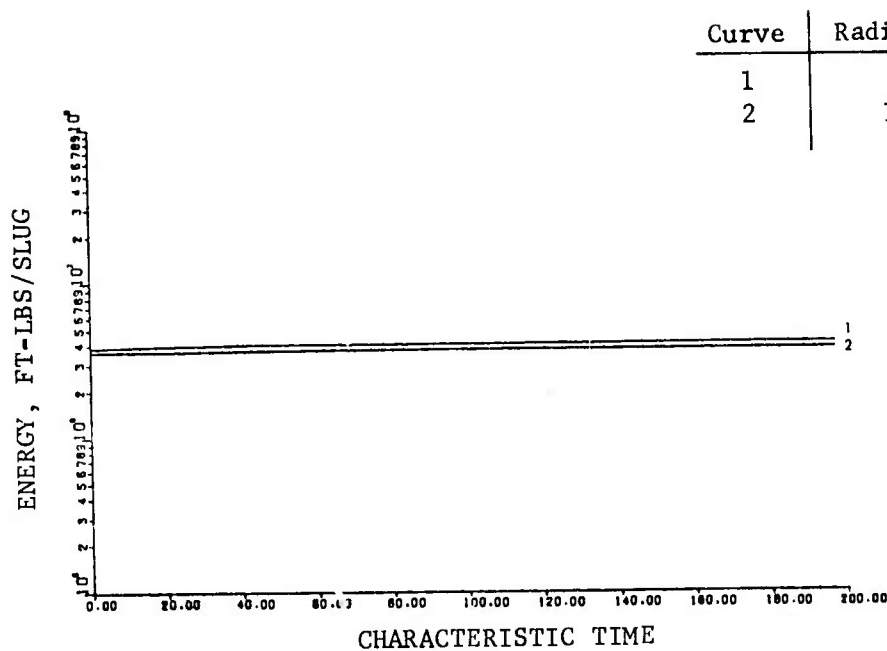| Curve	Radius (feet)
1	87.37
2	104.50

Figure 37. Specific Internal Energy and Pressure, vs. Time, at Various Points Along a Line Normal to the Centerline of an Atlas Booster During Ascent, and 171.86 ft Behind the Exit Nozzle. Data for the curves shown were generated by the AFTON 2A code using Mesh 8. (Problem 590.1; Altitude 394 kft; $E_\infty = .2836 \times 10^7$ ft-lbs/slug; $P_\infty = .5671 \times 10^{-4}$ psfa; $M_\infty = 8.054$; $Re_\infty = 1.17/\text{ft}$.)

Curve	Radius (feet)
1	87.37
2	104.50

RADIAL VELOCITY COMPONENT x 10^{-2} FT/SEC

110.00
90.00
70.00
50.00
30.00
10.00

0.00 20.00 40.00 60.00 80.00 100.00 120.00 140.00 160.00 180.00 200.00

CHARACTERISTIC TIME

AXIAL VELOCITY COMPONENT x 10^{-2} FT/SEC

100.00
80.00
60.00
40.00
20.00
0.00
-20.00

0.00 20.00 40.00 60.00 80.00 100.00 120.00 140.00 160.00 180.00 200.00
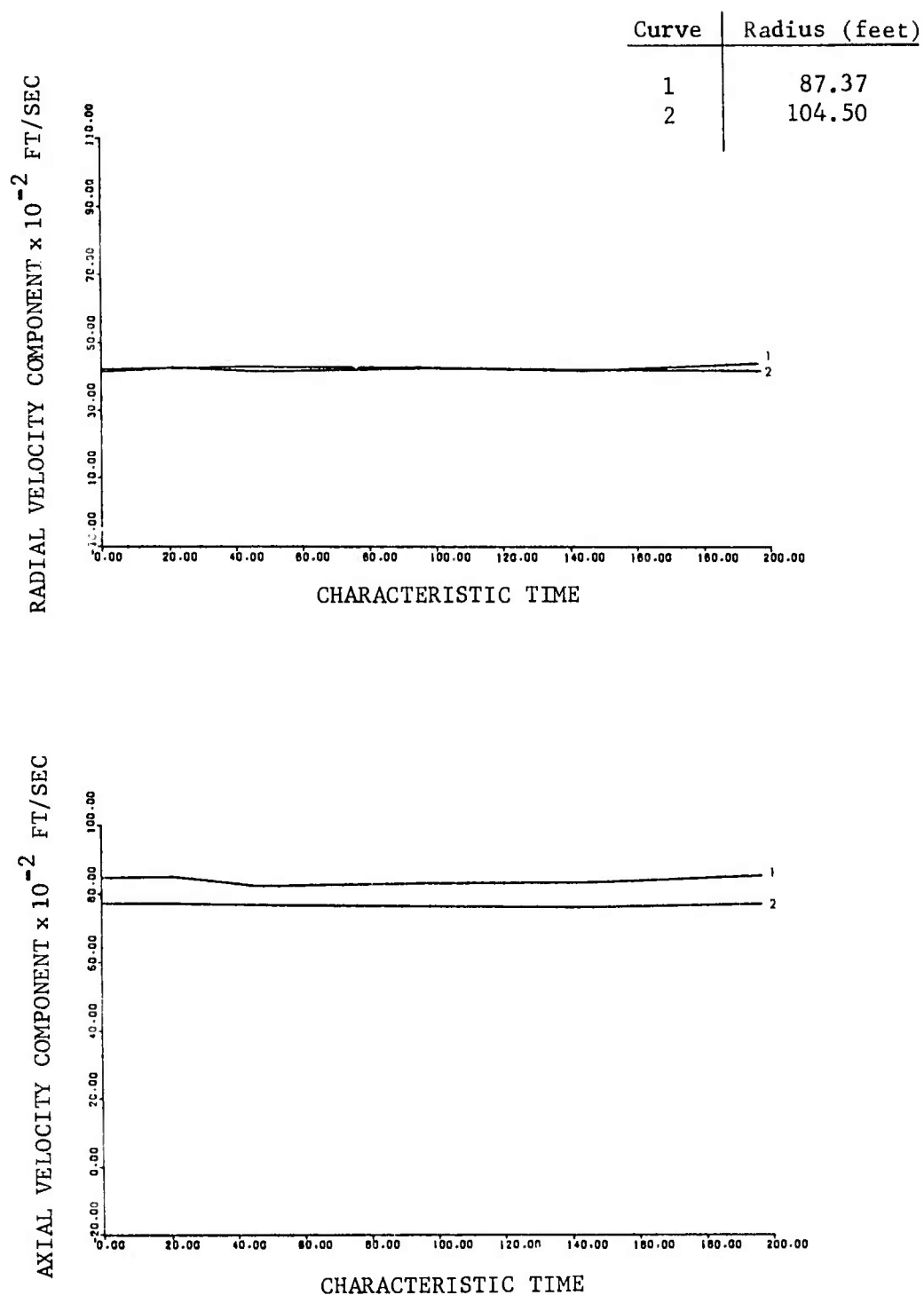
CHARACTERISTIC TIME

Figure 38. Radial and Axial Components of Velocity, vs. Time, at Various
Points Along a Line Normal to the Centerline of an Atlas
Booster During Ascent, and 171.86 ft Behind the Exit Nozzle.
Data for the curves shown were generated by the AFTON 2A
code using Mesh 8.   (Problem 590.1; Altitude 394 kft;
$U_\infty = 10150$ fps; $M_\infty = 8.054$; $Re_\infty = 1.17/ft.$)

59

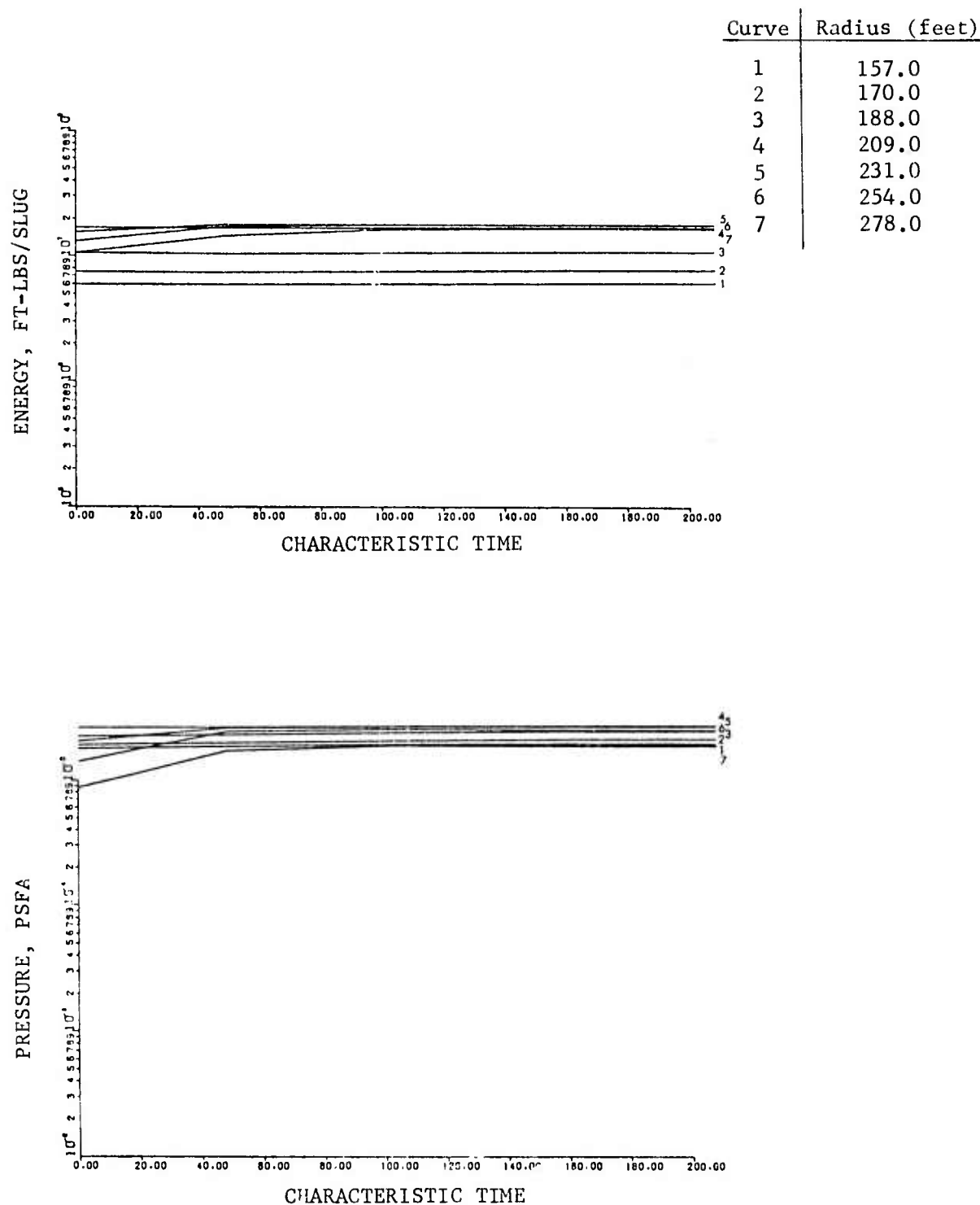| Curve	Radius (feet)
1	157.0
2	170.0
3	188.0
4	209.0
5	231.0
6	254.0
7	278.0

Figure 39. Specific Internal Energy and Pressure, vs. Time, at Various Points Along a Line Normal to the Centerline of an Atlas Booster During Ascent, and 171.86 ft Behind the Exit Nozzle. Data for the curves shown were generated by the AFTON 2A code using Mesh 9. (Problem 590.1; Altitude 394 kft; $E_\infty = .2836 \times 10^7$ ft-lbs/slug; $P_\infty = .5671 \times 10^{-4}$ psfa; $M_\infty = 8.054$; $Re_\infty = 1.17/ft$.)

60

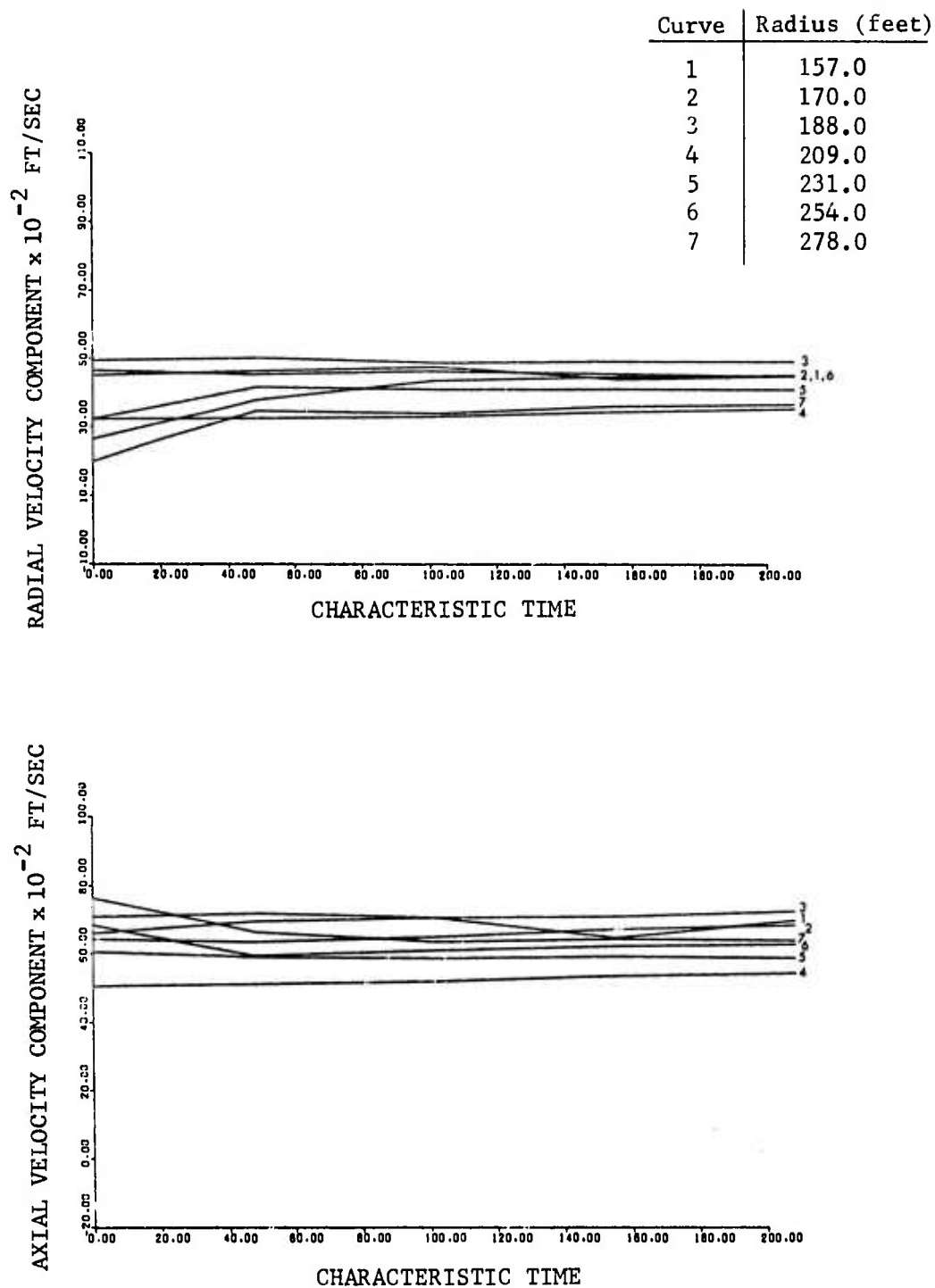| Curve	Radius (feet)
1	157.0
2	170.0
3	188.0
4	209.0
5	231.0
6	254.0
7	278.0

Figure 40. Radial and Axial Components of Velocity, vs. Time, at Various Points Along a Line Normal to the Centerline of an Atlas Booster During Ascent, and 171.86 ft Behind the Exit Nozzle. Data for the curves shown were generated by the AFTON 2A code using Mesh 9. (Problem 590.1; Altitude 394 kft; $U_\infty = 10150$ fps; $M_\infty = 8.054$; $Re_\infty = 1.17/\text{ft}$.)

61

SECTION 4

CONCLUSIONS

Several curves are presented in Figure 41 that
permit the AFTON 2A flow field to be compared with the field
predicted by a simpler model of Boynton.[6] Evidently the
AFTON 2A plume is considerably larger than Boynton's in the
near-field region. However, differences between the AFTON
and Boynton plumes diminish further downstream. At a dis-
tance of 100 ft behind the nozzle, the diameter of the AFTON
air shock is larger than Boynton's by a factor of about 2.2;
at 200 ft, the ratio is about 1.8 and at 300 ft the ratio has
the still-smaller value of about 1.5. As can be seen from
Figure 41, the two jet-shock loci agree more closely than do
the air shocks. The AFTON jet shock is larger than Boynton's
by factors of 1.5, 1.1 and 1.0, respectively, 100, 200 and
300 ft behind the nozzle.

Comments are made below on points of disagreement between
the AFTON flow-field and that of Boynton. However, it is a
major result of the present calculation that structural dif-
ferences between the AFTON and Boynton flow fields decrease
with downstream distance from the body. In fact, it seems
likely that over most of the region to two kilometers aft of
the body, an AFTON-calculated field would not differ signifi-
cantly from that of Boynton. Nevertheless, the relatively
large volume of high-temperature air in the AFTON near-field
might significantly alter the infra-red signature of the plume.
A calculation of radiation from the flow field would be needed
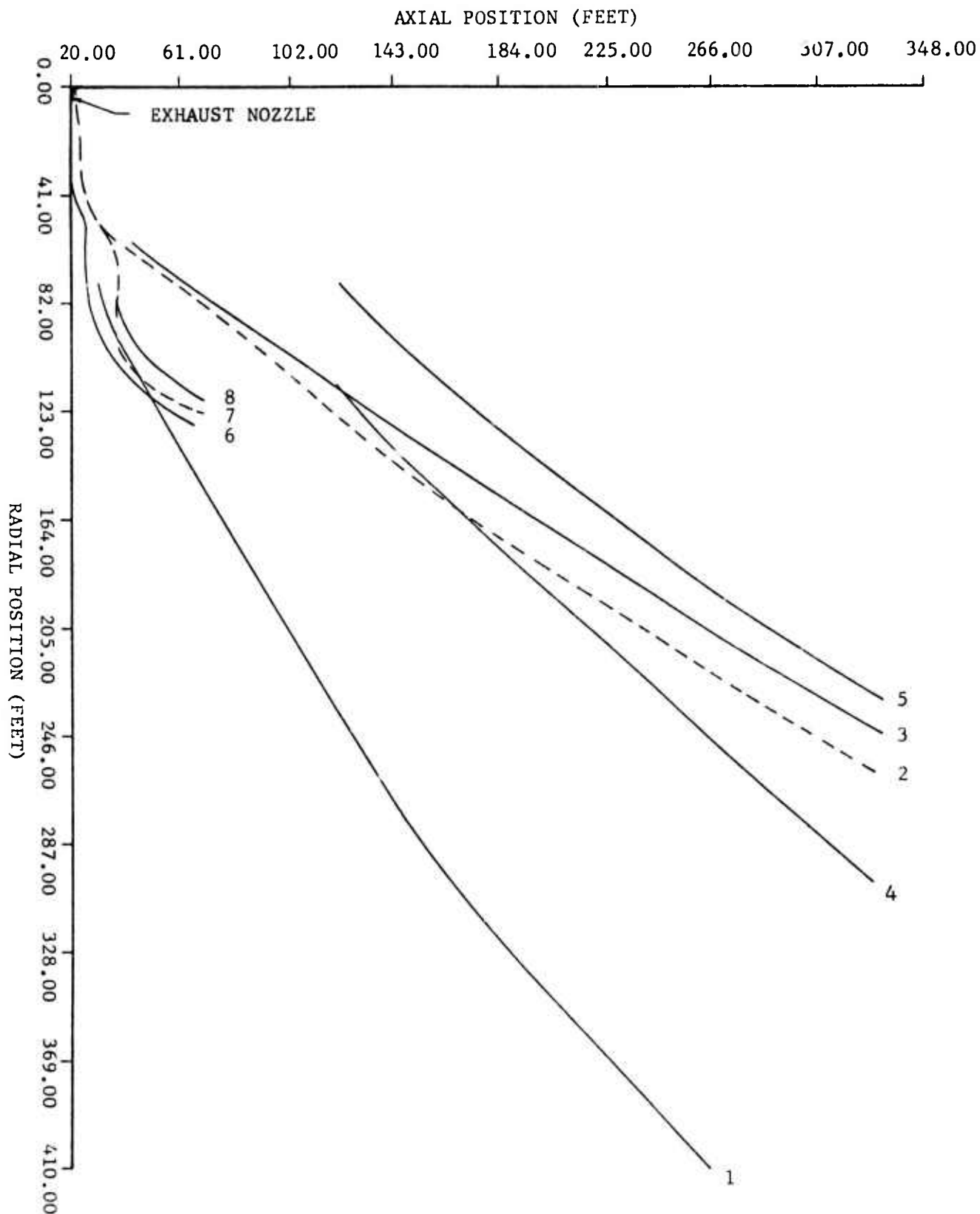to resolve that question.

Figure 41. Structure of the Flow Field Behind an Atlas Booster During Ascent. The field calculated with the Boynton Model is compared with the field generated by the AFTON 2A code. The AFTON 2A air shock, dividing streamline and jet shock are denoted by Curves 1, 2 and 3, respectively, while Curves 4 and 5 represent, respectively, the air and jet shocks of Boynton.[6] The previous AFTON 2A air shock, dividing streamline and jet shock are denoted by Curves 6, 7 and 8, respectively.[1] (Problem 590.1; Altitude 394 kft; $U_\infty = 10150$ fps; $M_\infty = 8.054$; $Re_\infty = 1.17/ft.$)

63

4.1 The Air Shock

The relatively large air-shock radius predicted by the AFTON code is consistent with a dividing streamline that makes an angle of about 90° with the plume axis near the nozzle, as opposed to an angle of less than 50° in Boynton's field. However, to explain why the two fields differ so greatly in the turning-angle of exiting exhaust gases, a detailed account is needed of the simpler calculation of flow near the nozzle; to our knowledge, the requisite details are as yet unpublished. In any event, by turning through a larger angle than that predicted by the simpler model, the AFTON dividing streamline presents a larger obstruction to the unimpeded flow of the incident airstream and gives rise to a stronger air-shock. Increasing shock strength implies increasing compression of shocked air, but the associated increase in turning-angle of the dividing streamline implies an increase by an even greater factor in the mass of air intercepted by the air shock. It is therefore reasonable that the volume of shocked air near the nozzle be greater in the AFTON field than in Boynton's field. Further, the stronger AFTON shock gives rise to more heating of shocked air. As a result, a consistently larger volume of shocked air is found in the AFTON field between the nozzle and any given cross-flow plane further downstream. In fact, while the two regions of shocked air differ in outer radius by a smaller and smaller factor with increasing downstream distance, their volumes differ by a factor that increases somewhat to a distance of 200 ft behind the nozzle, and then decreases.

4.2   Streamlines and Temperature Gradients

A principal assumption of most plume interaction
models is that gradients in velocity and temperature have
much larger components normal to streamlines than parallel
to them. With respect to that hypothesis, the calculated
AFTON Mach number and temperature contours shown in Fig-
ures 42 through 45 are of interest, as are the streamlines
shown for the AFTON field in Figure 28; for completeness,
density contours are also presented (Figures 46 and 47).
According to those figures, the hypothesis under discussion
is satisfied from the jet shock out to streamlines somewhat
larger in radius than the dividing streamline; that the hypoth-
esis is not valid near the centerline is of little consequence,
since gradients in Mach number and temperature are relatively
small in the core of the plume. Thus, it is not surprising
that the AFTON dividing streamline and jet-shock agree well
with those of Boynton, even at small distances from the
body. In the region of the air shock, however, the AFTON
code predicts a breakdown of the hypothesis in question:
the AFTON streamlines and isotherms do not coincide, even
roughly, near the air shock.

Non-coincidence of isotherms and streamlines consti-
tutes another reason for differences between the AFTON air-
shock and that of the simpler model. In particular, since
isotherms are not coincident with streamlines, heat flows
away from the air and into the exhaust gases less readily
in the AFTON field than in the field of Boynton, contribu-
ting both to greater downstream expansion of shocked air in
the AFTON field, and to higher shocked-air temperatures near
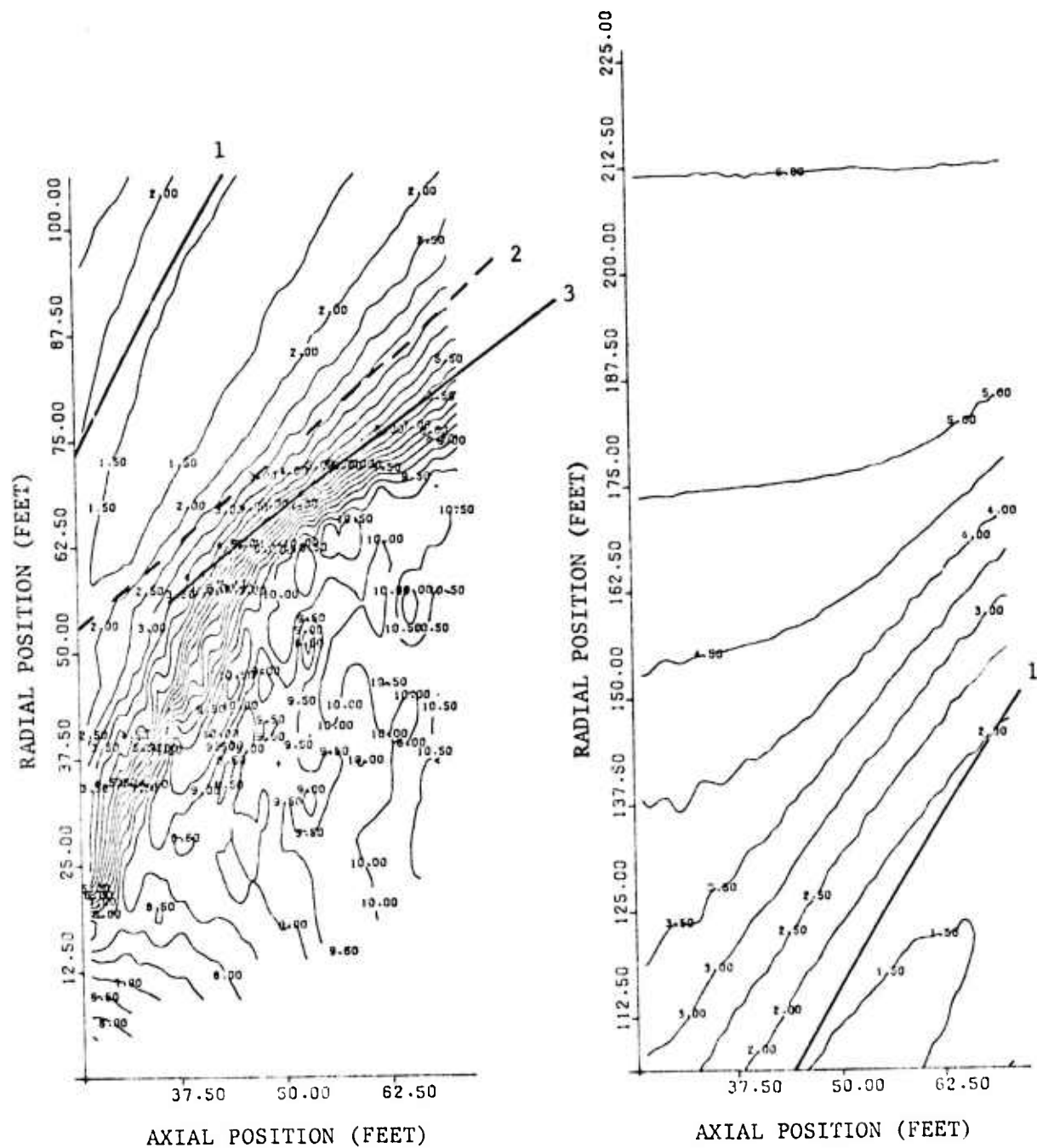the vehicle.

Figure 42. Mach Number Contours in the Steady Field Behind an Atlas Booster During Ascent. The field, which is shown between planes 3.58 ft and 44.36 ft aft of the body, was computed with the AFTON 2A code. The air shock, dividing streamline and jet shock are denoted by Curves 1, 2 and 3, respectively. (Problem 590.1; Altitude 394 kft; U_∞ = 10150 fps; M_∞ = 8.054; Re_∞ = 1.17/ft.)
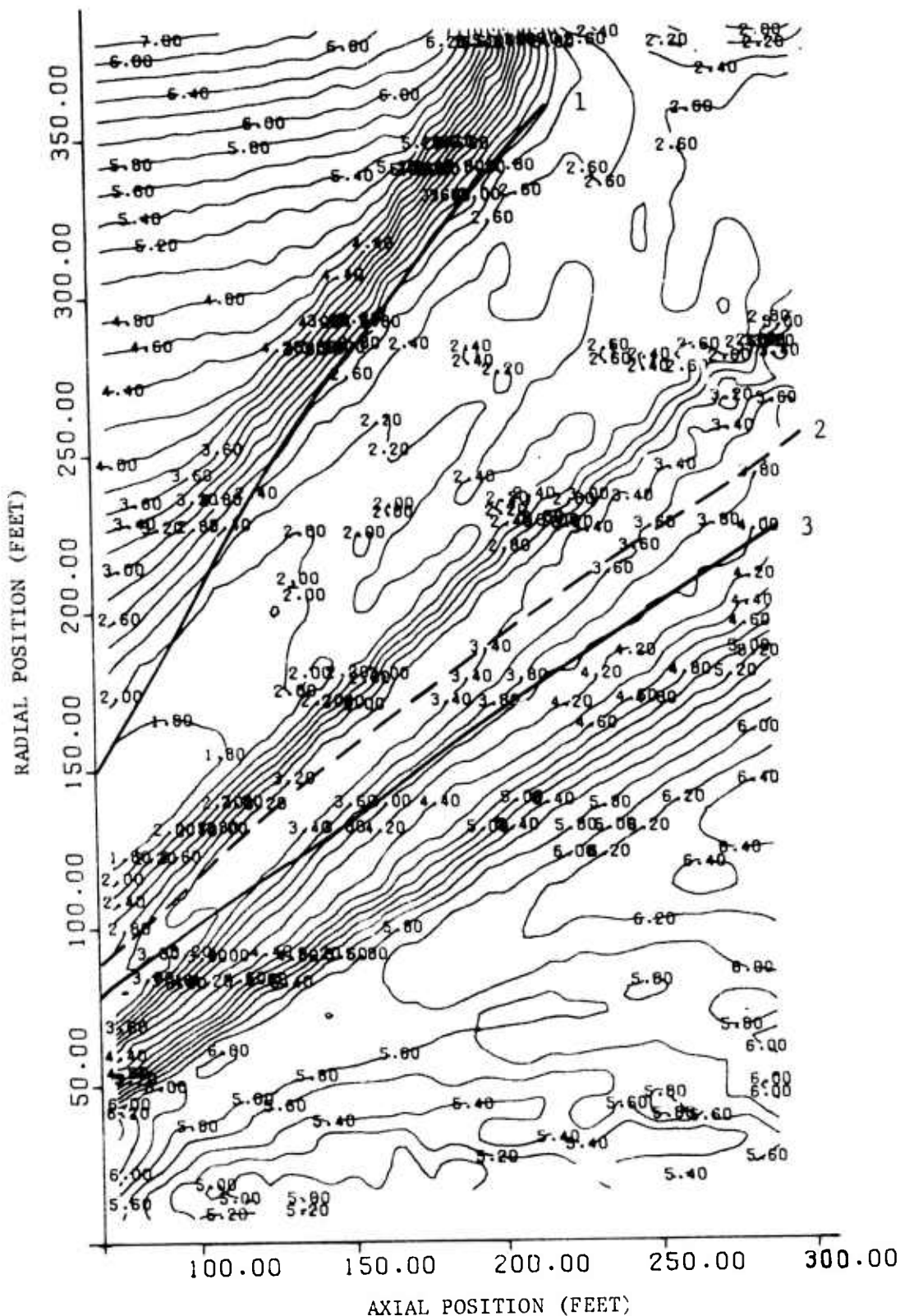
Figure 43. Mach Number Contours in the Steady Field Behind an Atlas Booster During Ascent. The field, which is shown between planes 44.36 ft and 302.01 ft aft of the body, was computed with the AFTON 2A code. The air shock, dividing streamline and jet shock are denoted by Curves 1, 2 and 3, respectively. (Problem 590.1; Altitude 394 kft; $U_\infty = 10150$ fps; $M_\infty = 8.054$; $Re_\infty = 1.17/\text{ft.}$)
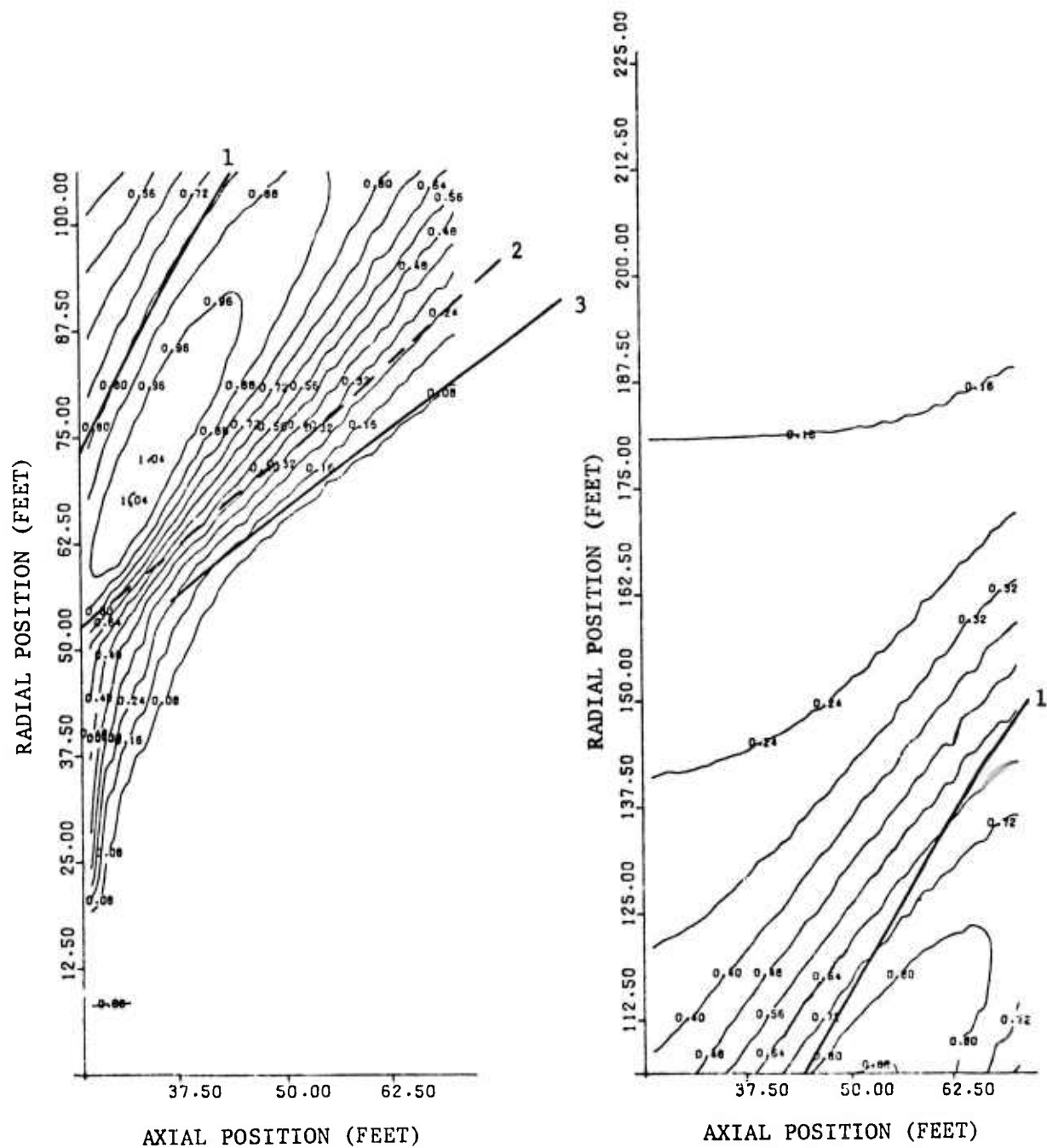
Figure 44.   Internal Energy Contours in the Steady Field Behind an Atlas
Booster During Ascent. The field, which is shown between
planes 3.58 ft and 44.36 ft aft of the body, was computed
with the AFTON 2A code. The air shock, dividing streamline
and jet shock are denoted by Curves 1, 2 and 3, respectively.
Contour parameter Z is defined as E/E_{STAG} where E_{STAG} is the
specific internal energy associated with free-stream stagnation.
(Problem 590.1; Altitude 394 kft; E_{STAG} = .3963x10^8 ft-lbs/slug;
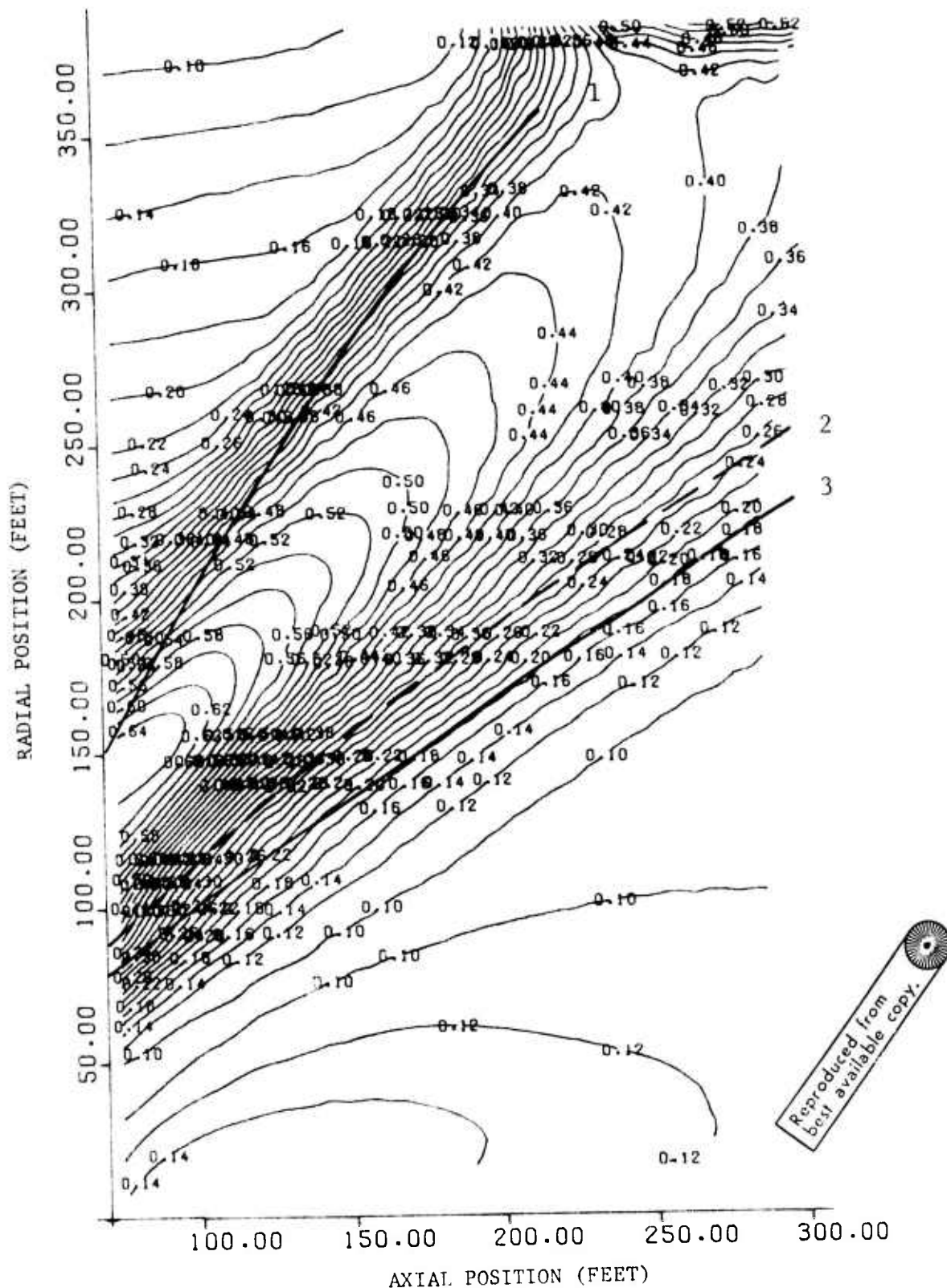M_∞ = 8.054; Re_∞ = 1.17/ft.)

Figure 45. Internal Energy Contours in the Steady Field Behind an Atlas Booster During Ascent. The field, which is shown between planes 44.36 ft and 302.01 ft aft of the body, was computed with the AFTON 2A code. The air shock, dividing streamline and jet shock are denoted by Curves 1, 2 and 3, respectively. Contour parameter Z is defined as E/E_{STAG} where E_{STAG} is the specific internal energy associated with free-stream stagnation. (Problem 590.1; Altitude 394 kft; $E_{STAG} = .3963 \times 10^8$ ft-lbs/slug; $M_\infty = 8.054$; $Re_\infty = 1.17/ft$.)
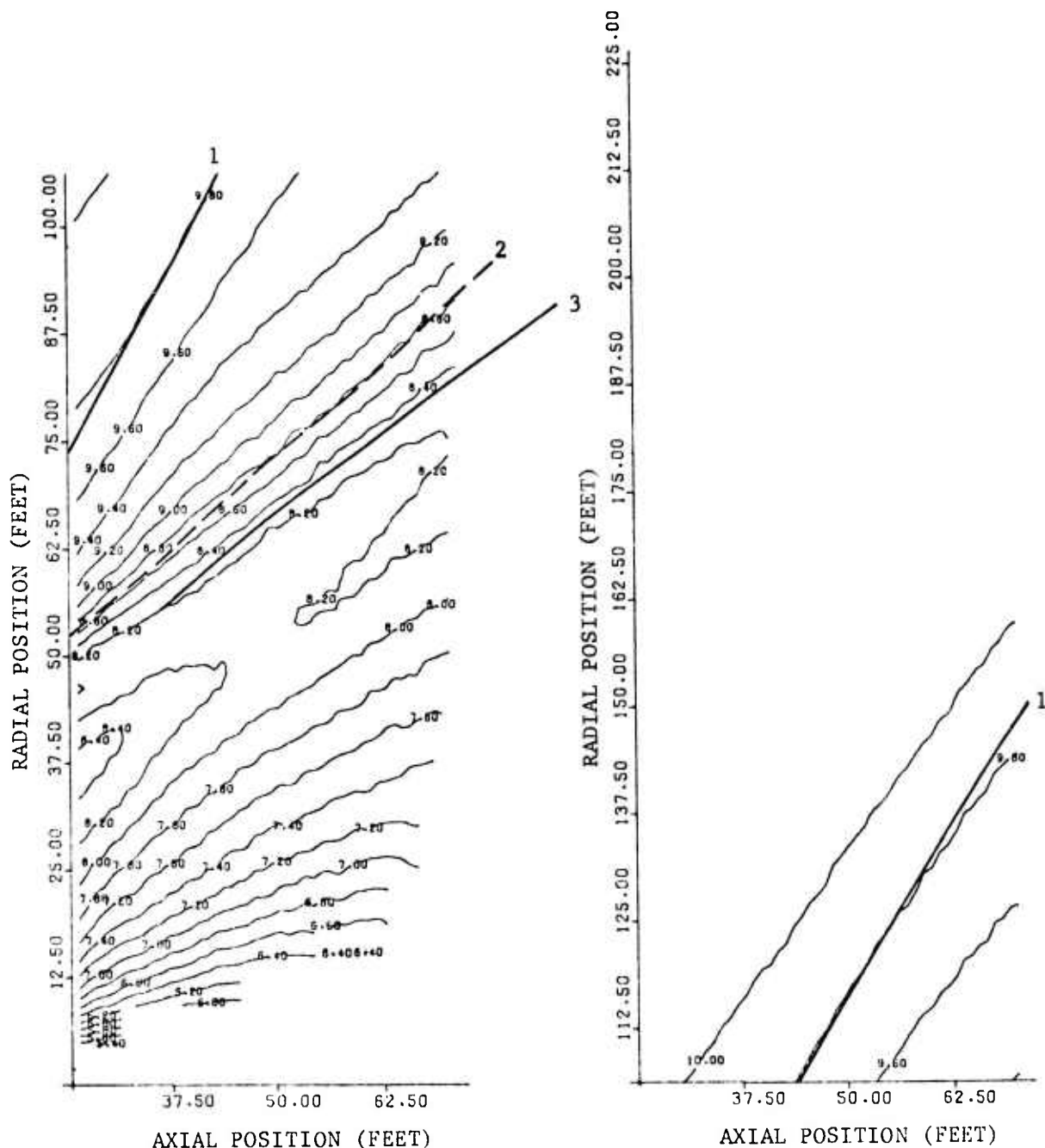
Figure 46. Density Contours in the Steady Field Behind an Atlas Booster During Ascent. The field, which is shown between planes 3.58 ft and 44.36 ft aft of the body, was computed with the AFTON 2A code. The air shock, dividing streamline and jet shock are denoted by Curves 1, 2 and 3, respectively. Contour parameter Z is defined as $Z = |\log_{10} \rho|$. (Problem 590.1; Altitude 394 kft; $\rho_\infty = 0.4999 \times 10^{-10}$ slug/ft^3; $M_\infty = 8.054$; $Re_\infty = 1.17/\text{ft.}$)
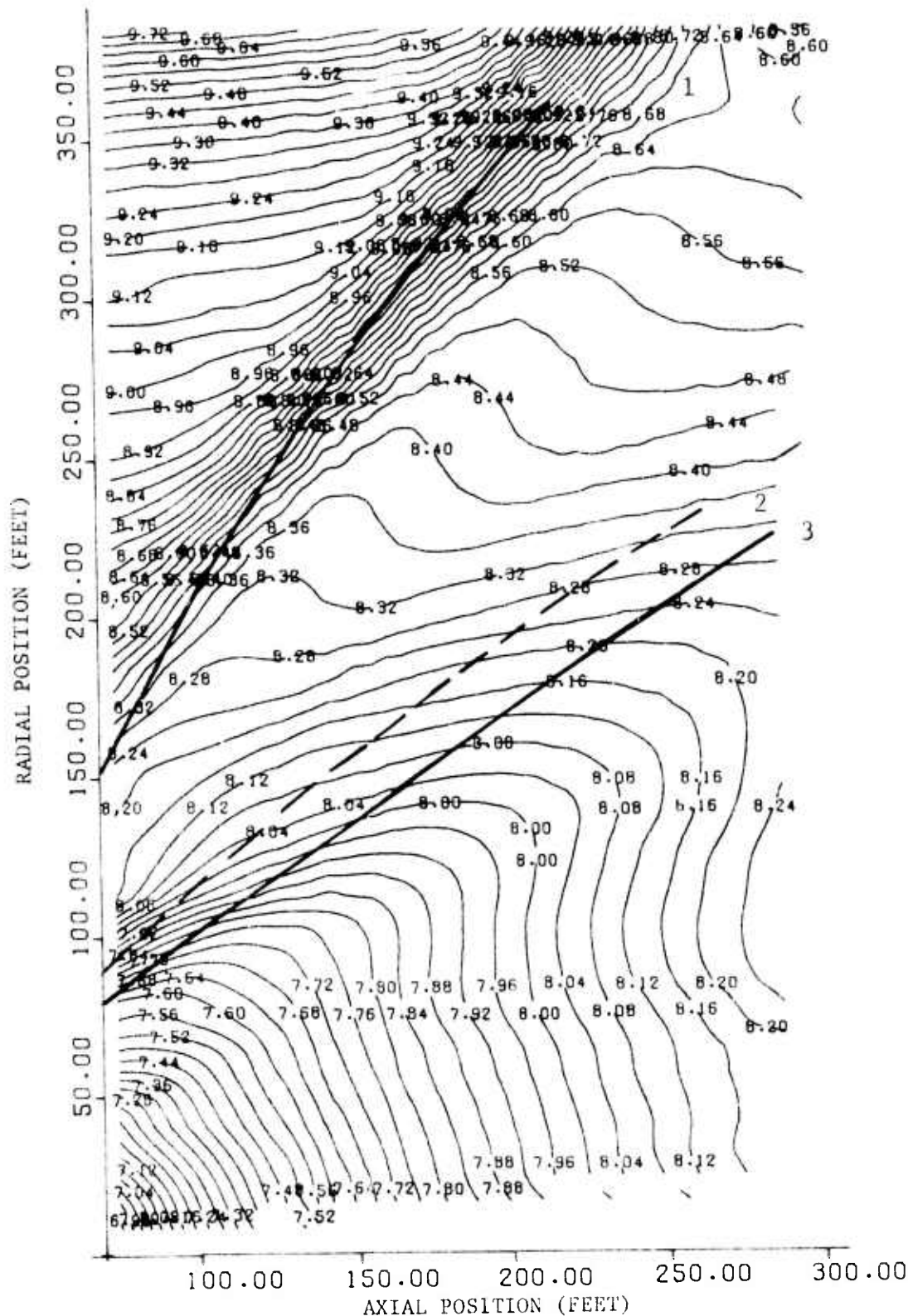
Figure 47. Density Contours in the Steady Field Behind an Atlas Booster During Ascent. The field, which is shown between planes 44.36 ft and 302.01 ft aft of the body, was computed with the AFTON 2A code. The air shock, dividing streamline and jet shock are denoted by Curves 1, 2 and 3, respectively. Contour parameter Z is defined as $Z = \frac{1}{3} |\log_{10} \rho|$. (Problem 590.1; Altitude 394 kft; $\rho_\infty = 0.4999 \times 10^{-10}$ slug/ ft^3; $M_\infty = 8.054$; $Re_\infty = 1.17/ft$.)

71

4.3   Shear Instabilities

The possibility of unstable growth of oscillations
at the interface between plume gases and air (i.e., at the
dividing streamline) is not taken into account in the simpler
plume models, but is calculable with the AFTON 2A code. The
mixing of gases that would attend such instability could
strongly affect the temperature of the interacting air and
plume gases, and hence their output of infra-red radiation.
However, careful examination of the velocity field pre-
sented in Figure 1 shows the shear layer to be free of
Helmholtz instability. The slight oscillations that can be
seen just upstream of the air shock at a radius of about
300 ft are not physical in origin. Velocity oscillations
like those noted are typically produced near a shock by dis-
crete time-marching equations of motion which, like the
AFTON 2A equations, describe transport terms in (formally)
second-order-accurate fashion.

REFERENCES

1. Walitt, L., "Exact Solution of the Navier-Stokes Equations for Rocket Plumes at 120 km Altitude", Paper prepared for Third Plume Physics Program Meeting, Institute for Defense Analyses, Arlington, Virginia, 8 November 1973.

2. Boynton, F.P., "Numerical Calculations of Viscous High-Altitude Exhaust Plume Flow-Fields", Research Institute for Engineering Sciences, Report No. RIES-70-18, College of Engineering, Wayne State University, Detroit, Michigan (1970).

3. Trulio, J.G., "Theory and Structure of the AFTON Codes", AFWL TR-66-19, Air Force Special Weapons Center, Kirtland Air Force Base, New Mexico (1966).

4. Trulio, J.G., "On the Eulerian AFTON Equations for Axisymmetric Fluid Flow", Applied Theory Report ATR-73-33-1, Los Angeles, California (1973).

5. DARPA Contractor's Meeting, The Aerospace Corporation, Los Angeles, California (April 1974).

6. Trulio, J.G., and Walitt, L., "Numerical Calculations of Viscous Compressible Fluid Flow Around a Stationary Cylinder", NASA CR-1465 (1970).